A Deep Photometric Survey of the Abell Cluster S0423. A Pilot Study for the UCT SALT Supercluster Survey.

J.P. Kotze

Department of Astronomy
University of Cape Town
South Africa

A dissertation submitted in partial fulfillment of the requirements for the degree M.Sc. in the Department of Astronomy, as part of the National Astrophysics and Space Science Programme
UNIVERSITY OF CAPE TOWN

May 2007

Supervisors: *Prof. R. C. Kraan-Korteweg, Dr. P. A. Woudt*

Abstract

The UCT SALT Supercluster Survey (USSS) will study galaxy transformation and evolutionary processes in high to lower density regions at various redshift ranges between z $\sim$ 0.15 - 0.60. This will be based on deep *UBVRI* band photometry and multi-object spectroscopy to be obtained with the Southern African Large Telescope (SALT). This thesis presents a study which evaluates the contribution that the Infrared Survey Facility (IRSF) can make to this project. Due to SALT's fixed constantly changing pupil size, it is necessary to calibrate its photometry using an independent facility. The feasibility of using the 1m telescope for these calibrations were also investigated.

To this end, deep multicolour photometry of the galaxy cluster Abell S0423 (z $\sim$ 0.138) were obtained during November/December 2005 and February 2006 at the South African Astronomical Observatory (SAAO) site of Sutherland. The multicolour photometry consists of near infrared (NIR) JHK_s band photometry obtained at the IRSF and optical *UBVRI* band photometry from the 1m telescope.

This work finds the IRSF to be an ideal instrument with which to obtain NIR photometry of galaxy clusters. Extending the wavelength range of the USSS to the NIR will result in better constrained galaxy evolution and transformation models.

Despite NIR colours being insensitive to morphological type, this work confirms previous studies by Jarrett *et al.* (2003) that find the NIR mean central surface brightness to be a rough morphological indicator.

Without SALT imaging performance data available, it is not possible to definitively discuss the feasibility of using the 1m telescope for this purpose. Preliminary results indicate that it is theoretically possible, but other avenues may need to be explored.

Acknowledgements

Firstly I would like to thank my supervisors. Prof. Renée Kraan Korteweg and Dr. Patrick Woudt. I am very gratefull for all your support, and for giving me the opportunity to share your knowledge. To my fellow students and very good friends I would like to extend a special thanks. Ros, thank you for being such a great office-mate, our friendship is cemented in our struggle with IRAF. To Ewald, the resident Python master, thank you for our great friendship and for all the help and support. To my family so far away, my two brothers, thank you for all your support. To my parents, thank you for all the sacrifices you have made over the years so that I can have the opportunity to be here today. I am forever gratefull for all the love and support you have given me.

Lastly, but most importantly, my Michelle. Thank you is only two words, it seems not nearly enough to describe my gratitude for everything you have done for me. Your unwavering love and support have seen me through the hard times and made the good times amazing. Thank you for all the sacrifices you made for me to finish my dissertation. I am forever grateful to have someone as wonderful as you in my life.

Contents

List of Figures

List of Tables

Chapter 1

Introduction

1.1 The UCT SALT Supercluster Survey (USSS)

The University of Cape Town Astronomy Department has set out to study superclusters at various intermediate redshifts (z $\sim$ 0.15, 0.30, 0.45, 0.60) to gain a better understanding of galaxy transformation and evolutionary processes in high to lower density regions. The observations will be carried out at the 10m class Southern African Large Telescope (SALT[1]) and the 1.4m Infrared Survey Facility (IRSF[2]), both located at the South African Astronomical Observatory (SAAO) site in Sutherland. The goal is to obtain deep *UBVRI* photometry using SALTICAM[3], making optimal use of SALT's blue sensitivity and wide 8×8 arcminute field of view and near infrared JHK_s photometry using SIRIUS[4] on the IRSF.

The study of galaxy transformation and evolution focuses on the effect that dense regions have on galaxies. Recent results show that transformation may start to occur farther away from the cluster core (3 $\sim$ 4 virial radii) than previously thought (Lewis *et al.* 2002; Gomez *et al.* 2003; Balogh *et al.* 2004 and Gerken *et al.* 2004). By extending this study out to various virial radii, we hope to address some of the big questions still unanswered today. What evolutionary and transformation processes are involved and to what extent? Where do various processes occur within the cluster and supercluster environment? What are their respective transition stages and end products? What are the timescales involved?

Detailed evolutionary modeling based on the acquired photometry, using models such as GALEV (Fritze -v. Alvensleben 2004; Bicker 2002), will form an integral part of the project. The large wavelength coverage and in particular, the unique blue sensitivity of SALT, will be of great importance in this respect. The deep photomet-

[1] www.salt.ac.za/

[2] www.z.phys.nagoya-u.ac.jp/~telescop/index_e.html

[3] SALT Imaging Camera

[4] Simultaneous-Color InfraRed Imager for Unbiased Survey.

ric study will be followed by SALT multi-object medium resolution spectroscopy of photometrically identified supercluster members using the Robert Stobie Spectrograph (RSS)[5].

Forming part of the project in the near future will be the Karoo Array Telescope (KAT[6]). Deep HI surveys of the superclusters at intermediate redshifts will provide valuable information on the actual HI content and distribution within superclusters, to be compared with the star formation histories as deduced from the GALEV modeling.

1.2 Outline of this Thesis

With the idea of using SALT as the main instrument for the USSS, the first step must be the verification of using SALT and the IRSF to reach the proposed goals. To test this, deep multi-colour photometry of a supercluster core at our lowest redshift range was obtained. Its richness and location was the main consideration for selecting the Abell cluster S0423 (Abell 1958) for this initial study. This cluster lies at the core of the galaxy supercluster SC -45.17 (Einasto *et al.* 2003) at a redshift of $z \sim 0.138$.

Given the constant changing pupil size of SALT, calibrating photometric data with standard stars is not possible. Therefore, a pilot study was initialised to investigate whether the 1m Elizabeth telescope, together with the SAAO CCD, could be used for calibrating SALT data.

The 1m is located at the same site as SALT. It has a 5.3×5.3 arcminute field of view and also uses the Johnsons-Cousins filter system. The SALT photometry was to be taken in parallel during the performance verification phase. Due to image quality problems, SALT data is still not available. Nevertheless, we continued the 1m feasibility study for SALT calibrations and obtained the first IRSF survey fields.

The deep multicolour images of the galaxy cluster Abell S0423 was obtained during November/December 2005 and February 2006 at Sutherland. The data presented in this thesis consist of near infrared (NIR) JHK_s band images obtained at the Infrared Survey Facility (IRSF) and optical *UBVRI* band images obtained at the 1m telescope. The deep NIR photometry forms part of the initial survey of the supercluster SC -45.17 for the USSS, whereas the optical data was reduced and analysed to give an indication whether the planned calibrations would be possible. Results from the observations were not only used to test the viability of using the IRSF for the "nearby" superclusters, but also whether the IRSF will suffice for imaging superclusters at higher redshifts. The data will also be used, together with future SALT data, as input for the galaxy evolutionary models.

[5]http://www.salt.ac.za/telescope/instrumentation/pfis/

[6]www.kat.ac.za

1.3 Overview

Chapter 2, will provide a brief introduction on galaxy evolution and transformation scenarios in clusters and superclusters. Together with a short description of the effects of possible transformation processes such as ram pressure stripping, harassment and galaxy mergers. GALEV evolutionary models will also be reviewed. Chapter 3 gives an overview of the target selection and discusses the data acquisition and reduction. Results will be shown in Chapter 4, with conclusions and future work of the USSS following in Chapter 5. Appendix A deals with the details of data reduction and Appendix B contains catalogues of the galaxies found in the IRSF survey of the supercluster SC -45.17.

Chapter 2

Overview of Galaxy Evolution and Transformation Processes in Clusters

2.1 Evidence for Galaxy Evolution and Transformation

Butcher & Oemler (1978) observed that the fraction of blue galaxies increases from $z = 0$ to $z \sim 0.5$. This has become known as the Butcher-Oemler effect. Van Dokkum *et al.* (2001) and Dahlén *et al.* (2004) found that the fraction of blue galaxies increases by a factor of 5 for that same redshift range. The blue galaxy population was found to consist mostly of spiral and irregular galaxies with ongoing star formation (SF) (Smail *et al.* 1997). This differs greatly from the the galaxy population found in local clusters, which consists mainly of elliptical and S0 galaxies (Fritze - v. Alvensleben 2004). Couch *et al.* (1998) and Fasano *et al.* (2000, 2001) have shown that the fraction of spiral galaxies decreases by a factor ~ 5 from $z \sim 0.5$ to $z = 0$ while the fraction of S0 galaxies increases by the same amount from $z \sim 0.5$ to $z = 0$. The fraction of elliptical galaxies stays almost constant.

This is compelling evidence for transformation of spiral galaxies into S0 galaxies between the redshift range of $z \sim 0.5$ to $z = 0$, i.e. over the past 5 Gyrs; transformation seems to be linked to the continuous infall of 'field' spiral galaxies into increasingly rich clusters (Fritze - v. Alvensleben 2004). A tracer for the evolution of galaxies in clusters is the effect the cluster has on the SF of a galaxy. This can be studied by comparing multicolour photometry of the cluster galaxies and field galaxies. Ongoing SF will make a galaxy appear bluer due to the younger stellar population while SF truncation will make a galaxy appear red due to the majority of stars being more evolved. A number of transformation and evolution scenarios have been proposed over the past few years. It seems that more than one process is needed to explain the observed phenomena. In the following, the most important

processes responsible for galaxy evolution and transformation will be discussed.

2.2 Galaxy Evolution and Transformation Scenarios

2.2.1 Ram Pressure Stripping

The possibility that ram pressure stripping could occur and result in the transformsation of a galaxy's morphology in dense environments was first investigated by the analytic work of Gunn & Gott (1972). They modeled the hydrodynamic effect a galaxy would experience as it orbits through a diffuse gaseous intra-cluster medium (ICM). Rapid motion of a galaxy through a tenuous ICM causes a large pressure front to build-up in front of the galaxy. If the binding energy of the galaxy's interstellar medium (ISM) is high enough, the ICM will flow around it. If not, the ICM will flow through the galaxy removing some or all of the diffuse ISM.

The first observations that support this mechanism were made by van den Bergh (1976), who found that spiral galaxies close to the centre of the Virgo cluster are redder on average. This is indicative of SF truncation. Cayatte *et al.* (1990) and Bravo-Alfaro *et al.* (2000) found increasingly truncated and displaced HI disks in spirals toward the centre of the Virgo and Coma cluster, respectively; an indication that the ICM density and pressure is comparable or higher than that of the ISM within the galaxies. Only recently, observations by Lewis *et al.* (2002), Gómez *et al.* (2003), Balogh *et al.* (2004) and Gerken *et al.* (2004) found that the galaxy population in clusters show reduced SF activity at much larger distances from the centre than previously thought, out to 3 - 4 R_{vir}. They suggest that the ICM densities that far out might still be high enough to drive away low density gas from galaxy halos, which would otherwise be used as a reservoir for disk accretion, hence, star formation (Larson *et al.* 1980).

If ram-pressure stripping is an effective mechanism for removing HI gas from spirals, one would expect that most cluster spirals would be HI deficient. But observational evidence for this is limited. The observations by Cayatte *et al.* (1990) and Bravo-Alfaro *et al.* (2000) clearly show the influence of ram pressure stripping on spirals near the Virgo and Coma clusters respectively through the displaced HI disks. Recent Hubble Space Telescope (HST) observations by Cortese *et al.* (2007) show two peculiar spirals with stellar and gas trails falling into the massive cluster Abell 1689. Their modelling suggests that the observed morphology is likely due to tidal interaction with the cluster potential and ram pressure stripping due to the ICM.

Mould *et al.* (1999) find no evidence of HI deficient spirals in a survey of 67 clusters. Moreover, based on modeling, Abadi *et al.* (1999) conclude that gas disks are not completely removed and that a significant portion of the cold gas remains

bound to the stellar disk. Ram pressure stripping alone can therefore not account for the morphological changes observed in infalling spirals.

2.2.2 Galaxy Mergers

Galaxy mergers, especially the role this mechanism plays in the evolution of cluster galaxies, has been the topic of much discussion (Mihos 2004; Fritze -v. Alvensleben 2004). For a merger to occur, the relative velocities of galaxies have to be relatively low. Mihos (2004) noted that galaxy clusters do not form by accreting random individual galaxies from the field, but rather through the infall of low mass groups along the filaments that make up the "cosmic web". The infalling groups have much lower velocity dispersions than that of the cluster, making the conditions for slow galaxy interactions more favourable. *N*-body simulations by Ghigna *et al.* (1998) show that merging has largely shut off at the core of massive clusters. Due to the high velocity dispersion of a virialised cluster, mergers are confined to the cluster periphery. They find no mergers within 1.6 Mpc of a cluster core situated at $z = 0$. Growing observational evidence reveal the importance of merging as a mechanism that can account for the change of the morphology of infalling spiral galaxies (Dressler *et al.* 1997).

Observations of rich clusters, for instance MS 1054-03, reveal a substantial number of major merger in the outer parts, consistent with the idea of enhanced merging in infalling groups (van Dokkum 1999). Mergers have been proposed as *the* mechanism to drive the formation of S0 galaxies. Evolutionary models by Fritze - v. Alvensleben (1998, 1999) suggest that the luminous S0 galaxies are the result of major mergers of gas-rich spirals, while minor mergers (e.g. mergers with mass ratio 3:1) or accretion events look to be viable mechanisms for the formation of intermediate or low luminosity S0s (Bekki 1998). However, cluster galaxies have to contend with the effects of the overall tidal field of the cluster. Simulations by Mihos (2004) indicate that the merger time scale is lengthened by cluster tidal effects. This implies that luminous S0s must have been preprocessed in the field or within infalling groups before being incorporated into clusters (Fritze - v. Alvensleben 2004).

2.2.3 Harassment

Galaxy harassment or frequent high speed galaxy encounters, is thought to be one of the dominant driving factors for morphological transformation in dense cluster environments. From their HST images Oemler *et al.* (1997) found disturbed spirals distributed throughout four rich clusters. They concluded that merging is implausible because the blue galaxy fraction is large and the merging probability low. With ram pressure stripping and global tidal effects only operating efficiently near the

cluster core (Oemler *et al.* 1997), another mechanism has to be considered. Moore *et al.* (1995, 1998) used numerical simulations and compared it to HST images of harassed cluster galaxies. They found that fast galaxy-galaxy encounters within the cluster potential destabilises the disks of infalling spirals, drag out short lived tidal tails, and tear away stars from the outer disk. This leaves the inner parts either as dwarf ellipticals, low-luminosity S0s or dwarf spheroidal galaxies. The remnants of this process will consist of the central parts of much more massive galaxies, which are expected to deviate from the Mg_2 - σ relation toward too high metallicities for their mass. Observations by Poggianti *et al.* (2001) of the Coma cluster found exactly these properties i.e. enhanced metallicities for their luminosities. Furthermore, the harassment timescale matches the interval of multiple starbursts found in spectroscopic observations by Couch *et al.* (1994) of a cluster at $z \sim 0.4$. A recent Sloan Digital Sky Survey (SDSS) study by Lisker *et al.* (2006) of dwarf elliptical galaxies in the Virgo supports harassment as a plausible formation scenario.

2.3 GALEV, an Evolutionary Model

Collaboration with Prof. Uta Fritze-v. Alvensleben, together with the Göttingen Galaxy Evolution Group, will play an integral role in the modeling of galaxy evolution in clusters through applying their models (GALEV) to our photometry. All strong galaxy interactions or mergers are observed to be accompanied by bursts of star formation if one or both galaxies are gas rich. When falling into a cluster, the spiral rich field population must somehow be transformed into an E/S0/dE rich cluster population. These transformation processes also involve interactions among individual galaxies or of an infalling galaxy with the cluster potential or hot ICM (Fritze - v. Alvensleben 2000). By studying interaction-triggered starbursts with spectrophotometric and chemical evolutionary synthesis models one can learn about the star formation process under interaction conditions.

The photometric evolution of various spirals, (with or without a preceding starburst) falling into a hot ICM have been investigated by Bicker *et al.* (2002). They conclude that the progenitors of low luminosity S0s can be Sa, Sb or Sc spirals that experienced star formation truncation > 3 Gyr ago, as well as Sa or Sb galaxies with SF truncation at ages between 6 and 9 Gyr ago. To date, models include detailed spectral evolution in a cosmological context, allowing the study of all types of field galaxies from the onset of various disturbances. The star formation histories can be followed through all the transitional stages at different redshifts (Bicker & Fritze - v. Alvensleben 2005). GALEV models follow the evolution of the gas, luminosity weighted stellar and gaseous metallicities, as well as emission lines which are tracers of star formation (Bicker *et al.* 2004). The models also allow for the determination

of very accurate photometric redshifts, provided U-band data is available. The blue sensitivity of SALT will play a major role in this respect.

2.4 USSS and Galaxy Evolution and Transformation

SALT is well suited for observing the distinct observational effects that clusters and superclusters have on galaxies. Deep imaging using SALTICAM in addition to multi-object spectroscopy using the RSS will be the key ingredient for this project. Time availability, SALT's large collecting area, a wide 8 $\times$ 8 arcminute field of view and unique blue sensitivity makes SALT ideal for a survey of this nature. The optical *UBVRI*, together with the NIR JHK_s photometry, will be used to derive photometric properties such as colours, morphology, galaxy distributions, mass, luminosity functions and photometric redshifts. The photometric survey will be used to identify candidates for follow-up spectroscopy. Multi-object medium resolution spectroscopy will give an indication of star formation histories, cluster dynamics and more accurate morphological classifications. Both these observational tools go hand in hand with the modeling of evolutionary and transformation processes. The transformation and evolutionary modeling will play a crucial role in quantifying observational phenomena. The future addition of KAT will provide valuable information on the actual HI content of the superclusters. All these world class observational and theoretical tools will make this a unique approach to the study of evolution and transformation processes in intermediate superclusters.

Chapter 3

Observations and Data Reduction

3.1 Target Selection: Abell S0423

The Abell cluster S0423 is situated at the heart of the supercluster SC -45.17 at a redshift of $z = 0.138$. SC -45.17 was classified as a supercluster by Einasto *et al.* (2003) using data obtained from the Las Campanas Redshift Survey (LCRS[7]) . That survey extends to a redshift of 0.2 and covers six 1.5×80 degree slices. Three slices are located in the Northern Galactic cap at Declinations δ (J2000) = -3°, -6°, -12°, and three slices are located in the Southern Galactic cap at Declinations δ (J2000) = -39°, -42°, -45°. The slices range in length from about five to seven and a half hours in Right Ascension, are approximately $7.5h^{-1}$Mpc thick at $z \approx 0.1$ ($H = 100$ km s^{-1} Mpc^{-1}) and contain a total of 23 697 galaxies with redshifts determined by Schectman *et al.* (1996). SC -45.17 is situated in the δ = -45° slice. This slice has a mean right ascension of $\sim 0^{\mathrm{h}}50^{\mathrm{m}}$ and a range of seven and a half hours in RA. It contains 3753 LCRS galaxies with redshifts.
Einasto *et al.* (2003) used density fields (DF) to identify regions of overdensity in the LCRS. Calculating density fields is done via the following steps:

- ▷ The co-moving distance of every galaxy in the LCRS is calculated using its redshift, with a cosmological model $\Omega_m = 0.3$ and $\Omega_\Lambda = 0.7$. Absolute magnitudes are calculated in the R-band, k-corrected and corrected for absorption due to the Milky Way.

- ▷ Assuming that every galaxy in the visibility window is part of an overdensity, weights are assigned to each of these galaxies. Weights are determined from the Schechter luminosity function (Schechter 1976). A total luminosity for

[7]http://qold.astro.utoronto.ca/~lin/lcrs.html

each galaxy is determined by

$$L_{tot} = L_{obs} W_L,$$

$$L_{obs} = L_{\odot} 10^{0.4(M_{\odot} - M_{obs})}$$

L_{obs} is the observed luminosity of a galaxy with absolute magnitude M and the weight is the ratio of the expected total luminosity in an expected visibility window.

$$W_L = \frac{\int_0^{\infty} L\phi(L)dL}{\int_{L_1}^{L_2} L\phi(L)dL}$$

The visibility window will lie between M_1 and M_2, with L_1 and L_2 given by $L_i = L_{\odot} 10^{0.4(M_{\odot} - M_i)}$.

- ▷ The coordinates and redshift of each galaxy are transformed into a two dimensional cartesian coordinate system. The position of each galaxy is given by an X and Y coordinate, which lies in the plane of the declination slice. The transformation yields a galaxy distribution independent of redshift, and thus free from projection effects.

- ▷ The coordinate system is divided up into a two dimensional grid with a cell size of 1 h^{-1}Mpc.

- ▷ A L_{tot} value is assigned to each galaxy in the transformed coordinates to produce the density field.

- ▷ The density field is smoothed using a Gaussian filter of smoothing length of $10h^{-1}$Mpc. The 10 h^{-1}Mpc smoothing length eliminates small scale irregularities and the 'finger-of-god' effect . To produce a surface density field that has a constant mean, the density is divided by the thickness of the slice at that particular distance. For identifying rich and compact clusters, a density threshold of $\delta = 1.8$ was calculated (Einasto *et al.* 2003). Superclusters having a density above $\delta = 1.8$ and areas greater than 100 $(h^{-1}Mpc)^2$ were included in the LCRS supercluster catalogue.

The supercluster SC -45.17 was chosen as the initial target for the USSS. Because of its richness and its location in the Southern hemisphere at δ = -45°, it is an ideal target for observations using SALT and the IRSF. Its intermediate redshift places it

in the range around $z = 0.15$, the starting point of the USSS. SC -45.17 was found to be one of the richest and more luminous superclusters in the LCRS survey. It contains 53 DF-clusters and has an estimated total luminosity (derived from the sum of the DF-cluster luminosities) of 115 $\times 10^{12}$ $L\odot$. It has a diameter of 71 Mpc and contains one Abell cluster.

We obtained multicolour images ranging from the optical to the NIR of the Abell cluster S0423, which lies at the core of SC -45.17. The NIR pilot fields will furthermore allow an evaluation on how deep the IRSF can probe superclusters at various redshifts (Section 3.2). The *UBVRI* data acquired with the 1m telescope was used to test the possibility of using the 1m photometry to calibrate future SALT data (Section 3.3). In Fig. 3.1 the distribution of all known galaxies in the area of our three target fields are shown. The NIR sources shown are from the Two Micron All Sky Survey extended source (2MASX) online data release (Skrutskie *et al.* 2006). The APM sources are from the U.K. Schmidt B band digitised plates (Maddox *et al.* 1990).

[8]http://nedwww.ipac.caltech.edu/

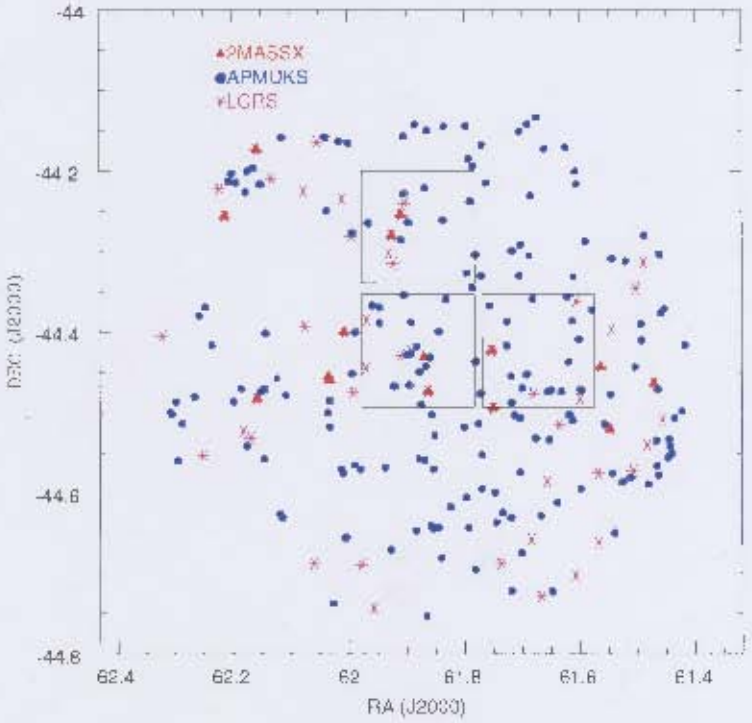

Figure 3.1: Distribution in equatorial coordinates of 244 known sources within a $20'$ radius from the centre of the Abell S0423 cluster as found in the the NASA Extragalactic Database[8]. Triangles indicate 2MASS extended sources; circles APM galaxies; asterisks LCRS galaxies. The large squares represent the observed fields.

3.2 Near Infrared Data Acquisition and Reduction

3.2.1 The Infrared Survey Facility and SIRIUS

The IRSF is located at the Sutherland observatory of the South African Astronomical Observatory. It is a 1.4m telescope equipped with a near infrared (NIR) detector capable of imaging three bands simultaneously. A 7.8′ x 7.8′ field of view and f/10 f-ratio makes it an ideal survey telescope.

The IRSF complements SALT very well. It has similar field of view and extends the wavelength coverage from U to the K_s (320nm to 2160nm). The SIRIUS detector consists of three HgCdTe (HAWAII) detectors and three broad-band filters covering J ($\lambda = 1.25\mu$m), H ($\lambda = 1.65\mu$m) and K_s ($\lambda = 2.15\mu$m). SIRIUS and 2MASS are closely matched in aperture. The IRSF has an f/10 f-ratio compared to the f/13.5 of 2MASS which enables it to observe deeper for the same exposure times. SIRIUS also has ~ 4 times better spatial resolution than 2MASS. See Table 3.1 and Fig. 3.2 for a comparison between 2MASS (Skrutskie *et al.* 2006) and the IRSF (Nagashima *et al.* 2002).

Table 3.1: Characteristics of SIRIUS versus 2MASS.

	SIRIUS	2MASS
Bands	J H K_s	J H K_s
Wavelength	1.25 1.65 2.15	1.25 1.65 2.16
Detector	HgCdTe	HgCdTe
Size (pixels)	1024x1024	256x256
Aperture (m)	1.4	1.3
Pixel Scale (″/pixel)	0.45	2
Field of view	7.8′	8.5′
F-ratio	f/10	f/13.5
Limiting magnitudes	20.6 19.4 19.1	16.5 15.8 15.0
Integration times	900sec	6×1.3sec

3.2.2 Near Infrared Observations in General

Near infrared observations differ from optical observations only through their detectors and observational technique. Both detectors use the same physical mechanism for detecting photons. The main difference lies in their architecture, composition and the way in which charge is handled.

A semiconductor material with a smaller bandgap than that of detectors working in the optical is required to detect NIR photons. HgCdTe (mercury cadmium telluride)

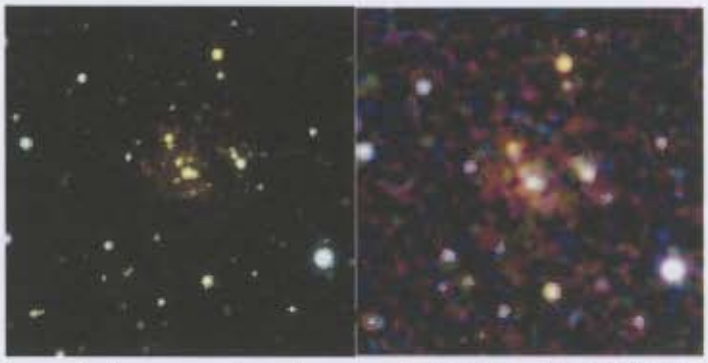

Figure 3.2: A resolution comparison between the IRSF and 2MASS. IRSF image on the left, 2MASS image on the right, field of view is $109'' \times 109''$ [9]. North is up and East is left. Seeing of the IRSF image is $\sim 1''$.

array detectors were initially developed by the Rockwell International Science Centre for the NICMOS instrument on the Hubble Space Telescope. The detector consists of two layers, HgCdTe on a sapphire substrate and a layer of silicone-based material known as the multiplexer (Glass 1999). The HgCdTe functions as the detector while the multiplexer is used for charge handling. The multiplexer is connected to the HgCdTe via indium pillars, this makes it possible for each pixel to be read out individually.

NIR observations are greatly affected by the atmosphere, more so than in the optical. NIR observations are hampered by scattering due to dust, air molecules, aerosols and absorption due to H_2O and CO_2 molecules. Because NIR observations take place at wavelengths where most objects radiate at ambient temperature, saturation of the NIR arrays occurs rapidly. Atmospheric emission and emission from the telescope itself are the main contributors. For $\lambda > 2$ μm, the IR emission is mostly due to airglow because of OH emission (Glass 1999). Variations of the OH emission and sky background takes place on the time scale of minutes. The high sky background can be overcome by reading out the array more frequently, avoiding saturation. The time variability of the atmospheric emission can be corrected by monitoring the sky frequently.

Dithering

The dithering employed by the IRSF is a simple observational technique whereby the telescope physically moves around the central pointing coordinates at a predefined offset called a dithering radius (see Fig. 3.3). This technique allows for the

[9] Image from Michelle Cluver, private correspondence, 2MASXJ08342749-4334516 in the ZOA.

creation of good sky frames to subtract from the data and compensates for bad pixels. Objects will fall on different parts of the detector as the telescope dithers. Object frames are created by first aligning, then combining overlapping image sections. Sky images are created by combining the overlapping image sections without aligning them (see Appendix A.1 for details).

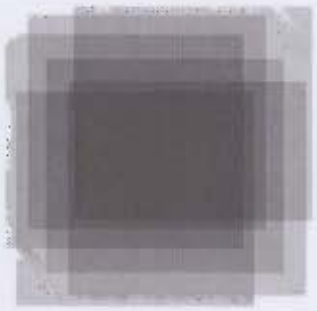

Figure 3.3: An example of dithered images. The dark section in the middle represents a final image. The dithered images typically have exposure times shorter than 20 - 30 sec to avoid saturation. The dithering radius should be large enough that after median combining, extended objects will not appear in the sky image. The larger the dithering radius, the smaller the final image.

3.2.3 IRSF Observations of Abell S0423

Observations took place in February 2006 at the Sutherland observatory of the SAAO. The target was the core of the Abell cluster S0423 plus the adjacent sky fields, (see Fig. 3.4). The total time spent on the target during the observing run was 1h39min40sec.

Persson standard stars were observed each night to calibrate the photometry (Persson *et al.* 1998). Few standard stars were observed each night due to us sharing the observation time with other observers. We could only observe standard stars for the first half of each night. Flat fields were taken at the beginning of each night and the dark frames at the end. To monitor the sky background variability a sky image of the same exposure as the object image was taken after object images. The sky images were taken $\sim 9'$ north and west of the central pointing (see Fig 3.4). Due to the data reduction process, one can reverse the data sets and use the original object images as the sky images and combine the original sky images as object images. A summary of the observations is given in Table 3.2. Individual exposure times for the observations was 20 sec. A $30''$ dithering radius was used.

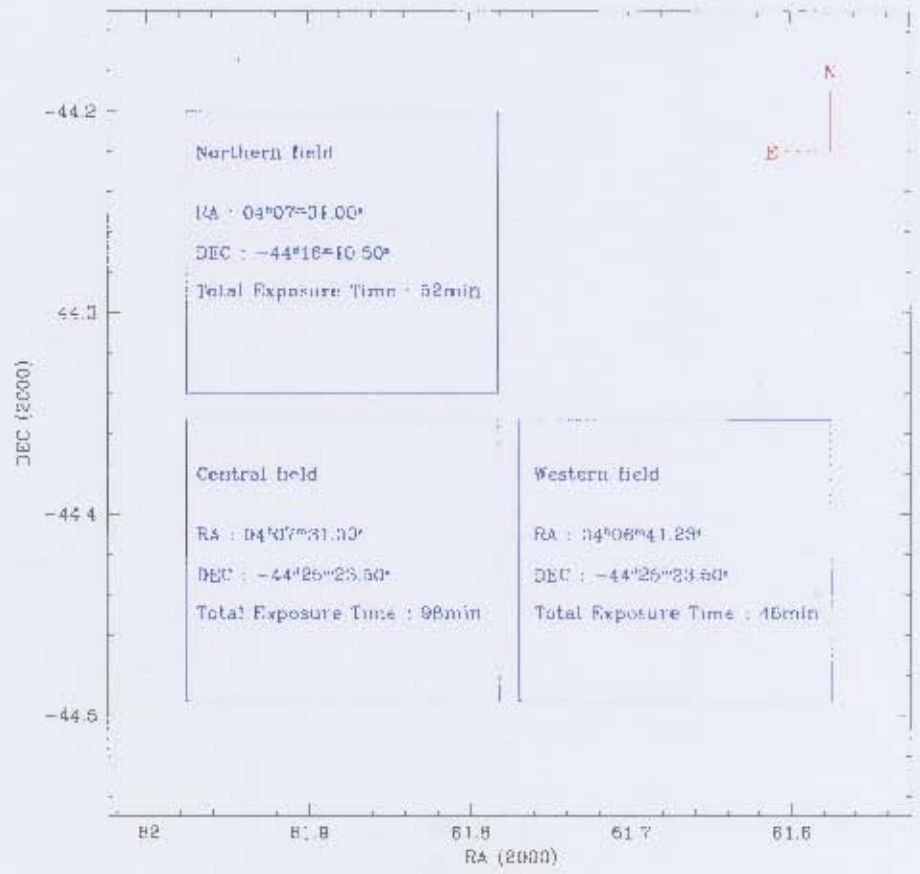

Figure 3.4: Location in equatorial coordinates of the three NIR fields observed. By using the original object image as the sky image, the so-called sky images can be combined as object images.

3.2.4 SIRIUS Data Reduction

The dithering technique employed by the IRSF and the simultaneous J, H and K_s imaging results in a large data set. The data was reduced with the SIRIUS pipeline[10]. It is loaded as a package in IRAF[11] and consists of IRAF scripts to flat field, dark subtract, sky subtract and combine images. The procedure for using the pipeline consists of a few vital steps.

[10] http://optik2.mtk.nao.ac.jp/%7Eyas/pipeline/manual/pipeline020510-e.html

[11] IRAF is distributed by the National Optical Astronomy Observatory, which is operated by the Association of Universities for Research in Astronomy, Inc., under cooperative agreement with the

Table 3.2: IRSF observations. Individual exposure times are 20 sec, with a 30″ dithering radius.

Observation Date	Seeing	Total Integration Time	Ave. Airmass	Sky
14/02/2006	∼1.2″	26min (78 × 20 *sec*)	1.11	North
15/02/2006	∼1″	20min (60 × 20 *sec*)	1.0	West
16/02/2006	∼0.95″	26min (78 × 20 *sec*)	1.11	West
17/02/2006	∼0.85″	26min (78 × 20 *sec*)	1.11	North

Flat fields are created using the `autotwflat` command in the `SIRIUS` package. The `obslog` file contains a list of all the images taken during a night. Editing the `obslog` file by adding suffixes to certain files will change the way the pipeline creates sky and object frames. If the "sky" suffix is added to images in the `obslog` file, the pipeline will distinguish the sky images from separate pointings of the object images. If the "self" suffix is added to the images in the `obslog` file, the pipeline will combine the non-aligned object images for sky images. For our observations, separate sky images were taken. To combine the sky images as object images, the "sky" suffix was added to the original object images and taken out of the sky images filenames.

The pipeline will use the `obslog` file to determine which dithered images need to be combined to produce a final image. The `pipelist` command will go through the `obslog` file and produce a file containing a list of dithered images to combine into a final image. The filename will be the name of the image in the `obslog` file and contain the filenames of the dithered exposures that makes up the final image. The pipeline is set in action with the `pipeline` command, see Appendix A.2.1 for details.

Astrometric Calibration

The three detectors of SIRIUS are not physically aligned. We therefore aligned the three filters before obtaining the astrometric solution to make the transformation only once and then apply it to the two other bands. The images were aligned using the K_s band as reference. We used the IRAF task `geomap` to set up a transformation matrix, and `geotran` to apply the transformation. The astrometric solution was computed using the IRAF task `ccmap` with the 2MASS point source catalogue as reference.

National Science Foundation.

combined images. Only two standard stars were observed which had similar colours so the colour term in the solution was set to zero. Due the lack of range in airmass the extinction coefficient was set to 0.06, 0.05 and 0.05 for the J,H and K_s bands respectively . These values were obtained from P.A. Woudt who observed through a full range of airmasses on the IRSF previously.

Table 3.3: The magnitude zeropoints for each night. The average of the four nights was used as the zeropoints for the combined deep image.

Zeropoints for the four nights.			
Date	J [mag]	H [mag]	K_s [mag]
14/02/2006	20.95±0.015	21.06±0.034	20.32±0.020
15/02/2006	20.94±0.020	21.08±0.020	20.33±0.028
16/02/2006	20.97±0.015	21.13±0.020	20.33±0.022
17/02/2006	20.93±0.015	21.10±0.017	20.32±0.028
Average	20.951±0.033	21.09±0.047	20.32±0.050

Source Detection and Photometry

The software package SExtractor (Source Extractor version 2.4.4; Bertin & Arnouts 1996) is used to obtain the photometry for the galaxies. SExtractor has the ability to handle large images fast. It deblends and extracts overlapping objects, determines magnitudes and distinguishes between point sources and extended sources.

The SExtractor output can be configured by changing the output parameter file. The object's world coordinates system (WCS) coordinates, magnitude and the star/galaxy classification parameter are needed for the data analysis.

The `CLASS_STAR` value is the parameter which discriminates between a star and galaxy through neural networks trained on simulated images. A value of 0 is assigned to extended objects, while 1 is assigned to objects with a good PSF, namely stars. It is up to the user to choose the optimal value between 0 and 1 given the quality of the data set. The star/galaxy classification is dependent on the pixel scale and the seeing FWHM only. It was found that 0.9 is a good value to distinguish between extended objects and stars. Tanaka *et al.* (2001) and Baker *et al.* (2003) used similar values for their star/galaxy classification.

SExtractor determines instrumental magnitudes. To convert these into apparent magnitudes, the magnitude zeropoint is needed, which was obtained from the standard star reductions. Magnitudes are determined by fitting Kron apertures around objects (Kron 1980). Kron aperture magnitudes are determined by fitting a flexible

ellipse around an object and determining the total flux in the elliptical aperture (see for instance Fig. 3.6). A very useful method for determining magnitudes of extended objects; see Appendix A.2.3 for details.

Figure 3.6: An extract of a SExtractor output image. This $\sim 120'' \times 120''$ image shows the Kron apertures drawn on the original K_s band image for the central field. North is up and East is left.

There is no fixed method for extracting magnitudes from an image. It depends on the parameters set by the user. Varying one parameter can change the magnitudes obtained, albeit by a small amount (see for example Fig. 3.7) and the number of sources detected. With such a multitude of parameters, each one able to affect the photometry and the source detection, it is not straight forward to decide on the optimal values of the parameters. By considering the influence the SExtractor parameters have on the photometry and source detection, it was decided to evaluate these parameters for each filter separately. Values for the parameters were chosen on the basis of their effect on Δm, the difference between IRSF and 2MASS magnitudes. The values are listed in Table 3.4.

Figure 3.8 was produced by separating the output catalogue of objects into stars (star/galaxy value > 0.90) and galaxies (star/galaxy value ≤ 0.90) and displaying their coordinates on the original K_s-band image of the central field. This enables a verification of the results by eye.

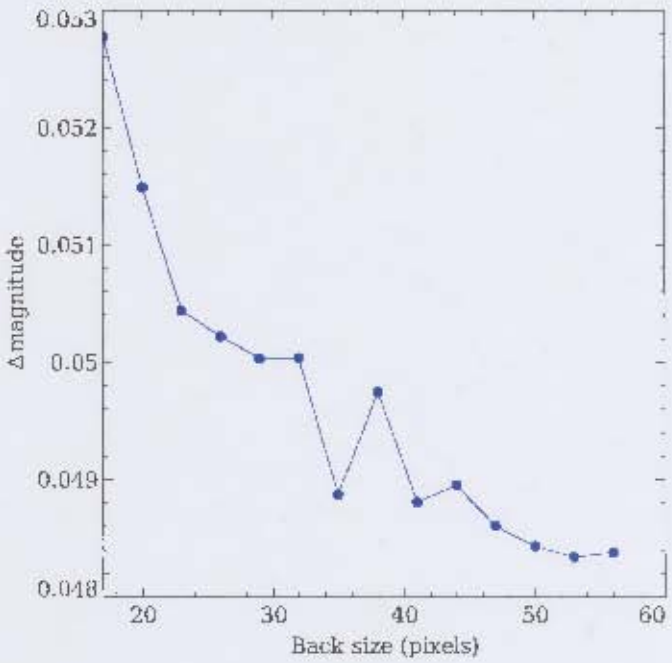

Figure 3.7: An example of the effect on the photometry of changing the BACK SIZE parameter. Δ magnitude is the average of the IRSF point-source magnitude minus the 2MASS point-source magnitude.

Table 3.4: The SExtractor parameters as set for the final magnitude determination. These values gave the best photometric results when compared to 2MASS point source photometry.

Parameter	J	H	K_s
σ detection	2	2	2
σ analysis	2	2	2
Back_size	17	53	32
Back filter size	5	5	4

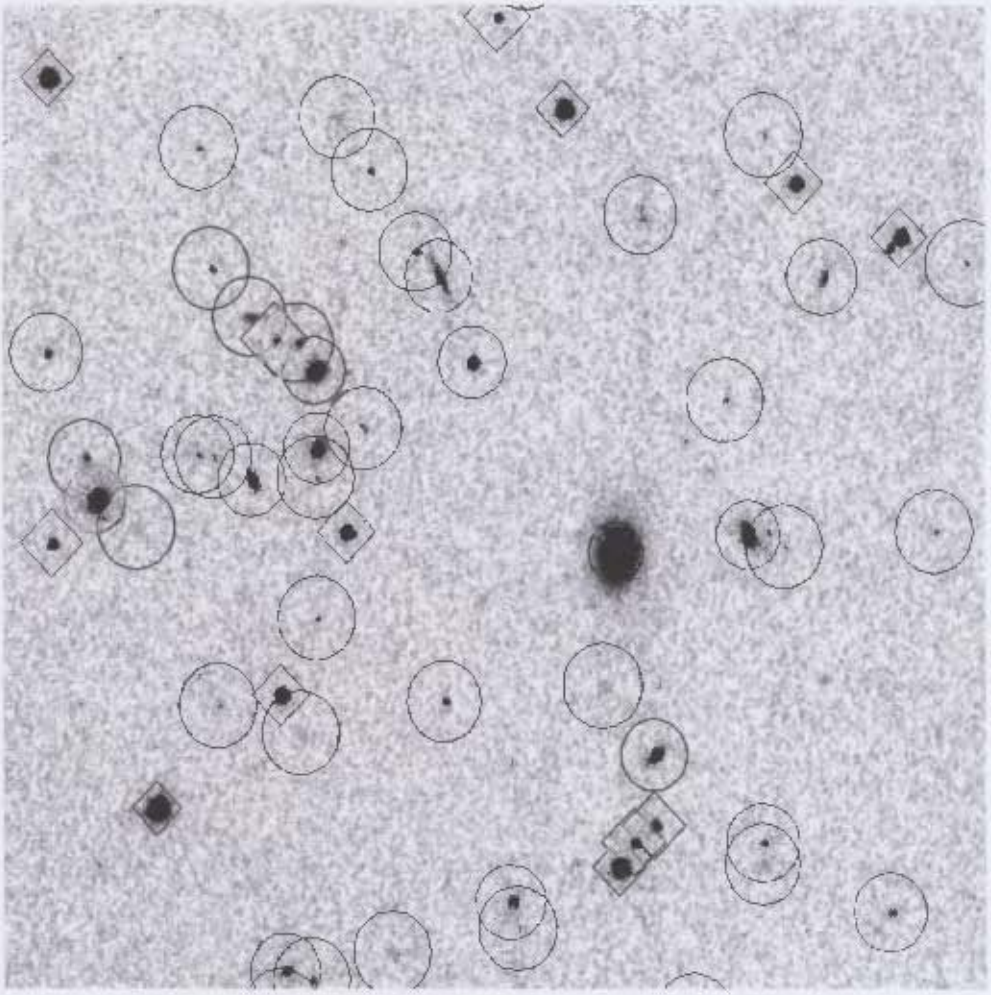

Figure 3.8: Example of star/galaxy classification. ◯ - extended objects; ◇ - point sources. By overlaying the source detection classification on the original image it is possible to gauge, by visual inspection, if the CLASS_STAR value produced realistic results. For this image, galaxies are defined as sources with a CLASS_STAR value of less or equal than 0.9. North is up and East is to the left; image size is $\sim 200'' \times 200''$.

3.3 Optical Data Acquisition and Reduction

3.3.1 The 1m Telescope and SAAO CCD

The 1m telescope is situated at the Sutherland observatory site of the SAAO. It is an equatorially mounted 1m Cassegrain focus telescope. Instrumentation consists of an acquisition/guider camera, filter box and the SAAO CCD. The SAAO CCD is a 1024x1024 pixel liquid nitrogen cooled CCD[12] (see Table 3.5). The Johnson-Cousins *UVBRI* photometric filter system was used to obtain the photometry.

Table 3.5: SAAO CCD characteristics.

Type	Thinned, back-illuminated
Material	Silicone-Telluride
Size (pixels)	1024x1024
Scale (arcsec/pixel)	0.31
Field of view (arcminute)	5.28x5.28

3.3.2 Observations

The aim of the 1m optical observations was to investigate the viability of using the 1m telescope and SAAO CCD to calibrate future SALT deep *UBVRI* photometry. Observations consisted of standard star observations and deep *UBVRI* imaging. Landolt standard stars (Landolt 1992) were observed at regular intervals during each night to calibrate the deep imaging of Abell S0423. The standard star observations enable the characterisation of the photometric response and performance of the SAAO CCD, and correct for atmospheric changes during observations. It is important to fully characterise the SAAO CCD's response in all the desired filters. Very deep photometry was obtained to investigate how deep the 1m could probe the Abell cluster S0423 and whether the data would allow SALT calibrations. All of the observations were done using 2×2 prebinning which corresponds to a pixel scale of $0.62''$/pix. Due to bad weather, we were able to obtain only two nights of photometric data. A summary of the observations is given in Table 3.6.

3.3.3 SAAO CCD Data Reduction

The data reduction consists of two parts: calibrating the standard star photometry and applying the calibrations to the deep photometry. Data reduction was done using various IRAF tasks. `flatcombine` in the `noao` package was used to produce flat

[12] http://www.saao.ac.za/facilities/instrumentation/1m-ccd-camera/tek8-detector/

Table 3.6: 1m observation log.

Date	Target	Exposure Time (sec)					Ave. Seeing
		U	B	V	R	I	
22/11/2005	PG0231+051	300	90	30	20	15	$\sim 1.6'' - 4''$
	SA95	90	20	5	3	3	
	AbellS0423	4×900	2×600	2×300	3×180	1×180	
23/11/2005	PG0231+051	300	90	30	20	15	$\sim 1.9''$
	SA95	90	20	5	3	3	
	AbellS0423	3×900	2×600	3×300	3×180	3×180	

field images for each filter. Each image was flat fielded, overscan bias corrected and bad pixel corrected with `ccdproc`. Object images were combined with `imcombine` in the `images` package.

Standard Star Photometry

To guarantee a good standard star solution the standard stars were observed in a range of airmass, colours and magnitude. Due to the moderately large field of view of the 1m telescope it was possible to observe at least four Landolt standard stars at once. This provided a larger range in colours and magnitude. Aperture-corrected photometry was performed on the standard stars and deep images due to the varying seeing (see Table 3.6). For the NIR photometry, aperture-corrected photometry would not have produced significantly different photometry due to the good and stable seeing during these observations. The aperture-corrected photometry was performed using `phot` in the `daophot` package with thirteen different size apertures. The total amount of flux in an aperture is determined by adding up the observed flux per pixel that lies a radial distance from the centroid of the star. Subtracting the total expected sky brightness from the total flux yields an estimate of the flux from the star alone. By making the aperture large enough it was ensured that all the light falls within a given aperture. However, the noise of the measurements increases rapidly with increasing aperture radius (Stetson 1990). Readout noise, noise due the diffuse sky background and flat field errors on small scales, all contribute to the total amount of noise. These errors grow as the square-root of the number of pixels, i.e. linearly with aperture size (Howell 1989). This results in a maximum signal-to-noise measurement at some intermediate aperture size and therefore requires the need for aperture correction, especially in the presence of bad seeing. To determine the aperture correction, an analytical model stellar profile was fitted to the observed

fluxes of each aperture. The aperture corrections were determined with the mkapfile task in the photcal package. Figure 3.9 shows the interactive output from mkapfile. The solid line is the stellar profile fit.

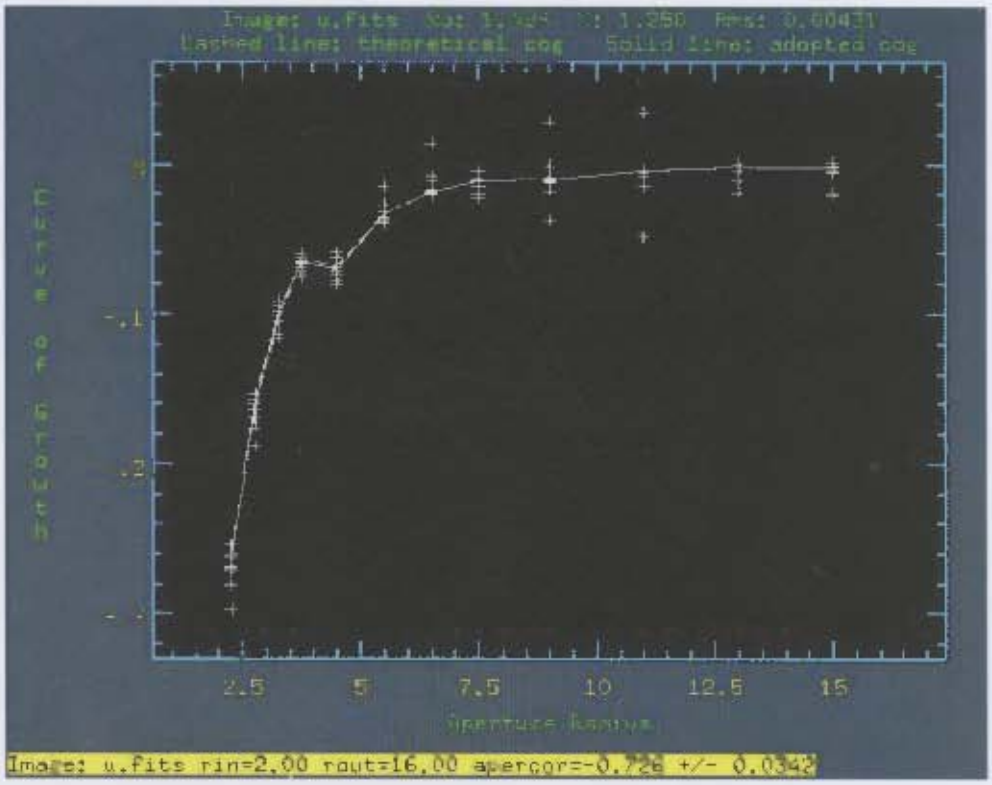

Figure 3.9: Example of a stellar profile fit of a standard star in the U band. The interactive output from mkapfile enables the user to discard bad points in the data to improve the model stellar profile fit. The values on the y-axis indicate the difference between the extrapolated total aperture magnitude from the model stellar profile fit and the magnitude determined with a particular size aperture.

The final output from `mkapfile` is a list of apertures with the corrections for each aperture. This correction denotes the offset between the total aperture magnitude determined from the stellar profile fit (integration over all apertures) and the aperture magnitude of the particular aperture, see Table 3.7.

Table 3.7: Example of aperture correction values obtained from U-band deep photometry reductions. Aperture radii were converted from pixels to arcseconds by multiplying the aperture size in pixels with the prebinning factor (2) and pixel scale (0.31″/pixel).

Aperture radius (arcsec)	Aperture correction (mag)
1.24	-0.726
1.55	-0.464
1.86	-0.307
2.17	-0.210
2.48	-0.145
3.10	-0.076
3.72	-0.044
4.34	-0.027
4.96	-0.017
6.20	-0.007
7.44	-0.003
8.68	-0.001

The aperture-correction has to be applied to the instrumental magnitude derived from `phot` to determine the total instrumental magnitude of the stars. Most of the stellar flux ($\sim$ 76%) will be contained within the FWHM of a Gaussian fit of the light distribution. Because the FWHM is dependent on the seeing, the seeing has to be taken into consideration when deciding upon an aperture, while bearing in-mind that the aperture has to be small enough to keep the noise to a minimum.

Figure 3.10 shows that a 4 pixel (2.48″) aperture radius will include most of the stellar flux. For such an aperture the aperture correction will be small and the noise will be sufficiently low to not play a significant role. `mknobsfile` will read through the output produced by `phot` and apply the aperture correction for the chosen aperture to the magnitude of the particular aperture. `mknobsfile` produces a list of objects and their aperture corrected instrumental magnitude. With the known apparent magnitudes of the Landolt standard stars, the instrumental magnitudes can now be transformed to apparent magnitudes with the `fitparams` task. `fitparams`

makes use of the interactive non-linear least squares fitting package (INLFIT) to solve the transformation equations which are of the general form:

$$imag = m + mzp + c1 \times X + c2 \times (mcol),$$

- $imag$ - instrumental magnitude
- m - apparent magnitude
- mzp - magnitude zeropoint
- $c1$ - extinction coefficient
- X - airmass
- $c2$ - colour coefficient
- $mcol$ - colour term

While solving for the standard star solution, $c1$ is kept fixed due to the lack in observations during the middle of the night. Thus, only the magnitude zeropoint and colour term can be derived. The extinction coefficients are typical values for each filter. The instrumental magnitudes of the object images can be calibrated with the magnitude offsets. Table 3.8 shows the zeropoints determined for each filter for the two observing nights.

Table 3.8: Magnitude zeropoints (mzp) for each filter. The typical extinction coefficients ($c1$) for each filter were fixed to obtain a good solution for the zeropoint magnitude fit. The colour coefficients ($c2$) were determined using the apparent colours shown in the table.

	22/11/2005					23/11/2005				
	mzp	$c1$	$c2$	$mcol$		mzp	$c1$	$c2$	$mcol$	
U	19.677±0.008	0.50	-0.086±0.010	U	B	19.682±0.030	0.50	-0.128±0.044	U	B
B	22.386±0.008	0.30	0.065±0.009	B	V	22.299±0.030	0.30	0.020±0.040	$B-V$	
V	22.664±0.006	0.15	-0.003±0.010	V	R	22.597±0.004	0.15	-0.032±0.008	$V-R$	
R	22.610±0.008	0.15	0.021±0.013	V	R	22.596±0.030	0.15	-0.017±0.038	V	R
I	22.208±0.020	0.15	-0.045±0.033	$R-I$		22.206±0.009	0.15	-0.015±0.014	R	I

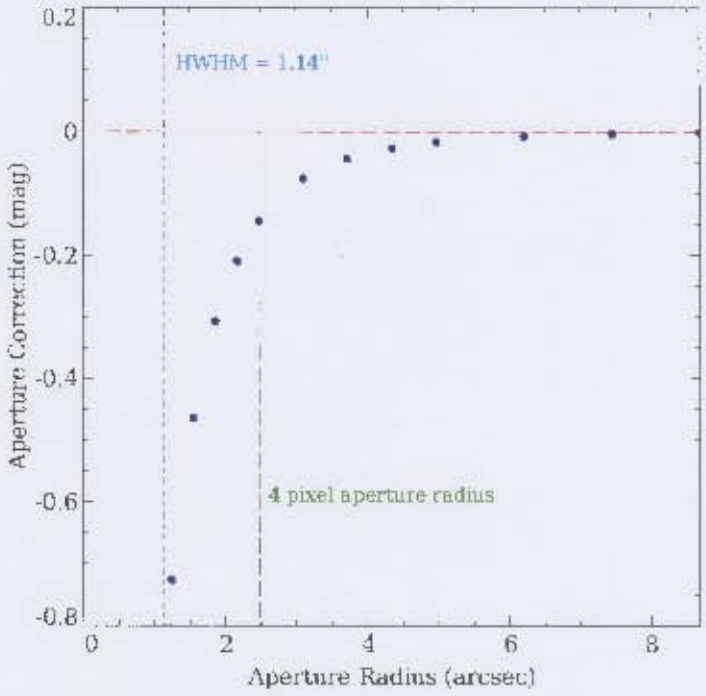

Figure 3.10: Example of aperture corrections. The dotted line represents the Half Width Half Maximum (1.14″) of one of the standard stars. The seeing was 2.28″. The dashed vertical line represents the 4 pixel aperture radius (2.48″) used for determining the aperture magnitude. The dashed horizontal line shows where the difference between the aperture magnitude and the total magnitude is zero.

Deep Field Photometry

The applied data reduction procedure for the deep images were the same as for the standard star data reduction. Aperture corrected magnitudes were determined for stars in the deep field. The magnitude offsets determined from the standard stars were applied to the deep images to therewith obtain the apparent magnitudes of the stars in the deep field.

Chapter 4

Results and Discussion

4.1 Accuracy of the IRSF photometry

4.1.1 Photometric Comparison with 2MASS

Investigating the accuracy of the IRSF photometry is not only important for the reproducibility of this work, but also relevant for future work. To this end, we compare the magnitudes of our point sources to the magnitudes of corresponding point sources in the 2MASS Point Source Catalogue (Skrutskie *et al.* 2006). Transformation between the photometric systems is not needed as 2MASS uses the same filter system as the IRSF. Only 2MASS point sources brighter than the completeness limit and with 'AAA' quality photometry were chosen for this comparison. 'AAA' refers to sources being detected in all three bands, having $\leq$ 10% measurement uncertainties and meeting the Level 1 Requirements of the 2MASS survey[13]. 2MASS magnitudes refer to either an 8″ aperture magnitude or aperture-corrected magnitude, depending on the flux of the object. IRSF point source magnitudes are also determined using an 8″ aperture. Due to the long exposure time, IRSF point sources brighter than 10^{m} are saturated. Therefore we only use IRSF point sources fainter than 10^{m} for the comparison. The mean magnitude offset ($< \Delta m >$ = IRSF − 2MASS) was derived for each field and filter separately. The standard deviation of the mean (σ) and the average error in magnitude difference ($< \varepsilon_{m} >$) were determined to quantify the results. The mean magnitude offset (Δm) derived for each field, standard deviation of the mean (σ) and average error in magnitude difference ($< \varepsilon_{m} >$) are shown in Table 4.1.

Because of small number statistics, the sources from the three fields are combined to determine the mean magnitude offsets in each filter. This can be done because the magnitudes from each filter are derived with the same SExtractor parameters. Figure

[13]See http://www.ipac.caltech.edu/2mass/releases/allsky/doc/requirements.html and Skrutskie *et al.* (2006).

Table 4.1: Magnitude offsets derived for stars in the three deep fields individually and combined.

Filter	$<\Delta$m$>$ [mag]	σ [mag]	$<\varepsilon_{\rm m}>$ [mag]	**Stars**
	Central Field			
J	0.003	0.034	0.033	20
H	0.029	0.040	0.040	20
K_s	0.018	0.040	0.040	14
	Northern Field			
J	−0.016	0.040	0.035	11
H	−0.003	0.052	0.039	12
K_s	0.047	0.024	0.040	8
	Western Field			
J	-0.010	0.035	0.035	10
H	0.013	0.048	0.041	10
K_s	0.044	0.043	0.041	5
	Combined fields			
J	-0.006	0.036	0.034	31
H	0.015	0.046	0.040	32
K_s	0.040	0.038	0.040	27

4.1 displays the photometric differences between the IRSF and 2MASS point sources for each filter. The means for each filter are indicated with the solid horizontal lines and the dotted horizontal lines represents the standard deviation. The vertical dotted lines show the 2MASS point source completeness limit in each filter (Skrutskie *et al.* 2006). Considering standard errors of individual points, it is found that 94%, 97% and 100% of sources in the J, H and K_s bands respectively, lie within one sigma (σ) of the mean.

As can be seen from Fig. 4.1, the J band comparison has the smallest offsets, and slight offsets are visible in the H and K_s bands. This was also found by Cluver (2005), who used the IRSF to observe galaxy cluster candidates. These offsets might be due to small differences in the filter systems. The 2MASS K_s filter is centred around 2.16μm and has a slightly different throughput (Fig. 4.2), compared to the SIRIUS K_s filter centred at 2.15μm.

The agreement between the IRSF and 2MASS magnitudes are good within the errors. This is reassuring since we plan to calibrate IRSF data directly using 2MASS photometry in future. This will reduce observing and data reduction time signifi-

cantly.

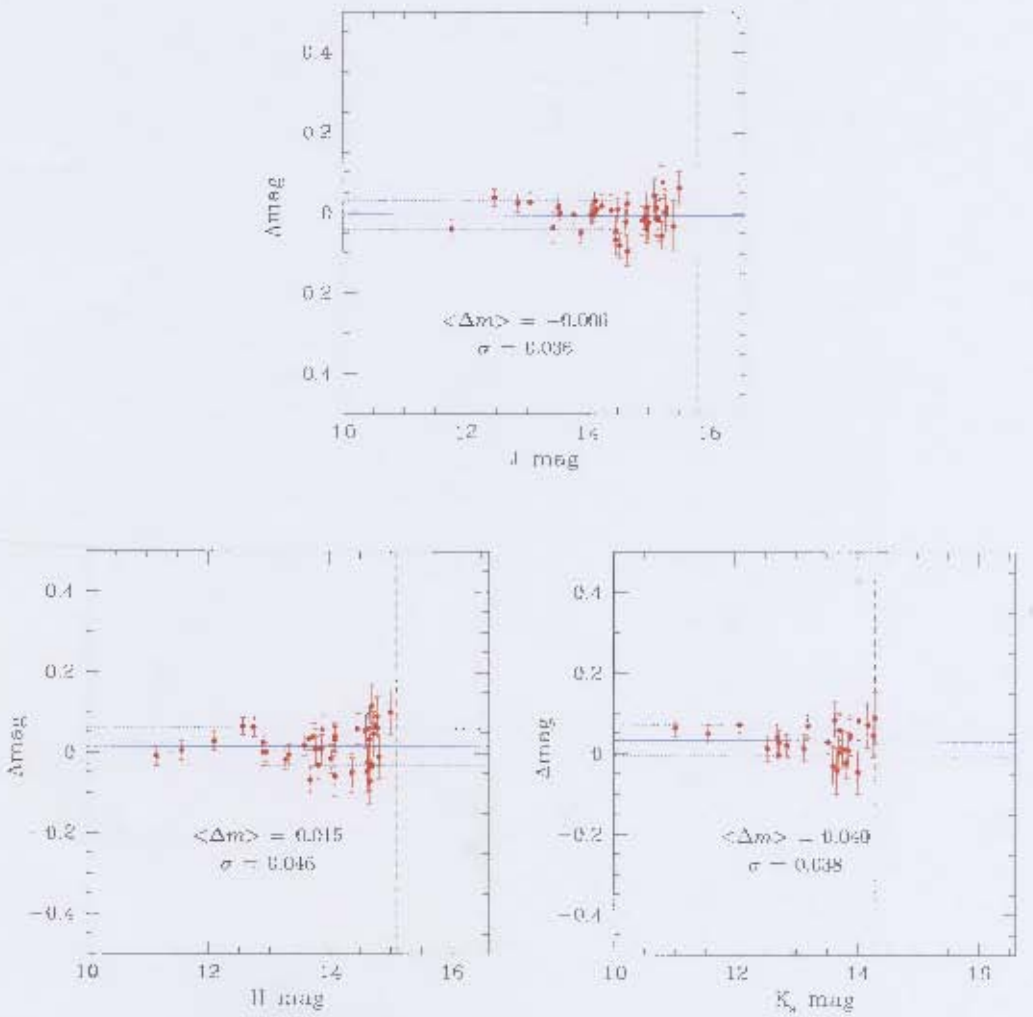

Figure 4.1: Magnitude offsets (Δm = IRSF mag − 2MASS mag) for sources in the three fields combined. The solid line represents the mean magnitude difference; dotted lines indicate the standard deviation and the dashed vertical line shows the 2MASS completeness limit.

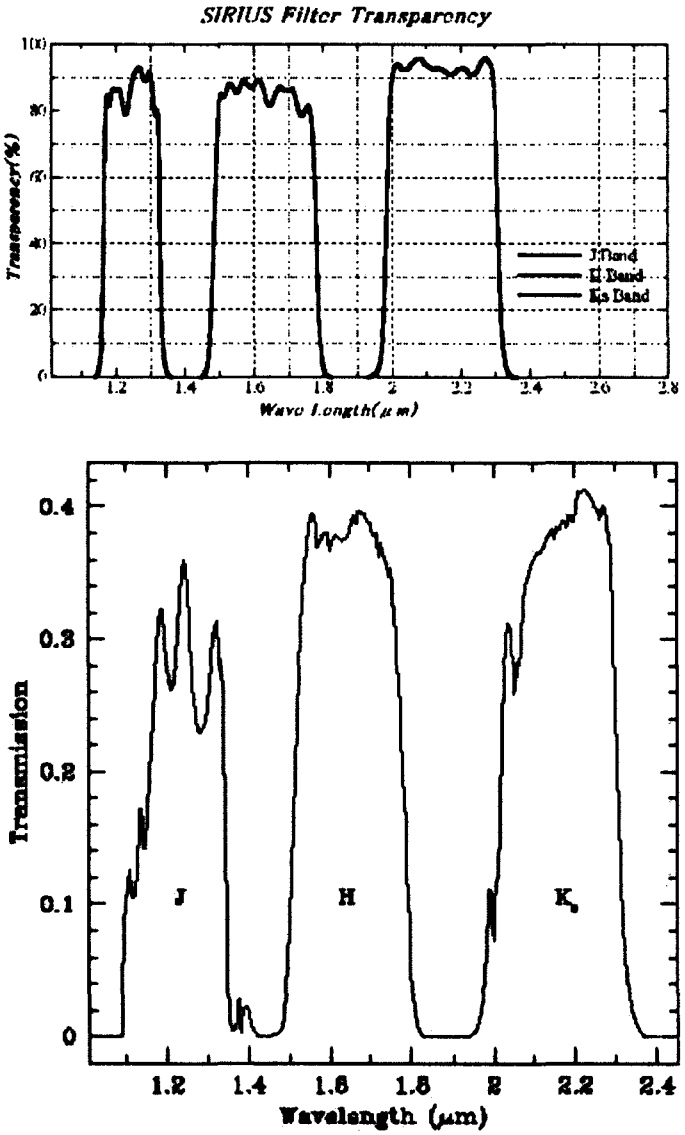

Figure 4.2: The top graph shows the SIRIUS filter transmission taken from http://www.z.phys.nagoya-u.ac.jp/~irsf/sirius/about/spec.html. The bottom graph shows the 2MASS filter transmission taken from Skrutskie *et al.* (2006). Although the differences in the filter systems cannot be quantified, there are obvious differences in the filters visible from the graphs.

4.1.2 Completeness Limits of the Extended Sources

Before investigating the properties of the galaxy sample, it is necessary to determine magnitude completeness limits in each band respectively, and because the exposure times are different for the three fields, also determining common completeness limits for the three fields.

The completeness limits were estimated using two different methods. The first method is based on the well known $\log N/\log S$ relation. Glazebrook *et al.* (1994) found that the increase of $\log N_{gal}(\mathrm{mag}^{-1}\ \mathrm{deg}^{-2})$ with K-mag for a galaxy sample complete within $14^{\mathrm{m}} < K < 20^{\mathrm{m}}$, has a slope of 0.45 at $K = 17$ mag, allowing the slope to vary between 0.3 and 0.6 to account for errors in magnitudes. Jarrett (2004) used the Glazebrook *et al.* (1994) results to verify the completeness for the 2MASS Extended Source Catalogue also derived using the $\log N/\log S$ method.

To estimate the completeness limit for the IRSF extended source photometry, $\log N_{gal}(\mathrm{mag}^{-1}\ \mathrm{deg}^{-2})$ per 0.5 mag bin was determined and a least squares line fitted. Due to the small number of sources per magnitude bin, the straight line is only fitted to points that give a slope between 0.3 and 0.6. The magnitude where $\log N_{gal}(\mathrm{mag}^{-1}\ \mathrm{deg}^{-2})$ deviates from the linear relation is used to define the completeness limit. Figure 4.3 shows the $\log N/\log S$ plot for the J band of the Central Field.

The second method is described in Garilli *et al.* (1999) and Andreon *et al.* (2000) (henceforth referred to as the maximum central surface brightness (MCSB) method). They estimate the completeness limit to be the magnitude at which galaxies are no longer detected due to the galaxies having a lower surface brightness than the detection threshold. To derive the completeness limit, a least square line is fitted to the data in a magnitude vs. maximum central surface brightness plot (Fig. 4.4). The standard deviation (σ) of the straight line fit is determined. The completeness limit is determined at the magnitude where the limiting maximum central surface brightness (vertical dotted line) intersects the (-1σ) line (lower dashed line). The completeness limits derived for each field and filter using the two methods are listed in Table 4.2. The sources in the Northern and Western fields were combined to reduce undersampling effects; this was possible because the total integration times for the two fields differed by only 6 min.

Both methods produce similar results (Table 4.2), but the $\log N/\log S$ method does have some caveats. The linear fit is affected by bin size and number of sources per magnitude interval. In Fig. 4.3 one can see the effect of undersampling of bright sources in the Central Field. Undersampled magnitude bins have to be ignored when performing the straight line fit in order to keep the slope as near as possible to the expected slope. By comparison, the MCSB method is more robust and easy to incorporate into data analysis software.

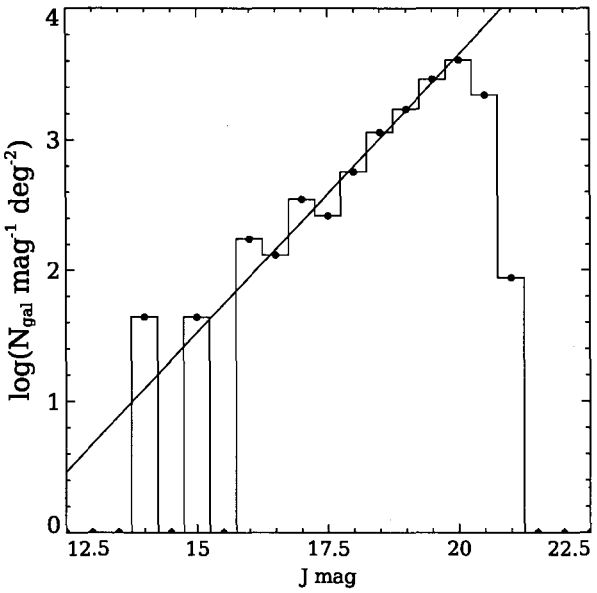

Figure 4.3: The $\log N/\log S$ for the J band of the Central Field. The slope of the fitted line is 0.42, which lies in the interval defined by Glazebrook *et al.* (1994). Undersampling at $J < 16^{\mathrm{m}}$ is evident from the plot.

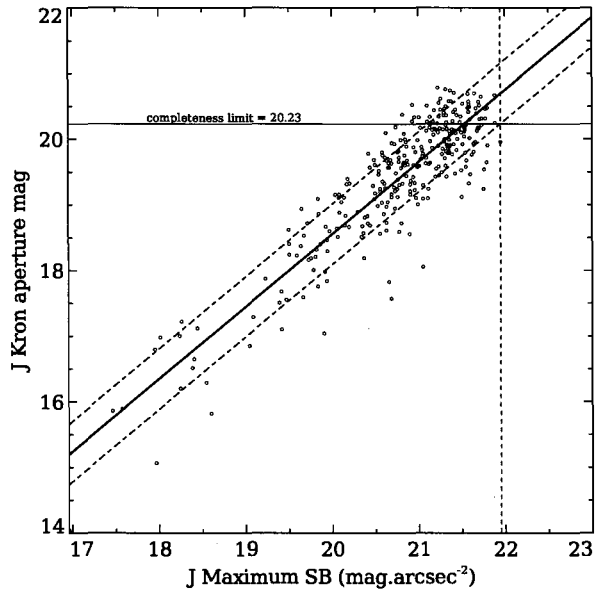

Figure 4.4: J band maximum central surface brightness vs. J Kron aperture magnitude of galaxies found in the Central Field. The solid horizontal line represents the estimated completeness limit.

Due to the longer exposure time of the Central Field, we expect it to have a fainter completeness limit than the Northern and Western Field combined. From our data we find that a doubling in exposure time will produce a $\sim$ 0.5 mag fainter completeness limit in the K_s band (see Table 4.2).

A comparison was made with Skelton (2007), who determined the K_s band luminosity function of the Norma cluster. She found the MCSB completeness limit in the K_s band to be 15.74 mag for a 600 s total integration time. Comparing that to the 18.30 mag completeness limit we derived from a 5880 s total integration time shows that a 10 times longer exposure time produces a $\sim$ 2.5 magnitudes fainter completeness limit. Thus, a doubling in integration time will produce a $\sim$ 0.5 mag fainter completeness limit, which is what we found previously. Having confirmed that the MCSB method predicts consistent completeness limits, the MCSB completeness limits will be used for all further analysis.

Table 4.2: Completeness limits for each filter from the log$N$/log$S$ and MCSB methods. Due to small number statistics, the Northern and Western fields sources were combined.

	Central Field		North/West fields	
	log$N$ [mag]	MCSB [mag]	log$N$ [mag]	MCSB [mag]
J	20.0	20.23	19.5	20.06
H	19.5	19.90	19.5	19.92
K_s	18.0	18.30	17.5	17.86

The magnitude distributions are shown in Fig. 4.5 in 0.5-mag intervals . Figure 4.6 shows the on-sky distribution of galaxies with $J < 20.06^{\mathrm{m}}$ completeness limit (see Table 4.2).

The Northern and Western Fields do not show any structure in the on-sky distribution. The galaxy distribution in the Central Field shows a concentration in the centre of the field, as one would expect for a galaxy cluster.

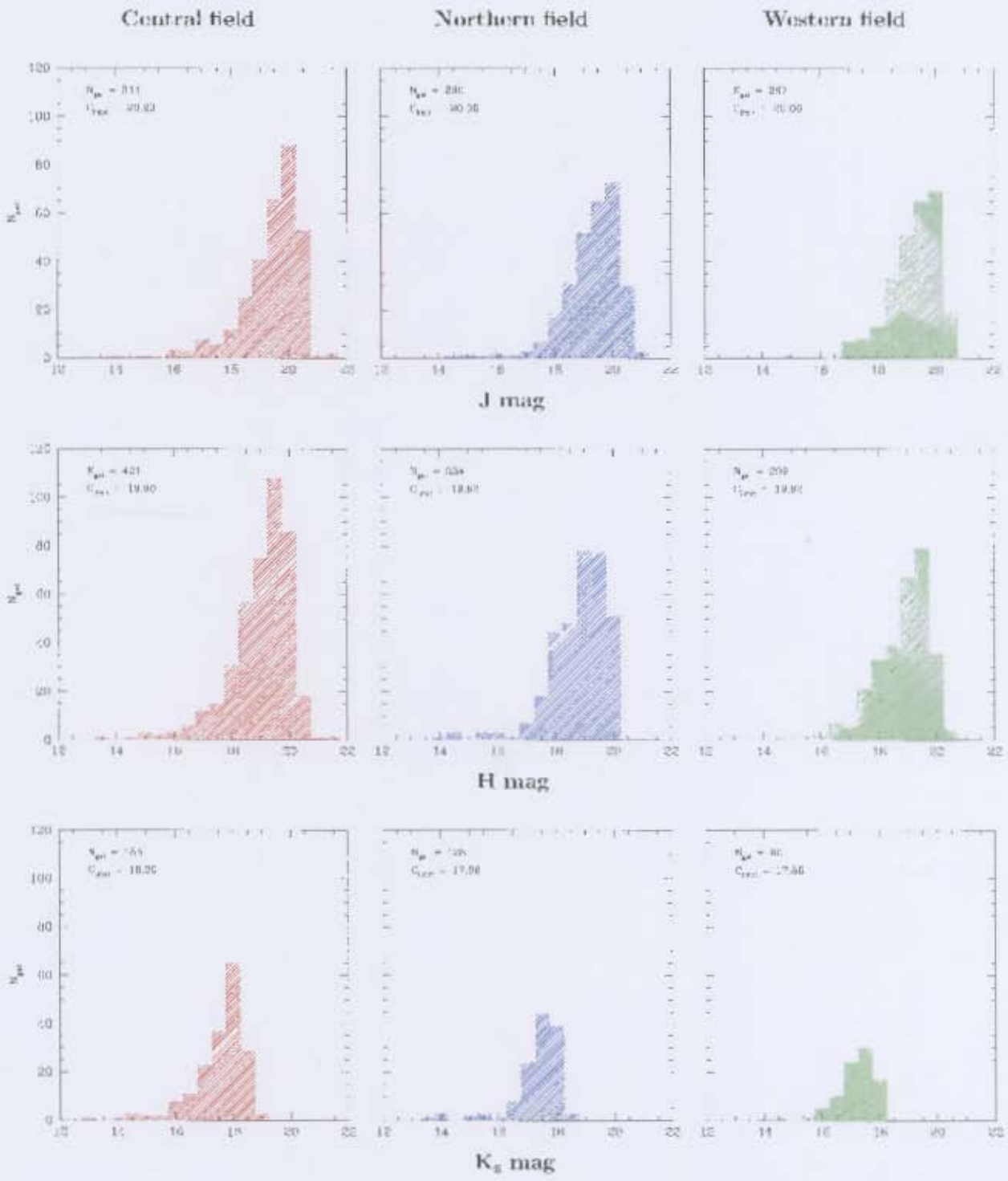

Figure 4.5: Magnitude distribution in 0.5 mag bins for the three fields (left to right) and the J, H and K_s bands (top to bottom).

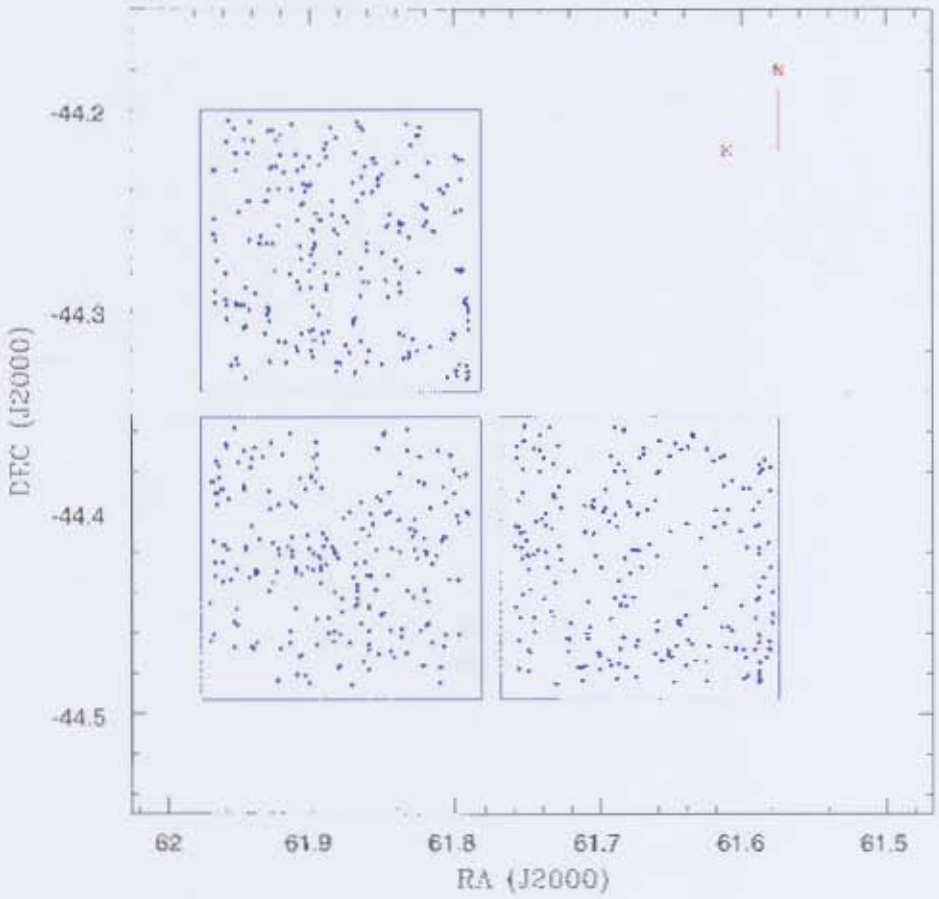

Figure 4.6: On-sky distribution in equatorial coordinates of sources brighter than the J band completeness limit of 20.06^{m}.

4.2 Near Infrared Galaxy Photometry Analysis

4.2.1 Intrinsic Near Infrared Galaxy Colours

Near infrared galaxy colours are not sensitive to star formation, making it a poor indicator of galaxy morphology and therefore, any evolutionary or transformation effects. This can be seen in Table 4.3 which shows the rest frame $(J - K_s)^0$ colour for different morphological types (McCall 2004). The small range in colour makes the NIR colours unsuitable for studying galaxy morphology; it is not possible to distinguish between different morphological types based on NIR colours alone.

Table 4.3: The intrinsic $(J - K_s)^0$ colour of galaxies of different morphological type.

Galaxy Type	$(J - K_s)^0$ [mag]
E	0.89
Sab	0.90
Sbc	0.90
Scd	1.00
Im	0.83

4.2.2 k-correction and Apparent Near Infrared Galaxy Colours

Due to the expansion of the universe, the recession velocity (redshift) of a galaxy increases with distance and so does the shift in the peak of the spectral energy distribution. To compensate for the effect redshift has on the spectral energy distribution of galaxies, k-corrections has to be applied. The k-correction depends on the morphology of a galaxy, its redshift and filter used for the observations. It is vital to apply k-corrections when calculating absolute magnitudes or determining intrinsic colours for redshifted galaxies.

With the goal to extract distance information from the 2MASS data, Jarrett (2004) found a linear relation between the NIR colours of nearby galaxies ($z \leq 0.2$) and their independently measured redshift. Figure 7 in Jarrett (2004) shows the linear relation and the associated errors, it suggests that NIR photometry could provide some crude indication of distance for galaxies in the local universe ($z \leq 0.15$), see Fig. 7 in Jarrett (2004).

With this in mind, the York Extinction Solver (YES)[14] (McCall 2004) was used to

provide an estimate for the $J - K_s$ colour expected for different galaxy morphologies at $z = 0.138$ (the redshift of Abell S0423). The Galactic extinction was approximated by zero (NED gives a selective extinction E(B-V) = 0.016 for Abell S0423) and the 2MASS filter system was used to determine the colours. The expected $J - K_s$ colours are shown in Table 4.4.

Table 4.4: $(J - K_s)^{\rm obs}_{z=0.138}$ colour and k-corrections.

Galaxy Type	$(J - K_s)^{\rm obs}_{z=0.138}$ [mag]	k-correction [mag]
E	1.14	0.25
Sab	1.15	0.25
Sbc	1.24	0.34
Scd	1.18	0.18
Im	1.08	0.25

Table 4.4 shows that we expect galaxies at a redshift of $z = 0.138$ to lie within the colours range of $\sim 1.08 \leq J - K_s \leq \sim 1.24$, with a small range in k-correction. If we include the average error in colour (0.06 mag), we can determine the boundaries of the likely colour range of galaxies, $\sim 1 \leq J - K_s \leq \sim 1.3$, that we expect galaxies at $z = 0.138$ to be in. Figure 4.7 shows the $(J - K_s)^{\rm obs}$ colour derived for the galaxies in the three observed fields. The expected colour range is indicated by dotted lines. For the comparison between the three fields, a completeness limit of 17.86 mag in the K_s band was used.

The relation found by Jarrett (2004) was used as a comparison for the expected values estimated by the York Extinction Solver. An extrapolation to higher redshift of the linear fit made by Jarrett (2004) is shown in Fig. 4.8 (dashed line). On the same graph, the $(J - K_s)^{\rm obs}$ colour for galaxies with different morphologies is shown as a function of redshift. As the k-correction becomes more significant at higher redshifts, the estimated colours using the York Extinction Solver start to deviate from the Jarrett line beyond $z \sim 0.15$. Thus, for objects at redshifts $z \geq 0.15$, one cannot be sure if the observed colours are due to morphology or redshift. Consider for example a galaxy with $(J - K_s)^{\rm obs} = 1.5$. This could either be a Sbc galaxy at $z = 0.28$ or it could be an E galaxy at $z = 0.68$. Therefore, it would seem that it is only possible to determine a very rough distance estimate for objects in the local universe ($z \leq 0.15$) using NIR colours. For objects with redshifts higher than $z \sim 0.15$, the k-correction becomes too large and deviates for different galaxy morphologies (read: different spectral energy distribution) and it is no longer

[14] http://www1.cadc-ccda.hia-iha.nrc-cnrc.gc.ca/community/YorkExtinctionSolver/index.html

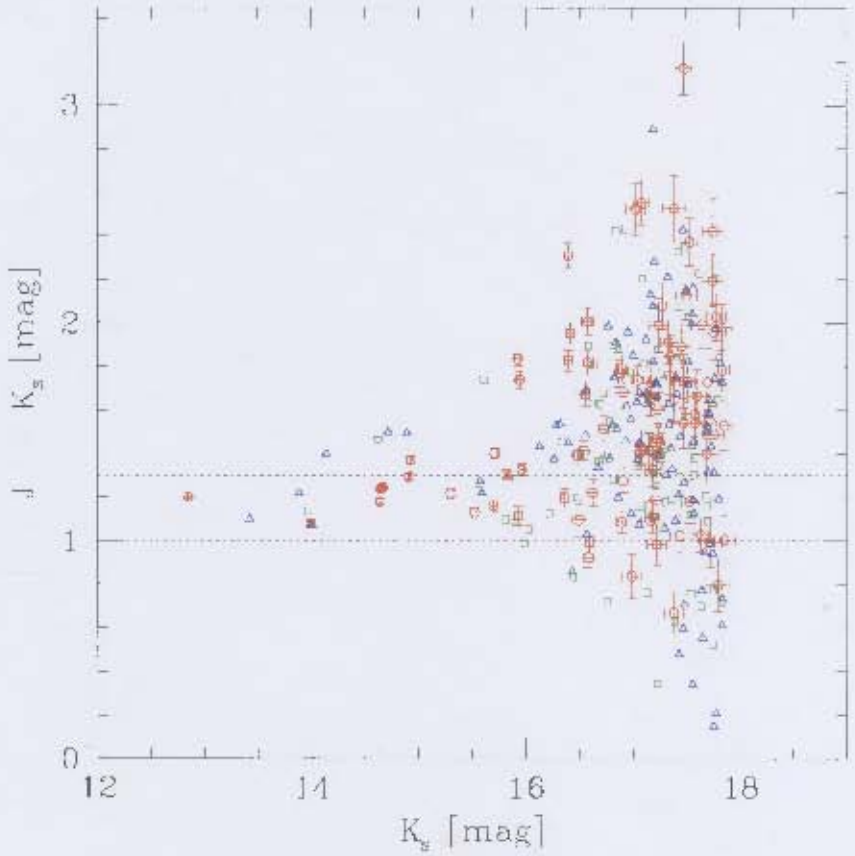

Figure 4.7: $(J-K_s)^{\rm obs}$ colour vs $(K_s)^{\rm obs}$ plot. The open circles are Central Field sources, triangles represent Northern Field sources; squares show Western Field sources. The errors in $(J-K_s)^{\rm obs}$ colour and $(K_s)^{\rm obs}$ magnitude are shown for the Central Field; for galaxies brighter that $15^{\rm th}$ mag, the errors are smaller than the plotting symbols. The dotted lines indicate the colour range predicted by the York Extinction Solver that we would expect galaxies at a redshift of $z = 0.138$ to have.

possible to use the $(J-K_s)^{\rm obs}$ colour to estimate distances.

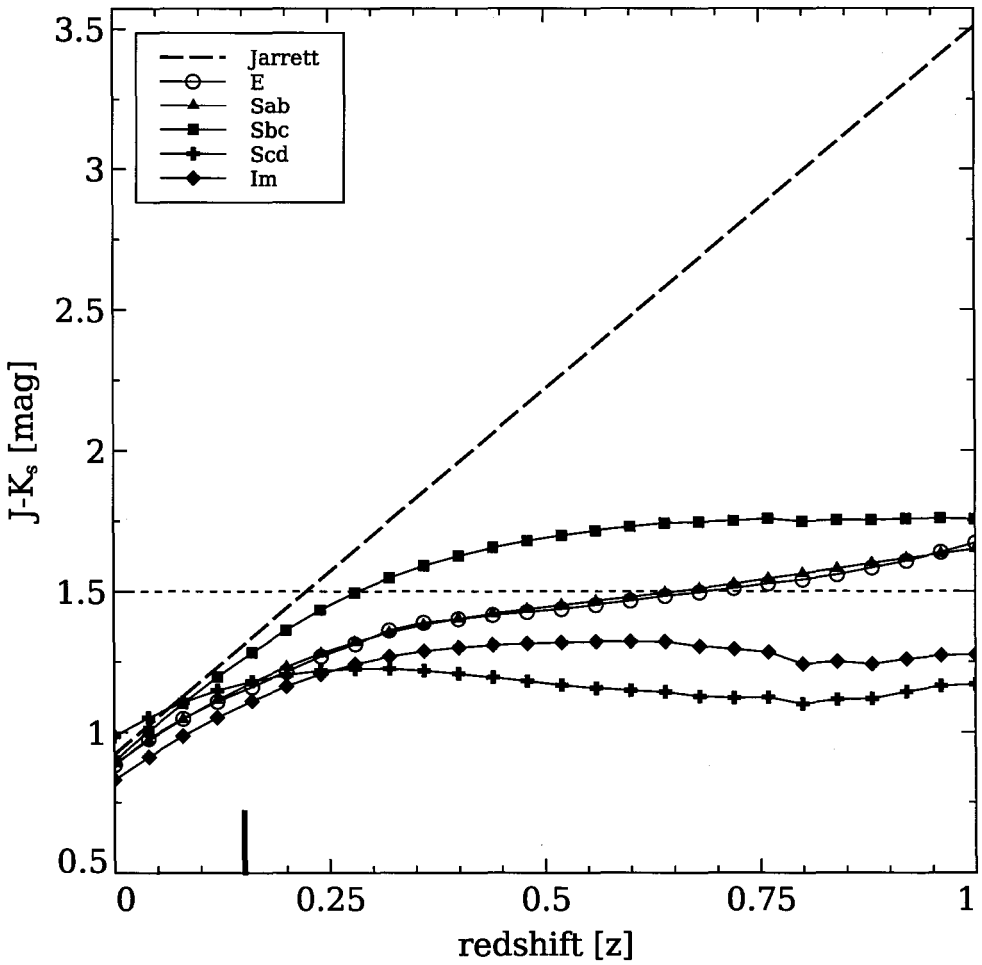

Figure 4.8: $(J - K_s)^{\rm obs}$ colour vs z plot. The dashed line is the extrapolated linear relation derived by Jarrett (2004) for $(J - K_s)^{\rm obs}$ colour vs. redshift. The various curves are the predicted $(J - K_s)^{\rm obs}$ colours of different morphological types with increasing redshift. Estimating distances from $(J - K_s)^{\rm obs}$ colours for redshifts $z \geq 0.15$ is not possible. The vertical solid line indicates the redshift of Abell S0423.

4.2.3 Morphological Information From NIR Photometry

Using Results rom the 2MASS Large Galaxy Atlas

As stated earlier, the NIR colours are poor indicators of galaxy morphology. This is not to say that NIR photometry cannot be used to provide morphological information. Jarrett *et al.* (2003) have found (for galaxies in the 2MASS Large Galaxy Atlas (LGA)) a relation between the mean central surface brightness (SB) and Hubble type (see Fig. 4.9). Early type galaxies are more compact and consequently have a higher mean central SB compared to late type galaxies. In Fig. 4.9 one can see the decrease in mean central surface brightness as a function of Hubble type. The mean central SB of the LGA is defined as a 10″ diameter (2.5 pixel radius) aperture magnitude (with units of mag and not mag/arcsec^2). For their nearby galaxy sample this size aperture samples only the central parts of galaxies.

If we use the same number of pixels to sample the mean central SB for our galaxies, it corresponds to a 2.25″ diameter aperture. The distance scale at $z = 0.138$ is 2.35 kpc/arcsec; so a 2.25″ aperture corresponds to a $\sim$ 5.3 kpc diameter. This is less than $\sim$ 10 kpc, the smallest expected diameter of galaxies, like irregulars, at that redshift. The method will become more inaccurate for smaller galaxies (and at larger distances). Due to the fixed aperture, an increasingly larger fraction of the galaxy will be sampled with increasing distance and smaller angular scale, producing a mean central SB brighter than expected for that galaxy's morphological type.

To ensure that the aperture we chose produces results that match the predicted morphology by Jarrett *et al.* (2003), we determined the mean central SB for two of the brighter galaxies in the Central Field which could still be classified using visual inspection. These galaxies are shown in Fig. 3.6. They are the central elliptical and the edge-on spiral to the upper left of the image. The mean central SB obtained for these two galaxies and the morphological classification using the Jarrett *et al.* (2003) method are given in Table 4.5.

Table 4.5: A morphological classification using the method described in Jarrett *et al.* (2003) of two galaxies in the Central Field with obvious morphology.

Visual Classification	Mean Central Surface Brightness [mag]			Estimated Morphology
	J	H	K_s	
Elliptical	17.15	16.37	15.82	E/S0
Spiral	19.49	19.16	17.09	Sc/Scd

The predicted morphologies match the visual classification of the two galaxies.

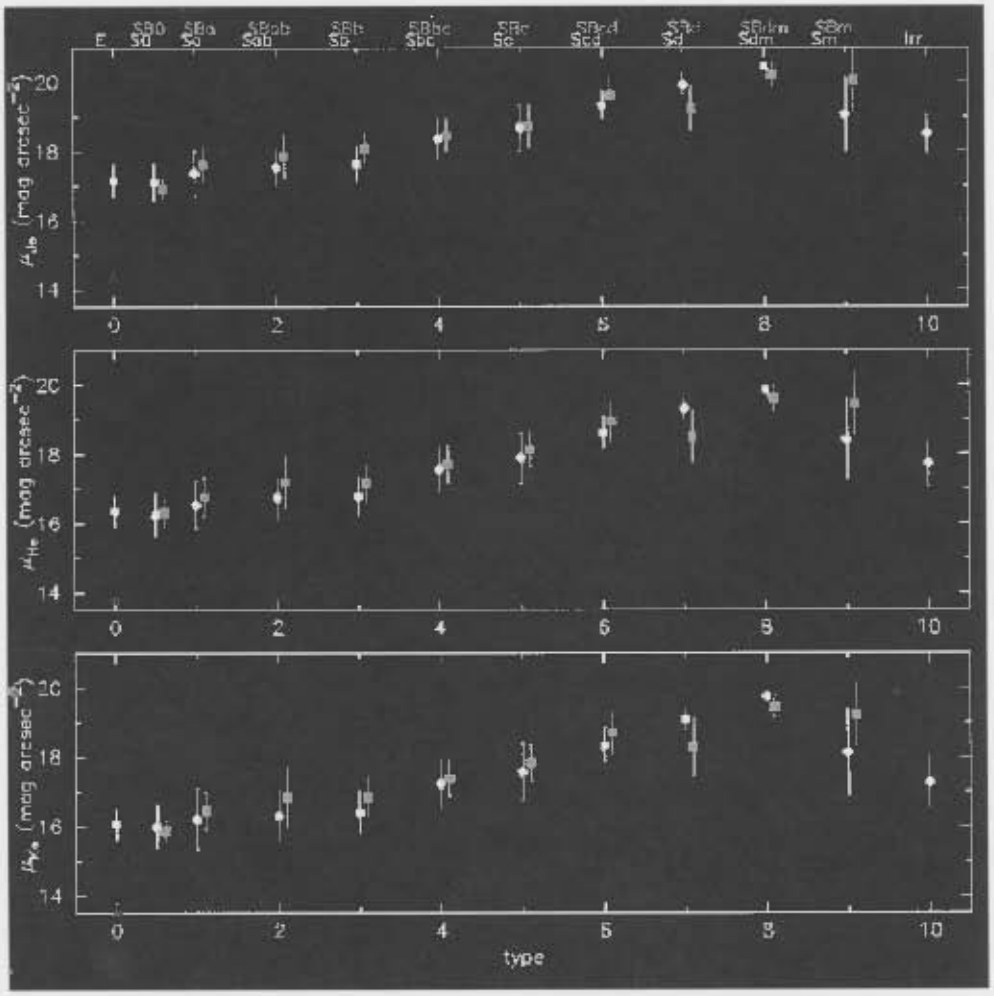

Figure 4.9: Figure 18 taken from Jarrett *et al.* (2003). It shows the relation between the mean central SB and Hubble type for galaxies in the 2MASS Large Galaxy Atlas.

The error bars in Fig. 4.9 shows that more than one Hubble type can be attributed to the same mean central SB. Therefore, we will use a broader morphological classification scheme for the galaxies in our sample.

4.2.4 Classification Scheme

We used the J band mean central SB for the galaxy classification as it had the most accurately calibrated photometry. A morphological classification was only made for galaxies brighter than the J band completeness limit of 20.06^{m}. As stated previously, the size of the galaxies needs to be considered when using a fixed aperture

to determine the mean central SB. SExtractor is capable of determining a Kron radius for all the detected sources. If we confine the classification to galaxies with a Kron radius $R_K > 3$ pixels (2.7" diameter), we will ensure that we sample the central parts of the galaxies. A 2.7" diameter at $z = 0.138$ corresponds to a diameter of 6.3 kpc, which is less that the ~ 10 kpc we expect for the smallest galaxies. From Fig. 18 in the Large Galaxy Atlas (Jarrett *et al.* 2003) it was decided to assign a "1" to galaxies having a mean central SB between 16.5 and 17.5 magnitudes. These will be early type galaxies and will include E, S0 and Sa galaxies. A "2" was assigned to early type spiral galaxies having a mean central SB between 17.5 and 18.5 magnitudes, which includes Sab, Sb and Sbc galaxies. A "3" was assigned to late type spirals having a mean central SB between 18.5 and 20.2 magnitudes, which includes Sc, Scd, Sd and Sdm galaxies. It is not possible to distinguish between Irregular galaxies since they have the same mean central SB as the late type spirals. The morphology for each of the galaxies that meet the above criteria is shown in Appendix B. Ninety seven of the 868 galaxies found in the *J*-band were given a morphological classification. Four galaxies were assigned to group "1", ten to group "2" and eighty three to group "3".

4.2.5 On-sky Morphology Distribution

As discussed in Chapter 2, one expects the fraction of red galaxies to increase towards the centre of clusters. This increase in the red galaxy fraction can be due to nature or nurture. One way to determine the degree of transformation in the cluster would be to compare the fraction of red galaxies in clusters at different redshift to that of ours. We have used our galaxy classification to study the distribution of red galaxies in our cluster using the morphological information. Red galaxies will be classified as early type galaxies using the Jarrett classification scheme, as they consist mostly of population II stars.

The on-sky distribution of the different morphological types using our classification scheme is shown in Fig. 4.10. No real structure is seen in the distribution of galaxies for the Western Field (bottom right panel). But, there is a clear concentration of galaxies around the centre of the cluster, consisting of the central elliptical galaxy and early type spirals.

This might be a very rough indication that galaxy transformation has occurred in the cluster. If we assume that the cluster has a velocity dispersion of $\sigma = 500$ - 1000 km.s^{-1}, which is typical for a cluster this size, the virial radius of the cluster is of the order of $R_{vir} \sim 10$ - 20 arcmin (Girardi *et al.* 1998). Thus, we can expect to observe transformation effects in all three fields.

The filament-like structure observed in the Northern Field might be one of the filaments described by Mihos (2004) (see Chapter 2) of groups of galaxies falling to-

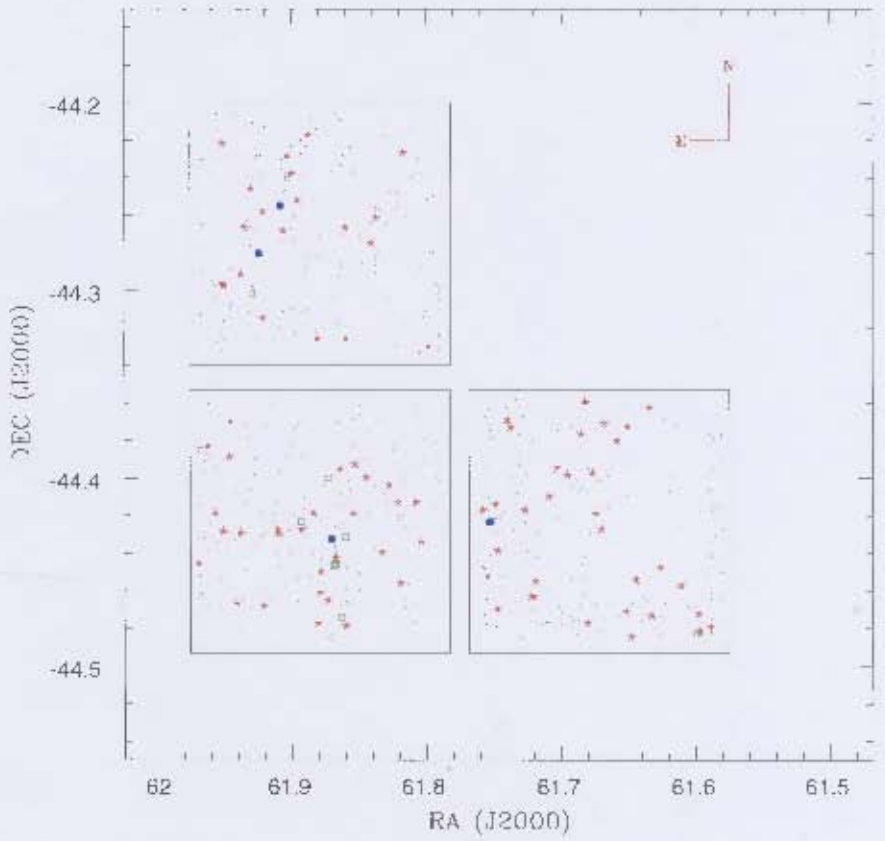

Figure 4.10: On-sky distribution of different morphological types. Solid circles are galaxies classified as "1" (early type); squares are "2"(early spirals); asterisks are "3"(late spirals). The dots are galaxies with no morphological classification.

wards the cluster centre. These groups might contain spiral galaxies that have been preprocessed into E or S0 galaxies. The early type spiral galaxies near the centre of the cluster might have undergone starformation truncation due to tidal interaction and ram pressure stripping. This is pure speculation, the proposed quantitative study using SALT multi-object spectroscopy is needed to reveal what is really happening in the cluster.

4.2.6 $B - K_s$ Colour Analysis

Given that the B band is sensitive to star formation, it is a better morphological indicator than any NIR band or colour. We therefore combined the NIR photometry with existing B band photometry to test the morphological estimates based on the mean central SB, as well as try and extract more detailed morphological information. b_J (henceforth B) band photometry was obtained from the APM galaxy survey (Maddox *et al.* 1990). The $(B - K_s)^{\rm obs}$ colour was determined for all galaxies in the three fields below the K_s completeness limit. This is shown in Fig. 4.11. The observed trend of decreasing $(B - K_s)^{\rm obs}$ value with fainter K_s magnitude was also found by Jarrett *et al.* (2003). They showed that this observed trend is correlated with Hubble type (Fig. 19 LGA).

Before we can use the $(B-K_s)^{\rm obs}$ colour as a morphological indicator, we need to correct for the distance dependent k-correction, as distance differences will introduce a scatter in the observed $(B - K_s)^{\rm obs}$ colour. To do this, we first determine the expected $(B - K_s)$ colour at $z = 0.138$ for different morphological types. This was done using the York Extinction Solver. The York Extinction Solver uses a Bessel B filter to compute the $(B - K_s)^{\rm obs}$ colour. The small (30 nm) difference between the Bessel B and b_J filter will not effect the $(B - K_s)^{\rm obs}_{z=0.138}$ colour and we will state all our results in terms of the B filter, results are shown Table 4.6.

Table 4.6: $(B - K_s)^0$ and $(B - K_s)^{\rm obs}_{z=0.138}$ colour and k-corrections for different morphological types.

Galaxy Type	$(B - K_s)^0$	$(B - K_s)^{\rm obs}_{z=0.138}$	k-correction
	[mag]	[mag]	[mag]
E	3.85	4.85	1.00
Sab	3.64	4.53	0.89
Sbc	3.63	4.30	0.66
Scd	2.74	3.30	0.56
Im	2.68	3.17	0.49

We then use the $(J - K_s)^{\rm obs}$ colour as our tentative distance indicator to select galaxies at $z \sim 0.138$ and use the $(B-K_s)^{\rm obs}$ colour to assign morphologies to these galaxies. The $(J - K_s)^{\rm obs}$ colour range for galaxies at $z \sim 0.138$ in the $(B - K_s)^{\rm obs}$ vs. $(J - K_s)^{\rm obs}$ colour plot is show in Fig. 4.12. The dashed lines indicate the $(J - K_s)^{\rm obs}$ colour range expected of galaxies at $z = 0.138$. The same morphological parameter was used for the $(B - K_s)^{\rm obs}$ colour. The values in Table 4.6 were used to assign a "1", "2" or "3" to a galaxy, referring to E/S0/Sa, Sab - Sbc and Sc - Sd

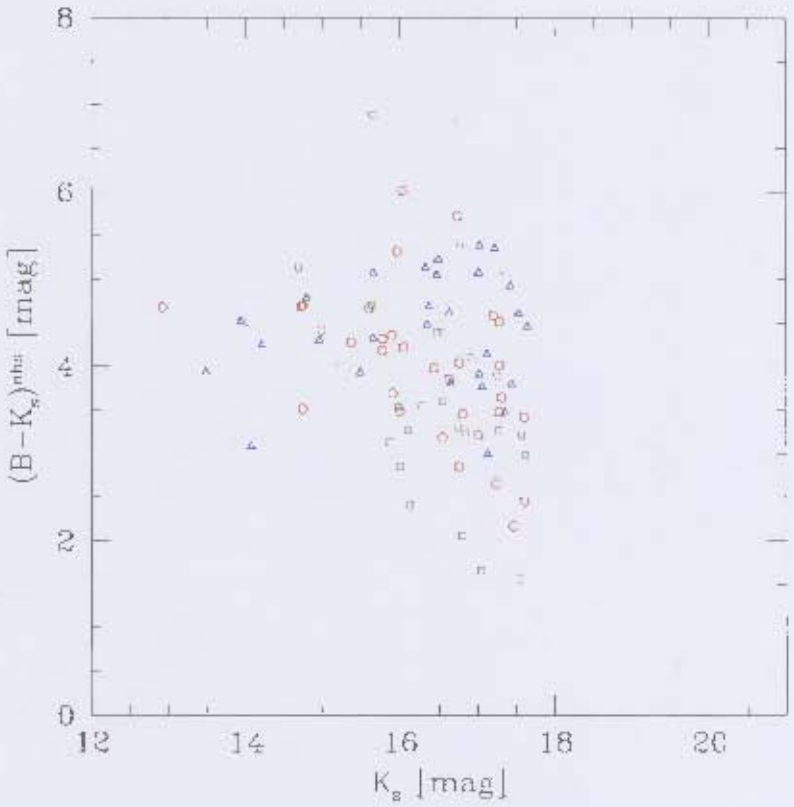

Figure 4.11: $(B-K_s)^{obs}$ colour vs $(K_s)^{obs}$ plot. The circles are Central Field sources, triangles are Northern Field sources and the squares represent Western Field sources.

galaxies respectively, the same as in section 4.2.4.

In Fig. 4.13 the $(B-K_s)^{obs}$ colours for those galaxies that lie in the expected $(J-K_s)^{obs}$ interval for the cluster distance are plotted against the $(K_s)^{obs}$ mean central SB, which, as discussed in the previous section also is a morphological indicator. The solid vertical lines represent the values assigned to the galaxies using the mean central SB classification scheme described above. These values for the morphology classification are shown on the top of the graph. The dotted horizontal lines and numbers on the right of the graph shows the $(B-K_s)^{obs}$ morphology classification.

Figure 4.13 indicates a general decrease in $(B-K_s)^{obs}$ with increasing $(K_s)^{obs}$ mean central SB. Jarrett *et al.* (2003) found the same trend for $B-K_s$ vs Hubble type (Fig. 19 in the Large Galaxy Atlas). For most of the galaxies in the $(J-K_s)^{obs}_{z=0.138}$ colour range it would seem that the $(B-K_s)^{obs}$ colour predicts the same morphology

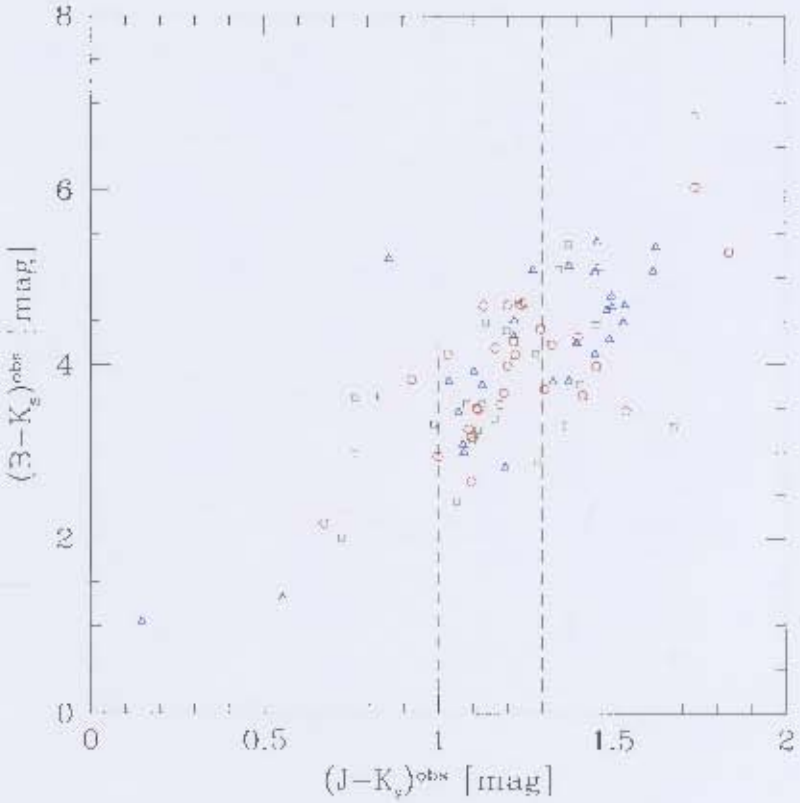

Figure 4.12: $(B-K_s)^{obs}$ colour vs $(J-K_s)^{obs}$ colour plot. The open circles are Central Field sources, triangles are Northern Field sources and the squares represent Western Field sources. The dashed lines indicate the $(J \quad K_s)^{obs}$ colour range we estimate galaxies at $z \sim 0.138$ to be in.

as the mean central SB.

But there are outliers. As the APM Galaxy Survey represents scanned photographic plates, some of the galaxies might have been misclassified as merged sources or have errors in the calculation of their magnitudes. The galaxy indicated with a solid circle in Fig. 4.13 is the central elliptical galaxy (PGC103218) in the Central Field. The $(B-K_s)^{obs}$ colour of this galaxy is far from the expected $(B-K_s)^{obs}$ for an elliptical galaxy. This prompted further investigation.

A NED search on PGC103218 revealed that the B and R magnitudes quoted in the downloaded APM catalogue[15] for the central elliptical galaxy were different to the photometry quoted by NED (see Table 4.7).

[15] http://www.ast.cam.ac.uk/~apmcat/

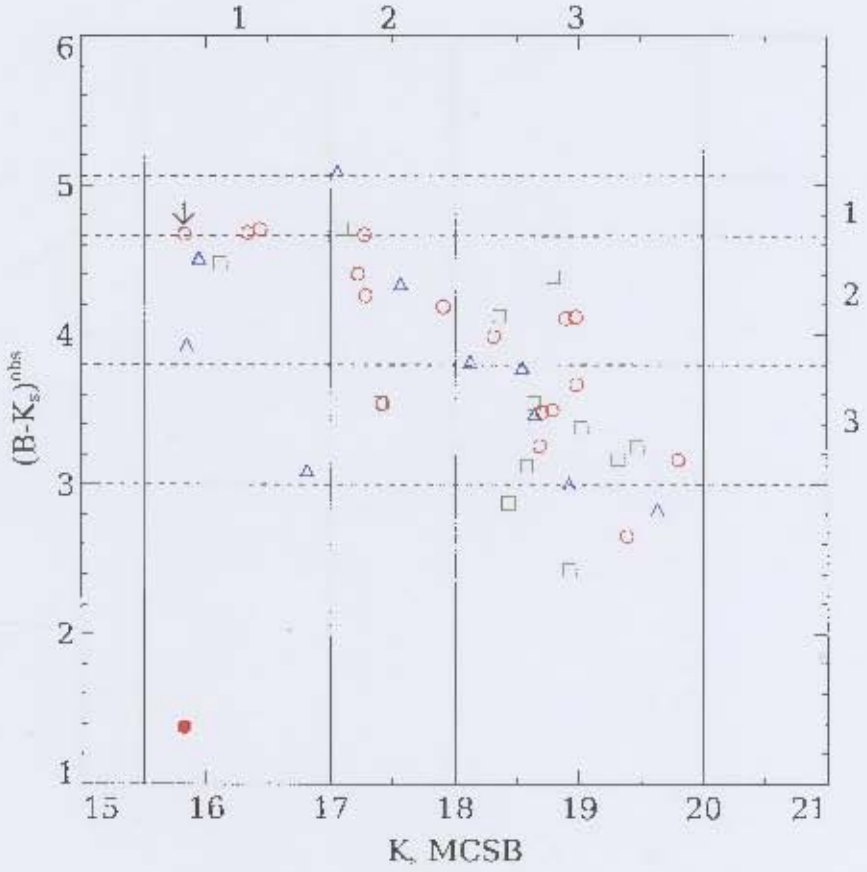

Figure 4.13: $(K_s)^{obs}$ MCSB vs. $(B \quad K_s)^{obs}$ colour . The open circles are Central Field sources, triangles are Northern Field sources and the squares represent Western Field sources. The solid dot indicates the $(B - K_s)^{obs}$ value when using the b_J photometry from the APM on-line catalogue and the arrow shows the corrected $(B - K_s)^{obs}$ value.

Table 4.7: The different B and R magnitudes quoted for PGC103218. APM magnitudes are from the on-line APM catalogue, APMCAT. NED magnitudes are from the NASA Extragalactic Database.

	APM	NED
	mag	mag
B	14.23	17.59
R	13.71	15.99

The magnitudes differences are quite significant and cannot be explained. The B magnitude quoted by NED results in a $(B - K_s)^{\rm obs}$ colour of 4.67 mag, quite close to the expected $(B - K_s)^{\rm obs}_{z=0.138} \sim 4.8$ mag (indicated by the arrow in Fig. 4.13). Objects in the APMCAT with NED photometry were corrected.

4.3 1m Results

4.3.1 Limiting Magnitudes for Point Sources

The fixed altitude design of SALT makes standard star observations unfeasible for calibration purposes. The aim of the 1m observations is to investigate the suitability of the 1m telescope as a SALT calibration instrument. During the pilot study we considered whether photometric calibrations would be possible, and whether the time it would take to complete a calibrated supercluster survey using the 1m telescope is realistic.

Due to the lack of SALT imaging performance data we could only test the performance of the 1m telescope for deep imaging. But the calibrations will be done using point sources. To this end we obtained deep $UBVRI$ photometry of Abell S0423 and determined the error in magnitude as a function of magnitude. This will provide an indication of the photometric performance of the 1m telescope in each filter. Photometric results for point sources in the deep Abell S0423 field are shown in Fig. 4.14. The individual exposure times, number of exposures combined and average seeing in each filter are shown. The red indicates observations on 22/11/2005 and blue shows observations taken on 23/11/2005. From the top, middle and lower left panels one can see that there is an almost exponential increase in error with magnitude. It was decided that the maximum allowable error for calibrations should be 0.02 magnitudes, indicated by the horizontal dotted line. This limits the magnitude of the point sources we can use to carry out accurate calibrations with. These limits are shown in Table 4.8.

From the top left panel in 4.14 one can see that it is possible to decrease the magnitude error as a function of magnitude by increasing the exposure time. This, implies than one would spend even more time on calibration observations.

Table 4.8: Limiting magnitudes in each filter for point sources derived from the 0.02 magnitude error cut off.

Filter	Mag	FWHM ["]	Exp. Time [min]
U	19.5	2.22	60
B	21	2.18	20
V	20.5	1.88	10
R	19.5	1.88	9
I	19	1.88	9

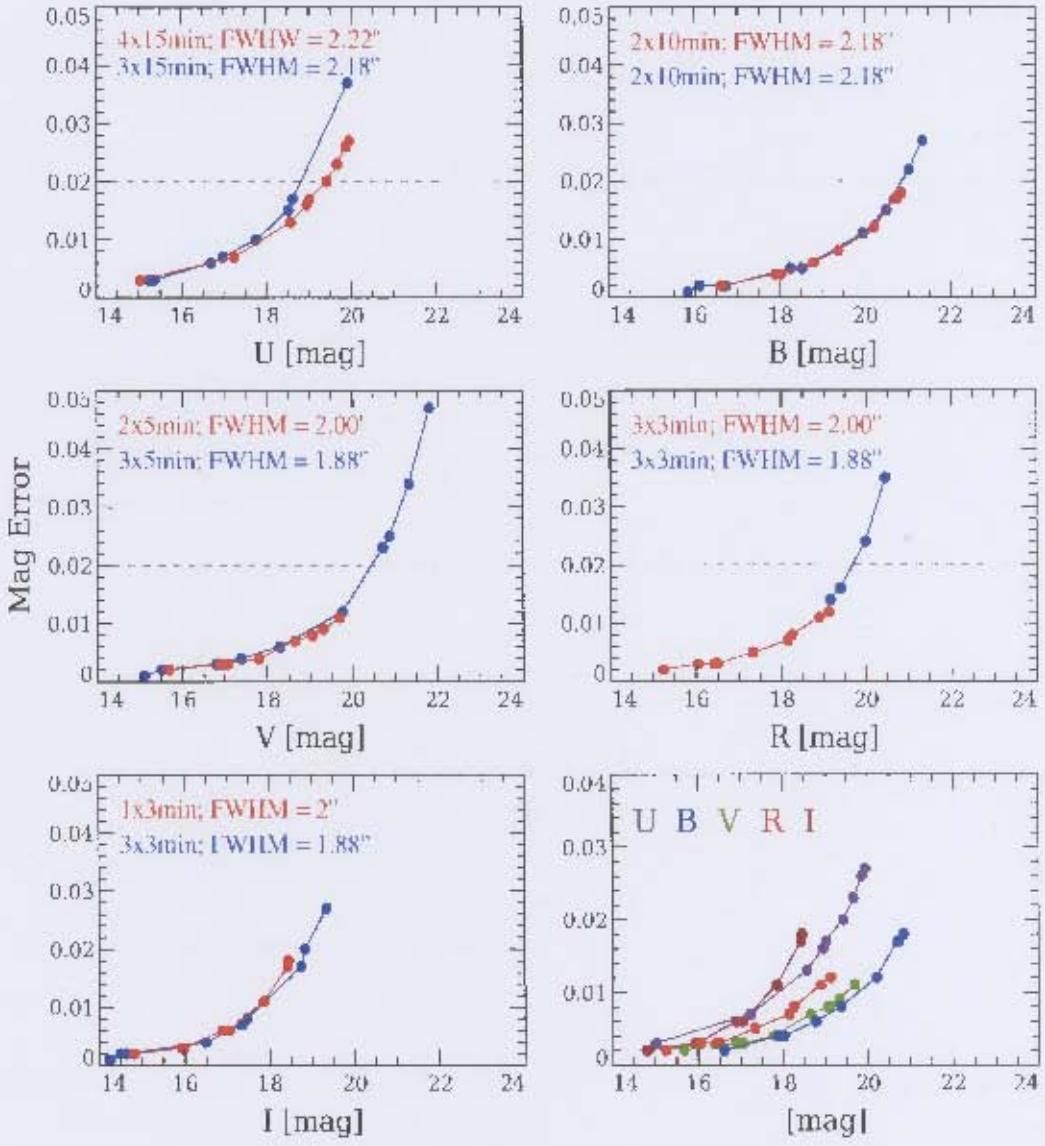

Figure 4.14: The magnitude error plots gives an indication of the range in magnitude for which the 1m telescope will produce accurate photometry.

4.3.2 Estimation of Time To Complete Survey

We now have an idea of the 1m telescope's photometric response, but without any SALT imaging performance data, we can only speculate on how to calibrate SALT photometry. Some of the biggest concerns would be the large difference in blue sensitivity of SALTICAM and the SAAO CCD; and the changing pupil size of SALT as it tracks. These effects might be very difficult to compensate for or it might not be possible at all. We can only make a final conclusion when we know more about SALT's imaging performance.

The planned survey strategy for the USSS is to observe supercluster members out to 3 or 4 virial radii, which will enable us to probe the onset of transformation in the supercluster. Such a survey would require ~30 SALT fields for the nearest redshift range ($z = 0.15$). In an attempt to estimate how long it would take to obtain calibrated data for an entire supercluster, without any SALT performace data available, we use the VLT exposure time calculator. The VLT has a smaller aperture and is setup to be more sensitive in the red than in the blue, compared to SALT. However, the VLT exposure time calculator provides a rough indication of what can be expected in terms of the time it will take to complete the survey using SALT.

To determine VLT exposure times we use a solar type star, 1.2″ seeing, airmass of 1.35 and the magnitudes listed in Table 4.8 for each filter. To guarantee a good signal-to-noise ratio, the exposure time needs to be long enough to sample faint objects, but short enough to ensure that stars with magnitudes listed in Table 4.8 are not saturated. Table 4.9 lists the total exposure times needed to probe superclusters at $z = 0.15$ in each filter; saturation times for each filter derived from the VLT exposure time calculator; number of images needed per filter per field and the total time on target. The total amount of time spent per field comes to $\sim$ 2 hours if one adds the readout time per image, but this is set by the depth of the desired survey of the supercluster (i.e. to encompass the dwarf population).

SALT has a maximum track time of $\sim$ 1 hour and one field needs $\sim$ 2 hours of observing. Thus, one field can be completed by observing the U and I bands as the target is rising and the B, V and R bands as the target is setting. During ideal conditions one would be able to observe 4 - 6 fields per night, making it possible to complete a supercluster survey in a week. If the supercluster is located far North or South, this time may be shortened due to the increase in SALT track time at far North and South declinations.

The IRSF will also take a week to complete a 30 field survey of a supercluster. The only other consideration that has to be made is the time it will take to acquire the calibration data on the 1m telescope. If we use the same exposure times as in Fig. 4.14, the total exposure time needed per field will be $\sim$ 2 hours. This does

Table 4.9: The total time was calculated by adding the readout time of SALTICAM which is 11.2 sec, to each image.

Filter	Total Exposure time (sec)	Saturation time (sec)	Images needed	Total time on target
U	1800	200	9	32min
B	1200	260	5	21min
V	1200	220	6	21min
R	1200	130	10	22min
I	1800	100	18	35min
Total time for 1 field: $\sim$ 2hours				

not include overheads, such as time spent observing standard stars, slewing the telescope and setting up guide stars, which could take up to 15 - 20min every time the telescope is moved. In ideal observing conditions, 2 fields and 3 - 4 standard star observations could be made in one night. The total time to complete such observations would be $\sim$ 2 weeks.

If it would be possible to observe on the 1m, IRSF and have SALT observations done in parallel, a supercluster survey could be completed in two weeks. Four weeks if parallel observations are not possible. The time it would take to observe a supercluster in $UBVRIJHK_s$ and obtain the calibration data seems reasonable. One should keep in mind that this does not include data reduction time, which could take much longer than the observations.

Chapter 5

Conclusions and Future Prospects

5.1 Summary of Results

This dissertation forms part of the pilot study for the UCT SALT Supercluster Survey. The aim is to establish what contributions the IRSF telescope can make to the USSS other than NIR photometric input for the galaxy evolutionary models. Another component to the dissertation is the feasibility study of the 1m telescope as a SALT calibration facility.

From the results of the 2MASS photometric comparison, we conclude that future photometric calibrations using 2MASS point sources will be feasible. This method will reduce the time spent on data reduction significantly, but is limited to fields with significant numbers of point sources with 'AAA' photometry.

The comparison between the two methods of determining completeness limits yielded similar results, which is reassuring. For future observations the MCSB method is preferable as it is better suited to be incorporated into data analysis software. The confirmed relation that a doubling of the exposure time results in a 0.5^{m} fainter completeness limit will be usefull when planning future observations of supercluster at higher redshifts.

It was shown that the insensitivity of the NIR colours to morphological type can be used as a rough distance indicator for the local universe ($z \leq 0.15$). But to distinguish background galaxies using this method will not work due the increasing effect of k-correction at higher redshifts ($z > 0.15$). To be able to use the $B - K_s$ colour as a morphological indicator, distance information is needed. The distance estimation from the $(J - K_s)^{\mathrm{obs}}_{z=0.138}$ colour was invaluable in this instance.

Using the work of Jarrett *et al.* (2003) it was possible to construct a simple morphological classification scheme. Using a fixed aperture we could derive the mean

central surface brightness for the galaxies in our fields. The predicted morphology from the mean central SB method compared well to the morphology estimated from the $(B-K_s)^{\rm obs}_{z=0.138}$ colour for galaxies at $z \sim 0.138$. From the deduced morphological information, a very crude picture of the transformation processes at work within Abell S0423 can be constructed.

The results from the NIR study of Abell S0423 illustrate that the IRSF can make a very useful contribution to the USSS. The IRSF enables us to extend the wavelength coverage of the survey to the near infrared, which is important for constraining the galaxy evolution and transformation models. The NIR data also enables us to study the morphology of galaxies in our sample on a very basic level. This was made possible through previous results by T. H. Jarrett and the researchers involved with 2MASS.

The investigation of the 1m telescope as a SALT calibration facility remains inconclusive until SALT imaging performance data become available. The calibrations are theoretically possible and we have quantified the photometric limits of the 1m telescope, but we do not yet know the practical aspects of calibrating SALT photometry.

5.2 Future Prospects

After the recommissioning of the RSS and SALTICAM we will continue the 1m telescope feasibility study during the performance verification phase of SALTICAM. This will be an ideal time to test the effectiveness of calibrations and plan future calibration strategies.

We should also explore the option of using other facilities or existing data for calibration purposes. SALT will soon be equipped with Sloan filters; this will make it possible to calibrate SALT photometry using SDSS photometry. The main disadvantage would be that targets would be confined to the Northern hemisphere. Another possibility is the Wide Field Imager (WFI)[16]. This 2.2m telescope has a 34 $\times$ 33 arcminute field of view is situated at the European Southern Observatory site of La Silla, which makes it ideal for imaging in the Southern hemisphere. The WFI will be capable of observing 17 SALT fields at once and has a blue cutoff at 350nm, which is much closer to the 320nm cutoff of SALT compared to the SAAO CCD. This will simplify the U and B band calibrations. The larger aperture of the WFI may also make it possible to use fainter stars for calibrations, reducing the number of SALT images needed to be combined, and so reducing the readout noise.

In the near future an Australian Southern Hemisphere survey called the Stromlo Southern Sky Survey will begin at Siding Spring Observatory. The survey will be

[16]http://www.ls.eso.org/lasilla/sciops/2p2/E2p2M/WFI/

carried out with the 1.3m Skymapper[17] telescope which is currently under construction. This survey will use Sloan filters which will extend the SDSS database to the Southern Hemisphere.

Plans for the near future involve NIR observations of the galaxy cluster Abell 1437. This very rich cluster is located in the Sloan supercluster, SDSS.N. Together with our collaborator Prof. U. Fritze, we will use the existing Sloan photometry together with newly obtained IRSF observations as input for the GALEV evolutionary and transformation models. From the evolution and transformation analysis, interesting targets will be identified for follow up RSS spectroscopy.

The 1m telescope calibration data, together with future targets for RSS spectroscopy, will provide us with the opportunity to work on SALTICAM and RSS data during the performance verification phase. The experience we will gain during this phase will provide us with invaluable information as to what is possible with SALT and the future of the UCT SALT Supercluster Survey.

[17] www.mso.anu.edu.au/skymapper/

Appendix A

Details on Data Reduction

A.1 Dithering

As with any detector, there are imperfections in the structure of the detector called cosmetic defects. These defects can lead to pixels not being sensitive to light at all, hence the name "bad pixels". To compensate for the effect of bad pixels the telescope employs a technique called dithering. This involves the telescope physically moving with a small offset around the centre coordinates of a target and ensures that any observed field falls on different parts of the array. Aligning each of the offset fields and median combining them eliminates the effect of a bad pixel.

As stated in Section 3.2.2, the OH emission varies on the timescale of minutes. This can be compensated for by frequently monitoring the sky. This is done by taking exposures of the same duration of a field close to the target field. The dithering technique is used to create the sky images. By not aligning the images before median combining them one essentially creates an image void of any objects and are left with only the background sky value. The object image is corrected by subtracting the sky image from it.

Due to the internal imperfections of a detector, pixels have varying sensitivity. To compensate for this effect one needs to illuminate the array with a uniform source of light and record the effect it has on each pixel. This is called a flat field, and is representative of each pixels' response to photons. Another effect is due to the thermal electrons produced by the array itself. The thermal electrons produced can be a significant fraction of charge accumulated during an exposure. To remedy this, the array is exposed with the cold shutter closed, so that any electrons produced in the array will be due to thermal effects. The dark frames need to have the same exposure time as the images taken during the night.

A.2 SIRIUS - Data Reduction

A.2.1 Pipeline Procedure

The first step consists of editing the `obslog` file by adding prefixes to filenames, so that the pipeline knows which files to use for creating sky images and which files will be used to create the final images. The next step is create the flat field images. This is done by making a file containing the filenames of the flat field images. One needs to insure that the flat field images have counts in the linear regime of the detector (counts less than 6000 for J and H and less than 4500 for the K_s band). `autotwflat` command will combine the flat field images.

Due to the dithering technique, each image consists of many dithered images. The pipeline needs to know which files to combine to produce an image. This is done by the `pipelist` command. `pipelist` reads through the `obslog` file and creates files which contain a list of the filenames of the dithered images to combine and produce an image. The filename of this list is the name of the final image. There will be files listing the names of images for the dark images, sky images and the object images to be combined. Sky images can be created in two ways. If separate sky frames were taken, these are median combined without aligning them to get rid of any objects in the final frame. If sky frames were not taken, self-sky frames are used. Self-sky frames are object frames median combined without aligning the images. The pipeline knows what type of sky image to produce because of the prefixes attached to filenames in the obslog file.

The final step is to run the pipeline with the `pipeline` command. The dark frames will be subtracted from all the images, including the flat fields and sky frames. Flat fielding is done on the sky images and object images. Finally, the sky images are subtracted from the object frames and the object frames are aligned and median combined to produce the final images.

A.2.2 Standard Star Photometry

The next step in the data reduction process is to obtain accurate photometry for the standard stars observed. The goal is to obtain the offset between the instrumental magnitude of the standard star and the apparent magnitude. If we know this offset for a night's observations then it will be possible to calibrate the other images taken on the night. Due to the fact that the SIRIUS pipline does not reduce the standard stars, this has to be done manually. Because images are dithered it is necessary to copy the overlapping parts of the images before combining them. This is done by running an IRAF script which searches in the FITS image header for the dithering offset. The IRAF task `imcopy` copies the image sections that overlap with the other images. The copied sections are aligned using `imalign` and then average combined

using `imcombine`.

Photometry is obtained by using the IRAF package `daophot`. The standard stars are the brightest sources in the images,thus, the task `daofind` with a high σ - detection value would only pick up the standard stars in the images.

A centroid centring algorithm is used to determine accurate positions. This algorithm makes use of a centring box and computes the intensity weighted mean and mean error of values between the minimum plus threshold and maximum minus threshold pixel value within the box. `Phot` was used to obtain aperture photometry. With the positions of the stars know, it was not necessary for `phot` to do photometry on all the objects in the image. This made the photometry fast because `phot` would produce the magnitude of the standard star.

When doing aperture photometry it is important to choose the correct aperture size and sky annulus. The average seeing during the observing run was $\sim 1\ ''$, thus, the FWHM (Full Width Half Maximum) of the standard images was ~ 2.2 pixels. Using the guidelines as in Massey & Davis (1992) the size of the aperture was chosen to be 4 or 5 times the FWHM and the sky annulus 5 pixels larger than that. The reason for this is to avoid under sampling of the object and good sky sampling. This makes the aperture ~ 12 pixels and the sky annulus ~ 17 pixels.

Determining the instrumental magnitudes is done by summing pixels in the aperture with a specific weighting function. A constant weighting function was used, where each pixel is assigned a weight of 1. For determining a sky value, an algorithm that determines the mean and median pixel values is used. A mode value is then determined which represents the sky value if the star was not present.

The next step is to obtain the magnitude offset, called the zeropoint magnitude. This is the systematic offset between the instrumental magnitude and the apparent magnitude. Transformation from instrumental to apparent magnitude is done using the IRAF package `photcal` which contains tasks to transform the instrumental magnitudes by solving colour and extinction terms for the Persson standard stars in the transformation equation. Because the same standard stars are observed during the night, the data is arranged in such a way that it contains the name of the standard star, filter, observation time, airmass, pixel coordinates and the instrumental magnitude. This is done by using `mknobsfile` which creates an observation file. `mkconfig` is used to organise the output data of `mknobsfile` such that the task `fitparams` knows which standard system is used. The final step is to use the `fitparams` task to solve the transformation equation by using the non-linear least squares package INLFIT. Because of the limited observation time each night, a full range of airmass could not be obtained and the second and third coefficients of the transformation equation had to be fixed. These coefficients are intrinsic to the telescope and instrument, they were obtained from Dr. P.A. Woudt who has observed extensively on

the IRSF. With the zero point magnitude known calibration of the object images are possible.

A.2.3 Source Detection and Photometry

To obtain photometry for the object images the software package SExtractor (Source Extractor version 2.4.4; Bertin & Arnouts 1996) was used. Written with the view to analyse large surveys, SExtractor has the ability to handle large images fast and to deblend and extract overlapping objects, measure the magnitude and classify objects as a star or galaxy.

SExtractor conducts the following procedures when analysing an image.

- ▷ Background and RMS noise determination.
- ▷ Subtraction of background.
- ▷ Filtering of the image to improve S/N ratio.
- ▷ Thresholding to isolate groups of connected pixels.
- ▷ Deblending of images.
- ▷ Measurement of shapes and positions of detections.
- ▷ Elimination of artifacts due to bright sources.
- ▷ Photometry and astrometry of detections.
- ▷ Star/galaxy classification.
- ▷ Output catalogue.

Parameters to be set before running SExtractor are specific to the observing conditions and the detector used. Setting these parameters as accurately as possible will ensure good photometry and source detection. `ANALYSIS_THRESH` is the threshold relative to the background RMS at which star/galaxy classification takes place and the FWHM of the object is determined. `DETECT_THRESH` is the lower limit of detection relative to the background RMS. Both of these parameters depend critically on the background RMS value. The RMS value in turn is strongly affected by the `BACK_` configuration parameters in the configuration file. These parameters are used to determine the background value for the image or, in other words, the pixel value that would be measured if an object was not present in the image. `BACK_SIZE` is the size of the mesh used for the background determination. If the mesh size is too small, random noise and objects affects the background value. This may cause

extended objects to be incorporated in the background value. If the value is set too large, small background variations will not be reproduced in the background map.

Parameters that depend on the detector is the magnitude zeropoint `MAG_ZEROPOINT`. This value was determined using `fitparams` and solving the transformation equation. The magnitude zeropoint will be subtracted from each magnitude determined for the objects in the image. `PIXEL_SCALE` is the pixel scale of the detector. Each night's seeing value `SEEING_FWHM` is used for separating stars and galaxies. The gain of the detector is also important and was determined by using the following formula as stated in Bertin (1999).

$$\text{Effective gain} = 2 \times \text{N} \times \text{gain} \div 3$$

where N is the number of frames combined to make the final image and the gain is $5e^-$ per ADU for the SIRIUS instrument.

SExtractor can be configured to output a range of object properties. Most important are the magnitude of the objects, their WCS position and the `CLASS_STAR` parameter. The `CLASS_STAR` parameter is a very powerful output parameter. It classifies stars or a galaxies using neural networks trained on simulated images. A value of 0 is assigned to extended objects, while 1 is assigned to objects with a good PSF, namely stars. The star/galaxy classification is dependent on the pixel scale and the seeing FWHM only. The value 0.9 was found to be a realistic discriminator between extended objects and stars, for our good and stable seeing conditions.

Kron magnitudes (Kron 1980) were determined by fitting a flexible ellipse around an object and determining the total flux in the elliptical aperture. This method is very useful for determining magnitudes of extended objects.

Appendix B

Catalogues

Table B.1, B.2, B.3 list all galaxies found in the J band with counter parts in the H and K_s. The columns are as follows:

Column 1: Indentification

Column 2: Right Ascension and Declination (J2000).

Column 3, 5, 7: Kron aperture magnitude and errors in J, H and K_s as derived using `SExtractor`.

Column 4, 6, 8: Central surface brightness in J, H and K_s as derived using `SExtractor` with the `MU_MAX` parameter.

Column 9: $J - K_s$ colours and errors if corresponding K_s band data is available.

Column 10: Diameter of the galaxies in the J band derived from the Kron radius using `SExtractor` with the `KRON_RADIUS` parameter.

Column 11: Position angle derived using `SExtractor` with the `THETA_J2000` parameter.

Column 12: Ellipticity, defined as $1 - \frac{minor\ axis}{major\ axis}$ derived using `SExtractor`.

Column 13: Class of the object as derived using `SExtractor`. 1 is assigned to point source like objects while 0 denotes extended sources. For our catalogue galaxies are defined as objects with a class of less or equal to 0.9.

Colomn 14: Morphology assigned to galaxies using the classification scheme described in Section 4.2.4. 1: E - Sa; 2: Sab - Sbc; 3: Sc - Sdm.

Table B.1: Galaxies found in the Central field.

Ident.	RA (J2000) h m s	DEC (J2000) ° ′ ″	J mag	μ_J^c mag/arcsec^2	H mag	μ_H^c mag/arcsec^2	K_s mag	$\mu_{K_s}^c$ mag/arcsec^2	$J-K_s$ mag	D_J ″	PA °	ε	Class	Morph
(1)	(2a)	(2b)	(3)	(4)	(5)	(6)	(7)	(8)	(9)	(10)	(11)	(12)	(13)	(14)
JPKS0423C-001	4 07 09.59	−44 24 03.1	19.55±0.08	21.20	19.07±0.11	21.06	17.09±0.09	19.30	2.46±0.12	3.7	-31	...	...	-
JPKS0423C-002	4 07 09.83	−44 23 22.0	20.14±0.06	20.62	...	...	17.94±0.11	19.54	2.19±0.13	2.7	59	0.86	0.86	-
JPKS0423C-003	4 07 09.89	−44 23 58.8	19.27±0.04	20.62	18.48±0.04	19.55	17.78±0.07	18.92	1.49±0.09	2.7	8	0.01	0.01	-
JPKS0423C-004	4 07 10.04	−44 22 52.3	20.01±0.06	20.69	19.76±0.08	20.48	...	...	...	2.7	13	0.80	0.80	-
JPKS0423C-005	4 07 10.44	−44 26 27.5	20.45±0.12	21.42	...	...	...	...	...	4.7	22	0.51	0.51	-
JPKS0423C-006	4 07 10.48	−44 24 56.2	20.26±0.12	21.48	19.69±0.07	20.52	...	...	...	5.7	44	0.15	0.15	-
JPKS0423C-007	4 07 11.15	−44 22 56.4	19.77±0.09	21.62	19.79±0.13	20.50	...	...	...	4.0	45	...	...	-
JPKS0423C-008	4 07 11.29	−44 27 39.3	19.15±0.04	20.14	...	...	18.21±0.09	18.86	0.94±0.10	2.7	-16	0.76	0.76	-
JPKS0423C-009	4 07 11.30	−44 24 18.3	19.01±0.07	20.99	18.81±0.08	20.18	...	...	...	5.5	37	...	...	-
JPKS0423C-010	4 07 11.40	−44 26 00.6	19.01±0.04	20.73	18.24±0.03	19.90	17.54±0.11	19.61	1.47±0.12	2.8	59	0.01	0.01	-
JPKS0423C-011	4 07 11.49	−44 24 06.3	19.87±0.07	20.72	19.31±0.07	20.00	...	...	...	2.9	45	0.58	0.58	-
JPKS0423C-012	4 07 11.74	−44 24 16.3	20.22±0.11	21.53	19.19±0.11	20.54	...	...	...	4.4	19	0.03	0.03	-
JPKS0423C-013	4 07 11.90	−44 26 15.7	20.30±0.12	21.59	...	...	...	...	...	6.2	-7	0.46	0.46	-
JPKS0423C-014	4 07 11.98	−44 23 26.4	19.09±0.05	19.84	...	...	18.23±0.09	18.73	0.86±0.10	4.0	-13	0.78	0.78	-
JPKS0423C-015	4 07 12.10	−44 22 45.9	19.43±0.08	20.94	18.46±0.06	20.34	...	...	...	4.5	11	0.02	0.02	-
JPKS0423C-016	4 07 12.69	−44 22 18.6	19.77±0.10	21.39	19.32±0.15	21.16	...	...	...	6.6	20	0.60	0.60	-
JPKS0423C-017	4 07 12.78	−44 24 37.4	20.69±0.16	21.57	...	...	...	...	...	5.4	85	0.60	0.60	-
JPKS0423C-018	4 07 12.92	−44 26 01.6	17.12±0.01	18.44	16.50±0.01	17.71	15.88±0.02	17.02	1.24±0.02	3.4	17	0.11	0.11	3
JPKS0423C-019	4 07 13.41	−44 27 38.4	19.21±0.05	20.91	18.28±0.05	20.25	...	...	...	3.2	-41	...	...	-
JPKS0423C-020	4 07 13.43	−44 23 42.7	19.68±0.05	20.61	18.36±0.06	19.93	17.98±0.12	19.00	1.70±0.13	2.7	-2	0.10	0.10	-
JPKS0423C-021	4 07 13.49	−44 24 43.6	18.59±0.03	20.37	17.69±0.02	19.47	16.65±0.05	18.64	1.94±0.06	3.0	-71	0.01	0.01	-
JPKS0423C-022	4 07 13.64	−44 21 52.9	21.37±0.13	21.43	...	...	...	...	...	2.7	-82	0.64	0.64	-
JPKS0423C-023	4 07 13.80	−44 23 16.7	19.81±0.06	21.05	18.78±0.07	20.27	17.99±0.10	19.02	1.81±0.12	2.7	10	0.09	0.09	-
JPKS0423C-024	4 07 13.86	−44 24 45.0	17.68±0.02	19.41	16.83±0.01	18.51	16.01±0.03	17.77	1.67±0.04	3.6	46	0.03	0.03	3
JPKS0423C-025	4 07 13.93	−44 27 59.4	18.61±0.04	20.63	17.91±0.03	19.63	17.29±0.07	18.70	1.32±0.08	3.4	75	...	...	-
JPKS0423C-026	4 07 13.99	−44 24 50.9	19.65±0.09	21.79	19.24±0.09	20.76	...	...	...	6.4	-82	...	...	-
JPKS0423C-027	4 07 14.11	−44 23 03.1	20.51±0.09	21.57	19.30±0.09	20.57	...	...	...	3.1	2	0.02	0.02	-

Table B.1 continued...

Ident.	RA (J2000) h m s	DEC (J2000) ° ′ ″	J mag	μ_J^c mag/arcsec^2	H mag	μ_H^c mag/arcsec^2	K_s mag	$\mu_{K_s}^c$ mag/arcsec^2	$J-K_s$ mag	D_J ″	PA °	ε	Class	Morph
(1)	(2a)	(2b)	(3)	(4)	(5)	(6)	(7)	(8)	(9)	(10)	(11)	(12)	(13)	(14)
JPKS0423C-028	4 07 14.36	−44 28 37.0	19.52±0.05	20.74	18.75±0.05	19.83	18.34±0.13	19.12	1.18±0.14	2.7	32	0.01	0.01	-
JPKS0423C-029	4 07 14.42	−44 24 55.8	20.13±0.12	21.41	19.17±0.08	20.40	...	...	...	5.0	-47	0.03	0.03	-
JPKS0423C-030	4 07 14.46	−44 29 05.9	19.92±0.10	21.51	19.20±0.09	20.42	18.17±0.12	19.44	1.76±0.15	6.5	74	0.42	0.42	-
JPKS0423C-031	4 07 14.72	−44 22 09.8	19.70±0.05	20.87	18.75±0.05	20.09	18.00±0.08	19.35	1.71±0.10	2.7	-74	0.14	0.14	-
JPKS0423C-032	4 07 15.01	−44 25 18.1	20.06±0.07	20.99	19.01±0.05	19.94	18.44±0.11	19.17	1.62±0.13	2.7	74	0.21	0.21	-
JPKS0423C-033	4 07 15.30	−44 26 30.5	20.40±0.12	21.29	19.55±0.11	20.58	...	...	...	4.0	38	0.36	0.36	-
JPKS0423C-034	4 07 15.32	−44 27 22.9	20.38±0.08	21.55	19.39±0.11	20.81	...	...	...	2.7	-1	...	...	-
JPKS0423C-035	4 07 15.36	−44 24 03.7	20.17±0.13	21.53	20.10±0.14	21.01	...	...	...	5.2	57	0.01	0.01	-
JPKS0423C-036	4 07 15.63	−44 25 32.6	19.17±0.05	20.69	18.42±0.05	19.75	17.65±0.09	18.96	1.51±0.10	3.1	14	0.01	0.01	-
JPKS0423C-037	4 07 15.68	−44 27 52.8	19.58±0.05	20.66	18.60±0.04	19.69	18.29±0.09	18.95	1.29±0.10	2.7	-19	0.04	0.04	-
JPKS0423C-038	4 07 15.70	−44 28 08.4	20.53±0.15	21.58	20.18±0.15	21.09	...	...	...	5.4	-22	0.09	0.09	-
JPKS0423C-039	4 07 15.91	−44 25 09.5	20.15±0.08	21.20	19.46±0.08	20.52	...	...	...	3.2	44	0.01	0.01	-
JPKS0423C-040	4 07 16.12	−44 23 52.2	19.61±0.05	20.50	18.69±0.05	19.81	18.03±0.08	18.76	1.58±0.09	2.7	-5	0.22	0.22	-
JPKS0423C-041	4 07 16.24	−44 27 18.9	19.57±0.07	20.44	19.00±0.06	19.94	...	...	...	4.0	2	0.80	0.80	-
JPKS0423C-042	4 07 16.50	−44 24 33.7	20.13±0.13	21.36	19.84±0.09	20.82	...	...	...	5.8	15	0.21	0.21	-
JPKS0423C-043	4 07 16.52	−44 26 40.4	19.37±0.08	20.91	18.64±0.06	19.77	17.97±0.12	18.98	1.40±0.15	5.6	26	0.05	0.05	-
JPKS0423C-044	4 07 16.63	−44 25 14.6	18.69±0.04	20.15	17.53±0.02	18.96	16.97±0.05	18.24	1.72±0.06	3.6	-20	0.02	0.02	-
JPKS0423C-045	4 07 16.70	−44 27 21.1	18.72±0.03	19.72	...	...	17.79±0.11	19.04	0.93±0.12	3.3	24	0.54	0.54	3
JPKS0423C-046	4 07 16.83	−44 25 10.1	19.68±0.08	20.63	19.26±0.07	20.08	...	...	...	4.2	-13	0.29	0.29	-
JPKS0423C-047	4 07 16.98	−44 26 18.6	19.52±0.08	20.54	19.06±0.08	19.93	...	...	...	4.3	9	0.46	0.46	-
JPKS0423C-048	4 07 17.01	−44 21 45.1	20.65±0.10	21.42	18.54±0.05	19.70	17.55±0.07	18.67	3.10±0.12	2.7	31	0.15	0.15	-
JPKS0423C-049	4 07 17.01	−44 23 09.7	18.51±0.04	20.34	17.81±0.03	19.56	17.15±0.07	18.70	1.36±0.08	4.1	-35	0.01	0.01	-
JPKS0423C-050	4 07 17.03	−44 24 46.9	18.19±0.03	19.75	17.32±0.02	18.84	16.98±0.05	18.25	1.21±0.06	3.2	-33	0.03	0.03	3
JPKS0423C-051	4 07 17.09	−44 25 21.9	20.15±0.11	21.39	19.72±0.08	20.55	...	...	...	4.0	-31	...	...	3
JPKS0423C-052	4 07 17.16	−44 28 35.2	19.57±0.09	20.80	18.81±0.07	20.23	18.06±0.12	19.33	1.51±0.15	4.8	20	0.31	0.31	-
JPKS0423C-053	4 07 17.49	−44 28 52.8	20.28±0.08	21.10	19.58±0.10	20.38	...	...	...	2.7	-46	0.09	0.09	-
JPKS0423C-054	4 07 17.63	−44 22 56.2	20.82±0.09	21.22	19.46±0.11	20.95	...	...	...	2.7	-37	0.56	0.56	-
JPKS0423C-055	4 07 17.78	−44 22 22.2	19.62±0.08	21.12	18.77±0.07	20.33	...	...	...	4.1	14	0.03	0.03	-
JPKS0423C-056	4 07 17.78	−44 27 31.5	19.36±0.07	20.58	18.63±0.05	19.68	17.35±0.08	18.62	2.01±0.11	4.3	33	0.36	0.36	-
JPKS0423C-057	4 07 17.95	−44 23 05.0	19.28±0.05	20.47	18.41±0.05	19.78	18.13±0.12	18.88	1.15±0.13	3.1	44	0.25	0.25	-

Table B.1 continued...

Ident.	RA (J2000) h m s	DEC (J2000) ° ′ ″	J mag	μ_J^c mag/arcsec^2	H mag	μ_H^c mag/arcsec^2	K_s mag	$\mu_{K_s}^c$ mag/arcsec^2	$J-K_s$ mag	D_J ″	PA °	ε	Class	Morph
(1)	(2a)	(2b)	(3)	(4)	(5)	(6)	(7)	(8)	(9)	(10)	(11)	(12)	(13)	(14)
JPKS0423C-058	4 07 18.07	−44 22 04.5	20.10±0.12	21.17	19.51±0.10	20.71	...	...	...	5.9	-16	0.71	0.71	-
JPKS0423C-059	4 07 18.12	−44 25 22.2	18.47±0.03	19.50	17.64±0.03	18.92	18.34±0.14	19.35	0.13±0.14	2.7	-89	0.83	0.83	-
JPKS0423C-060	4 07 18.39	−44 21 35.2	20.43±0.15	21.57	...	...	...	...	...	5.9	85	0.22	0.22	-
JPKS0423C-061	4 07 18.48	−44 24 35.0	19.30±0.08	21.06	18.80±0.07	20.17	18.25±0.13	19.25	1.05±0.15	4.8	-21	0.01	0.01	-
JPKS0423C-062	4 07 18.61	−44 29 06.7	20.25±0.08	21.53	19.62±0.14	20.78	...	...	...	2.7	-66	...	...	-
JPKS0423C-063	4 07 18.65	−44 25 06.9	19.80±0.07	20.58	...	...	...	...	...	3.8	44	0.89	0.89	-
JPKS0423C-064	4 07 18.72	−44 24 13.7	18.60±0.04	19.97	17.89±0.03	19.17	17.25±0.06	18.33	1.35±0.07	3.6	0	0.05	0.05	3
JPKS0423C-065	4 07 18.86	−44 26 32.6	19.80±0.06	20.42	...	...	...	...	...	2.7	16	0.86	0.86	3
JPKS0423C-066	4 07 18.92	−44 27 34.3	20.41±0.12	21.40	19.76±0.08	20.51	...	...	...	4.9	27	0.43	0.43	3
JPKS0423C-067	4 07 19.02	−44 24 43.6	19.81±0.11	21.64	19.55±0.08	20.87	...	...	...	4.7	-43	...	...	-
JPKS0423C-068	4 07 19.39	−44 24 30.1	19.13±0.06	20.76	18.30±0.05	20.11	17.65±0.10	19.62	1.47±0.11	3.6	-42	0.05	0.05	-
JPKS0423C-069	4 07 19.59	−44 25 04.3	20.37±0.12	21.44	19.58±0.08	20.54	...	...	...	5.1	-24	0.17	0.17	-
JPKS0423C-070	4 07 19.78	−44 26 21.2	18.40±0.03	19.86	17.90±0.03	19.20	17.28±0.07	18.80	1.12±0.08	3.6	-41	0.03	0.03	3
JPKS0423C-071	4 07 19.80	−44 21 33.0	17.96±0.02	19.78	17.18±0.02	19.14	16.61±0.04	18.47	1.35±0.04	2.7	-52	0.02	0.02	3
JPKS0423C-072	4 07 19.94	−44 29 03.8	20.08±0.11	21.37	19.70±0.14	20.84	...	...	...	5.0	72	0.06	0.06	3
JPKS0423C-073	4 07 19.98	−44 22 09.0	19.10±0.06	20.97	18.16±0.04	19.72	17.41±0.06	18.72	1.69±0.09	4.1	86	...	...	-
JPKS0423C-074	4 07 20.09	−44 28 12.7	19.33±0.06	20.61	18.67±0.05	19.98	18.00±0.12	19.26	1.33±0.13	3.4	-16	0.13	0.13	-
JPKS0423C-075	4 07 20.35	−44 28 17.6	20.17±0.10	21.25	19.70±0.10	20.41	...	...	...	4.5	-0	0.66	0.66	-
JPKS0423C-076	4 07 20.76	−44 27 42.6	19.36±0.04	20.20	18.62±0.05	19.66	...	...	...	2.7	2	0.85	0.85	-
JPKS0423C-077	4 07 20.93	−44 27 29.1	19.33±0.07	20.81	18.48±0.06	20.09	18.49±0.12	19.11	0.84±0.14	4.4	8	0.03	0.03	-
JPKS0423C-078	4 07 20.95	−44 25 11.3	19.23±0.08	20.96	18.65±0.07	19.98	17.31±0.09	19.00	1.92±0.12	5.1	38	0.04	0.04	-
JPKS0423C-079	4 07 20.98	−44 22 51.9	19.27±0.08	20.72	18.44±0.06	19.74	17.67±0.09	19.00	1.60±0.12	5.8	-3	0.14	0.14	-
JPKS0423C-080	4 07 21.07	−44 26 16.1	20.54±0.14	21.51	20.16±0.14	21.23	...	...	...	5.0	47	0.32	0.32	-
JPKS0423C-081	4 07 21.20	−44 26 38.0	20.31±0.13	21.70	19.63±0.12	21.21	...	...	...	6.2	-87	0.48	0.48	-
JPKS0423C-082	4 07 21.26	−44 24 14.6	19.10±0.06	21.11	18.27±0.06	20.54	...	...	...	4.6	-69	...	...	-
JPKS0423C-083	4 07 21.75	−44 25 18.6	20.70±0.12	21.64	19.80±0.10	20.85	...	...	...	3.9	-46	0.18	0.18	-
JPKS0423C-084	4 07 21.91	−44 21 39.9	20.51±0.08	20.90	18.86±0.07	20.15	18.24±0.14	19.52	2.27±0.16	2.7	-41	0.57	0.57	-
JPKS0423C-085	4 07 22.01	−44 28 20.0	19.05±0.04	20.64	18.20±0.03	19.83	18.06±0.11	19.34	0.99±0.12	3.0	-35	0.01	0.01	-
JPKS0423C-086	4 07 22.28	−44 21 41.3	20.32±0.08	20.79	19.77±0.13	20.71	...	...	...	2.7	-26	0.53	0.53	-
JPKS0423C-087	4 07 22.33	−44 23 26.2	20.34±0.12	21.13	19.04±0.06	20.18	18.72±0.15	19.26	1.62±0.19	4.0	-0	0.77	0.77	-

Table B.1 continued...

Ident.	RA (J2000) h m s	DEC (J2000) ° ′ ″	J mag	μ_J^c mag/arcsec^2	H mag	μ_H^c mag/arcsec^2	K_s mag	$\mu_{K_s}^c$ mag/arcsec^2	$J-K_s$ mag	D_J ″	PA °	ε	Class	Morph
(1)	(2a)	(2b)	(3)	(4)	(5)	(6)	(7)	(8)	(9)	(10)	(11)	(12)	(13)	(14)
JPKS0423C-088	4 07 22.45	−44 22 29.8	20.12±0.12	21.53	19.28±0.12	21.01	...	...	...	7.2	90	0.68	0.68	-
JPKS0423C-089	4 07 22.47	−44 25 04.2	19.88±0.11	20.94	19.24±0.07	20.05	18.77±0.16	19.28	1.12±0.19	4.7	17	0.07	0.07	-
JPKS0423C-090	4 07 22.71	−44 28 09.3	19.83±0.12	21.44	19.54±0.09	21.11	...	...	...	5.6	17	...	...	-
JPKS0423C-091	4 07 22.71	−44 27 31.1	19.62±0.07	20.50	19.05±0.08	19.85	...	...	...	3.7	18	0.48	0.48	-
JPKS0423C-092	4 07 22.77	−44 23 58.7	16.86±0.01	19.04	16.24±0.01	18.32	15.76±0.03	17.75	1.09±0.03	3.1	-73	0.03	0.03	3
JPKS0423C-093	4 07 22.94	−44 23 24.1	19.21±0.06	20.73	18.55±0.04	19.84	17.55±0.10	19.06	1.67±0.12	4.3	-4	0.02	0.02	-
JPKS0423C-094	4 07 23.05	−44 25 52.7	19.16±0.05	20.04	...	...	18.30±0.11	19.06	0.86±0.12	3.7	29	0.68	0.68	-
JPKS0423C-095	4 07 23.41	−44 24 02.2	19.20±0.07	20.56	18.21±0.04	19.59	17.42±0.07	18.60	1.78±0.09	4.4	-60	0.01	0.01	-
JPKS0423C-096	4 07 23.64	−44 21 36.8	19.89±0.07	21.03	18.90±0.05	20.13	17.97±0.09	19.10	1.92±0.11	2.7	61	0.05	0.05	-
JPKS0423C-097	4 07 23.74	−44 21 59.5	20.11±0.12	21.41	19.92±0.12	20.76	...	...	...	5.6	4	0.58	0.58	-
JPKS0423C-098	4 07 23.81	−44 21 41.2	19.88±0.09	21.35	19.21±0.07	20.39	...	...	...	3.9	26	0.01	0.01	-
JPKS0423C-099	4 07 23.91	−44 27 01.2	18.51±0.04	20.07	17.90±0.04	19.27	17.25±0.07	18.62	1.26±0.08	4.4	65	0.04	0.04	-
JPKS0423C-100	4 07 23.98	−44 27 33.1	20.74±0.10	21.36	19.66±0.08	20.47	18.44±0.14	19.16	2.30±0.17	2.7	-65	0.30	0.30	-
JPKS0423C-101	4 07 24.19	−44 27 04.5	19.47±0.11	21.60	19.22±0.10	20.80	...	...	...	6.5	-70	...	...	-
JPKS0423C-102	4 07 24.27	−44 23 38.5	19.71±0.06	20.83	18.99±0.06	20.20	...	...	...	3.0	65	0.09	0.09	-
JPKS0423C-103	4 07 24.30	−44 22 52.7	20.07±0.12	21.17	...	...	...	...	...	5.0	-27	0.08	0.08	-
JPKS0423C-104	4 07 24.78	−44 28 13.7	20.02±0.12	21.59	18.75±0.08	20.42	...	...	...	6.2	19	0.02	0.02	-
JPKS0423C-105	4 07 24.84	−44 22 06.5	19.90±0.08	21.35	17.95±0.03	18.94	17.60±0.08	18.79	2.31±0.11	3.2	45	...	...	-
JPKS0423C-106	4 07 24.90	−44 23 33.4	18.24±0.02	19.50	17.41±0.02	18.80	16.79±0.05	18.24	1.45±0.06	3.3	29	0.04	0.04	3
JPKS0423C-107	4 07 24.95	−44 22 56.0	20.18±0.10	21.13	19.16±0.06	20.25	18.23±0.12	19.40	1.95±0.15	3.5	11	0.27	0.27	3
JPKS0423C-108	4 07 25.08	−44 25 07.0	17.84±0.02	19.94	17.20±0.02	19.31	16.69±0.06	18.69	1.15±0.06	3.4	14	0.02	0.02	3
JPKS0423C-109	4 07 25.13	−44 26 19.2	19.34±0.08	20.96	18.72±0.07	20.28	...	...	...	4.5	-68	0.01	0.01	-
JPKS0423C-110	4 07 25.62	−44 24 22.1	19.92±0.11	21.41	19.47±0.12	20.68	...	...	...	5.5	-45	0.08	0.08	-
JPKS0423C-111	4 07 25.67	−44 27 59.4	20.49±0.13	21.58	19.50±0.10	20.71	...	...	...	5.1	-89	0.50	0.50	-
JPKS0423C-112	4 07 25.82	−44 25 55.4	19.66±0.06	21.01	19.11±0.08	20.15	18.30±0.14	19.46	1.36±0.16	2.7	-68	0.02	0.02	-
JPKS0423C-113	4 07 25.96	−44 24 02.6	19.99±0.11	21.35	18.87±0.09	20.76	...	...	...	5.3	54	0.06	0.06	-
JPKS0423C-114	4 07 26.10	−44 23 57.9	20.52±0.14	21.70	19.77±0.13	20.71	...	...	...	6.1	44	0.24	0.24	-
JPKS0423C-115	4 07 26.13	−44 24 41.5	19.61±0.09	20.94	19.16±0.10	20.20	18.39±0.09	19.22	1.22±0.13	4.5	-12	0.06	0.06	-
JPKS0423C-116	4 07 26.15	−44 25 52.8	18.89±0.04	20.09	...	...	...	...	...	3.5	19	0.22	0.22	-
JPKS0423C-117	4 07 26.17	−44 28 19.3	20.47±0.16	21.66	18.75±0.09	20.68	...	...	...	6.5	44	0.17	0.17	-

Table B.1 continued...

Ident.	RA (J2000) h m s	DEC (J2000) ° ′ ″	J mag	μ_J^c mag/arcsec^2	H mag	μ_H^c mag/arcsec^2	K_s mag	$\mu_{K_s}^c$ mag/arcsec^2	$J-K_s$ mag	D_J ″	PA °	ε	Class	Morph
(1)	(2a)	(2b)	(3)	(4)	(5)	(6)	(7)	(8)	(9)	(10)	(11)	(12)	(13)	(14)
JPKS0423C-118	4 07 26.23	−44 27 32.4	19.86±0.11	21.34	19.33±0.08	20.37	...	...	...	6.0	-3	0.30	0.30	-
JPKS0423C-119	4 07 26.24	−44 26 48.6	18.57±0.05	20.55	17.85±0.03	19.40	17.22±0.07	18.46	1.35±0.08	4.3	74	0.01	0.01	-
JPKS0423C-120	4 07 26.26	−44 26 52.7	19.43±0.10	21.32	18.68±0.08	20.36	17.77±0.12	19.72	1.66±0.15	5.1	25	...	...	-
JPKS0423C-121	4 07 26.38	−44 28 42.5	18.67±0.03	19.93	17.88±0.03	19.25	17.71±0.07	18.68	0.96±0.08	3.1	40	0.03	0.03	3
JPKS0423C-122	4 07 26.39	−44 27 57.0	19.62±0.06	20.69	18.57±0.05	19.66	17.90±0.08	18.97	1.72±0.09	2.7	17	0.11	0.11	3
JPKS0423C-123	4 07 26.43	−44 28 07.2	19.75±0.06	21.09	18.93±0.08	20.20	...	...	...	2.7	56	0.01	0.01	3
JPKS0423C-124	4 07 26.49	−44 25 53.2	16.21±0.01	18.25	15.42±0.01	17.48	14.98±0.01	16.89	1.23±0.02	3.0	-28	0.03	0.03	2
JPKS0423C-125	4 07 26.58	−44 22 44.9	20.61±0.10	21.25	19.32±0.11	20.93	...	...	...	3.6	46	0.44	0.44	2
JPKS0423C-126	4 07 26.89	−44 25 29.0	20.00±0.06	20.79	18.76±0.08	19.93	18.22±0.10	19.02	1.78±0.12	2.7	-7	0.67	0.67	2
JPKS0423C-127	4 07 27.04	−44 24 51.3	20.57±0.13	21.69	19.51±0.14	20.73	...	...	...	4.8	-89	0.14	0.14	2
JPKS0423C-128	4 07 27.17	−44 28 27.8	15.07±0.00	17.96	14.32±0.00	17.29	14.06±0.01	16.90	1.01±0.01	3.1	-18	0.03	0.03	2
JPKS0423C-129	4 07 27.35	−44 28 03.4	20.32±0.13	21.77	19.53±0.11	20.93	...	...	...	6.8	45	0.29	0.29	2
JPKS0423C-130	4 07 27.41	−44 24 30.5	20.01±0.08	20.84	18.67±0.07	20.34	...	...	...	3.5	-2	0.12	0.12	-
JPKS0423C-131	4 07 27.51	−44 27 19.6	19.61±0.09	20.84	18.44±0.05	19.90	18.12±0.12	19.65	1.48±0.15	4.2	-73	0.01	0.01	-
JPKS0423C-132	4 07 27.53	−44 23 41.9	18.89±0.03	19.65	...	...	...	...	...	2.7	49	0.49	0.49	3
JPKS0423C-133	4 07 27.62	−44 25 36.3	20.15±0.10	21.28	19.44±0.13	20.51	...	...	...	4.3	-64	0.07	0.07	3
JPKS0423C-134	4 07 27.76	−44 22 13.5	20.33±0.20	21.00	18.48±0.05	20.05	18.46±0.10	19.26	1.87±0.22	5.1	14	0.01	0.01	3
JPKS0423C-135	4 07 27.77	−44 24 09.8	20.39±0.13	21.67	18.51±0.07	20.53	18.37±0.14	19.34	2.02±0.19	4.1	4	...	...	3
JPKS0423C-136	4 07 27.82	−44 22 03.0	21.46±0.39	21.30	18.98±0.07	20.35	...	...	...	4.9	16	0.06	0.06	3
JPKS0423C-137	4 07 28.21	−44 26 20.3	19.58±0.14	21.55	19.03±0.10	20.67	...	...	...	7.1	-86	...	...	-
JPKS0423C-138	4 07 28.24	−44 26 45.3	16.98±0.01	18.02	...	...	...	...	...	2.8	-30	0.78	0.78	2
JPKS0423C-139	4 07 28.25	−44 26 32.9	16.65±0.01	18.40	15.96±0.01	17.57	15.59±0.02	16.94	1.06±0.02	3.2	51	0.03	0.03	3
JPKS0423C-140	4 07 28.31	−44 26 10.4	19.93±0.13	21.64	...	...	...	...	...	6.1	-27	0.01	0.01	-
JPKS0423C-141	4 07 28.34	−44 26 12.9	19.53±0.09	21.49	...	...	...	...	...	7.2	19	0.29	0.29	-
JPKS0423C-142	4 07 28.36	−44 26 26.3	20.13±0.14	21.68	...	...	...	...	...	7.2	5	0.22	0.22	-
JPKS0423C-143	4 07 28.43	−44 24 55.4	17.83±0.04	20.66	19.54±0.11	21.28	17.06±0.09	19.42	0.77±0.10	5.0	-0	...	...	-
JPKS0423C-144	4 07 28.46	−44 25 33.2	19.12±0.08	21.50	...	...	...	...	...	6.0	71	...	...	-
JPKS0423C-145	4 07 28.59	−44 26 48.5	16.80±0.01	17.95	16.46±0.01	17.41	...	...	...	3.0	-34	0.89	0.89	2
JPKS0423C-146	4 07 28.67	−44 28 57.9	20.71±0.24	21.41	18.13±0.04	20.29	18.58±0.14	19.34	2.13±0.28	6.4	42	0.37	0.37	2
JPKS0423C-147	4 07 28.88	−44 25 56.5	14.05±0.00	16.96	13.28±0.00	16.18	12.92±0.00	15.66	1.13±0.00	3.1	6	0.03	0.03	1

Table B.1 continued...

Ident.	RA (J2000) h m s	DEC (J2000) ° ′ ″	J mag	μ_J^c mag/arcsec^2	H mag	μ_H^c mag/arcsec^2	K_s mag	$\mu_{K_s}^c$ mag/arcsec^2	$J-K_s$ mag	D_J ″	PA °	ε	Class	Morph
(1)	(2a)	(2b)	(3)	(4)	(5)	(6)	(7)	(8)	(9)	(10)	(11)	(12)	(13)	(14)
JPKS0423C-148	4 07 29.11	−44 29 09.0	19.63±0.06	20.77	17.63±0.03	19.54	17.57±0.10	18.52	2.06±0.11	3.0	-3	0.01	0.01	-
JPKS0423C-149	4 07 29.15	−44 26 19.6	20.25±0.19	21.88	18.52±0.08	20.78	18.68±0.21	19.87	1.56±0.28	5.9	-0	...	...	-
JPKS0423C-150	4 07 29.16	−44 22 52.6	20.51±0.14	21.10	...	...	...	...	...	3.6	-15	0.14	0.14	-
JPKS0423C-151	4 07 29.43	−44 29 05.8	20.67±0.20	21.88	18.61±0.06	20.64	...	...	...	6.0	1	...	...	-
JPKS0423C-152	4 07 29.48	−44 24 00.3	17.23±0.01	18.26	...	...	...	...	...	2.8	-3	0.87	0.87	2
JPKS0423C-153	4 07 29.56	−44 27 53.9	18.23±0.04	19.59	17.24±0.02	18.73	16.62±0.04	18.06	1.61±0.06	4.5	-19	0.03	0.03	3
JPKS0423C-154	4 07 29.63	−44 26 51.9	20.32±0.17	21.73	19.28±0.11	20.80	...	...	...	6.1	48	...	...	3
JPKS0423C-155	4 07 29.80	−44 22 16.1	20.23±0.12	21.13	19.41±0.07	20.35	...	...	...	4.7	12	0.42	0.42	3
JPKS0423C-156	4 07 30.45	−44 24 11.4	19.68±0.08	20.68	18.94±0.07	19.92	18.05±0.08	18.67	1.64±0.12	4.1	-69	0.13	0.13	-
JPKS0423C-157	4 07 30.58	−44 23 12.5	20.60±0.09	21.37	19.53±0.09	20.60	...	...	...	2.7	52	0.27	0.27	-
JPKS0423C-158	4 07 30.64	−44 29 10.1	20.34±0.10	20.95	18.90±0.05	19.99	17.94±0.11	18.95	2.41±0.15	3.7	-68	0.75	0.75	-
JPKS0423C-159	4 07 30.82	−44 26 59.3	17.56±0.02	19.47	17.01±0.01	18.70	16.43±0.04	18.14	1.13±0.04	3.1	-1	0.03	0.03	3
JPKS0423C-160	4 07 30.87	−44 26 34.1	20.00±0.10	21.35	19.51±0.07	20.45	...	...	...	4.4	-1	0.06	0.06	-
JPKS0423C-161	4 07 31.06	−44 28 34.4	19.24±0.08	21.11	18.82±0.05	20.27	17.82±0.10	19.48	1.42±0.13	5.2	51	...	...	-
JPKS0423C-162	4 07 31.09	−44 27 39.0	17.51±0.02	19.39	17.08±0.02	18.70	16.65±0.04	18.17	0.86±0.05	4.1	15	0.03	0.03	3
JPKS0423C-163	4 07 31.47	−44 28 38.2	18.53±0.04	19.68	19.98±0.09	20.88	18.26±0.12	19.35	0.28±0.13	4.0	-5	0.46	0.46	3
JPKS0423C-164	4 07 31.48	−44 25 22.1	17.01±0.01	18.24	16.29±0.01	17.48	...	...	...	2.7	14	0.21	0.21	3
JPKS0423C-165	4 07 31.89	−44 25 14.5	19.62±0.10	20.88	18.94±0.09	20.14	...	...	...	4.3	29	0.37	0.37	-
JPKS0423C-166	4 07 32.01	−44 27 34.2	19.32±0.09	20.91	18.95±0.07	20.12	18.27±0.09	19.11	1.05±0.12	5.5	49	0.01	0.01	-
JPKS0423C-167	4 07 32.02	−44 26 23.1	19.24±0.06	20.75	18.37±0.04	19.60	17.58±0.07	18.66	1.66±0.09	3.9	-20	0.03	0.03	-
JPKS0423C-168	4 07 32.06	−44 25 06.7	17.04±0.02	19.91	16.40±0.01	19.05	16.00±0.04	18.47	1.05±0.04	3.6	-27	0.01	0.01	3
JPKS0423C-169	4 07 32.25	−44 27 51.6	19.80±0.11	21.35	19.34±0.10	20.34	...	...	...	5.3	-40	...	...	-
JPKS0423C-170	4 07 32.49	−44 25 02.2	18.81±0.05	20.38	17.99±0.04	19.35	17.22±0.08	18.46	1.60±0.09	4.5	32	0.03	0.03	-
JPKS0423C-171	4 07 32.55	−44 22 11.4	20.12±0.11	21.40	19.02±0.06	20.55	...	...	...	4.7	9	0.05	0.05	-
JPKS0423C-172	4 07 32.73	−44 25 56.8	20.46±0.15	21.77	19.80±0.13	20.98	...	...	...	6.1	-29	0.11	0.11	-
JPKS0423C-173	4 07 33.00	−44 27 08.0	19.64±0.08	21.13	19.13±0.10	20.46	18.29±0.14	19.47	1.35±0.16	3.8	-58	0.01	0.01	-
JPKS0423C-174	4 07 33.22	−44 27 36.9	19.25±0.06	20.55	18.21±0.04	19.51	17.40±0.07	18.66	1.85±0.10	4.2	25	0.01	0.01	-
JPKS0423C-175	4 07 33.33	−44 24 47.6	19.66±0.08	20.77	18.88±0.05	19.80	18.04±0.08	18.73	1.62±0.11	3.9	-78	0.09	0.09	-
JPKS0423C-176	4 07 33.45	−44 25 34.0	19.16±0.05	20.50	17.96±0.05	19.75	18.07±0.11	18.95	1.09±0.12	3.0	6	0.01	0.01	-
JPKS0423C-177	4 07 33.85	−44 25 00.3	19.58±0.08	21.23	19.25±0.07	20.44	...	...	...	4.4	-57	...	...	-

Table B.1 continued...

Ident.	RA (J2000) h m s	DEC (J2000) ° ′ ″	J mag	μ_J^c mag/arcsec^2	H mag	μ_H^c mag/arcsec^2	K_s mag	$\mu_{K_s}^c$ mag/arcsec^2	$J-K_s$ mag	D_J ″	PA °	ε	Class	Morph
(1)	(2a)	(2b)	(3)	(4)	(5)	(6)	(7)	(8)	(9)	(10)	(11)	(12)	(13)	(14)
JPKS0423C-178	4 07 33.87	−44 24 38.2	18.60±0.04	20.90	17.90±0.04	20.27	17.87±0.12	19.81	0.73±0.12	2.9	14	...	...	-
JPKS0423C-179	4 07 34.01	−44 26 14.3	20.35±0.13	21.23	19.99±0.14	20.89	...	...	...	5.1	-47	0.57	0.57	-
JPKS0423C-180	4 07 34.09	−44 23 17.0	18.26±0.03	20.37	17.63±0.03	19.79	17.23±0.08	19.20	1.03±0.09	2.7	-75	0.01	0.01	-
JPKS0423C-181	4 07 34.32	−44 25 37.6	16.52±0.01	18.39	15.82±0.01	17.66	15.37±0.02	17.12	1.15±0.02	3.1	36	0.03	0.03	3
JPKS0423C-182	4 07 34.35	−44 26 08.0	18.89±0.03	19.85	...	...	18.23±0.14	18.95	0.66±0.14	2.7	-43	0.81	0.81	3
JPKS0423C-183	4 07 34.35	−44 25 42.9	18.83±0.04	20.41	18.20±0.05	19.55	18.05±0.14	19.08	0.78±0.14	3.4	-45	0.01	0.01	-
JPKS0423C-184	4 07 34.35	−44 25 23.6	15.89±0.00	17.46	15.17±0.00	16.71	14.72±0.01	16.08	1.17±0.01	2.8	47	0.04	0.04	2
JPKS0423C-185	4 07 34.66	−44 25 18.7	18.90±0.05	20.30	18.06±0.04	19.43	17.24±0.08	18.47	1.66±0.10	4.4	18	0.18	0.18	-
JPKS0423C-186	4 07 34.67	−44 26 28.6	20.41±0.11	21.57	19.12±0.10	20.61	18.27±0.14	19.69	2.15±0.18	4.8	-47	0.17	0.17	-
JPKS0423C-187	4 07 34.85	−44 22 16.5	20.04±0.12	21.53	19.49±0.08	20.76	...	...	...	5.6	36	0.01	0.01	-
JPKS0423C-188	4 07 34.96	−44 27 56.8	18.05±0.03	21.05	17.30±0.04	20.71	17.45±0.09	19.76	0.60±0.10	4.1	-74	...	...	-
JPKS0423C-189	4 07 34.97	−44 27 11.4	18.71±0.03	20.20	17.45±0.03	19.09	16.46±0.05	18.06	2.24±0.06	2.7	38	0.02	0.02	-
JPKS0423C-190	4 07 35.03	−44 23 04.5	18.22±0.02	19.72	17.15±0.02	18.86	16.46±0.04	17.91	1.76±0.05	2.7	14	0.03	0.03	-
JPKS0423C-191	4 07 35.12	−44 21 54.5	19.94±0.06	21.11	18.68±0.07	20.21	17.82±0.10	19.09	2.13±0.12	2.7	46	0.21	0.21	-
JPKS0423C-192	4 07 35.13	−44 22 41.6	19.35±0.05	20.78	18.34±0.05	19.71	17.52±0.09	18.81	1.83±0.10	3.0	31	0.11	0.11	-
JPKS0423C-193	4 07 35.37	−44 22 36.6	20.13±0.07	20.73	19.18±0.07	20.05	...	...	...	2.7	-38	0.71	0.71	-
JPKS0423C-194	4 07 35.51	−44 25 13.8	18.71±0.03	20.35	17.69±0.03	19.58	17.32±0.09	18.88	1.39±0.09	2.7	-85	0.01	0.01	-
JPKS0423C-195	4 07 35.52	−44 25 43.2	17.29±0.01	19.09	16.48±0.01	18.30	16.03±0.02	17.67	1.26±0.03	2.7	-20	0.03	0.03	-
JPKS0423C-196	4 07 35.52	−44 22 22.9	19.77±0.06	20.96	18.75±0.05	19.81	18.06±0.08	19.07	1.71±0.10	2.7	50	0.03	0.03	-
JPKS0423C-197	4 07 35.77	−44 22 56.9	19.81±0.06	20.84	19.16±0.07	20.22	17.99±0.11	19.13	1.81±0.12	2.7	84	0.37	0.37	-
JPKS0423C-198	4 07 35.98	−44 22 56.7	19.90±0.09	21.23	19.16±0.07	20.22	17.99±0.11	19.13	1.91±0.14	4.5	42	0.56	0.56	-
JPKS0423C-199	4 07 36.15	−44 26 23.9	20.50±0.12	21.31	19.48±0.11	20.30	18.27±0.13	19.40	2.23±0.17	4.8	-44	0.61	0.61	-
JPKS0423C-200	4 07 36.21	−44 25 39.0	20.16±0.11	21.32	19.33±0.07	20.30	18.01±0.12	19.30	2.15±0.16	5.6	-22	0.51	0.51	-
JPKS0423C-201	4 07 36.22	−44 25 05.2	18.86±0.05	20.60	18.31±0.04	19.79	17.93±0.10	18.92	0.94±0.11	4.8	-23	0.03	0.03	-
JPKS0423C-202	4 07 36.28	−44 29 07.4	19.57±0.07	20.65	19.44±0.12	20.24	...	...	...	4.3	29	0.62	0.62	-
JPKS0423C-203	4 07 36.46	−44 24 43.5	19.18±0.04	20.49	18.52±0.04	19.75	18.23±0.09	19.02	0.95±0.10	2.7	6	0.08	0.08	-
JPKS0423C-204	4 07 36.50	−44 22 04.2	20.29±0.08	21.46	19.37±0.11	20.61	...	...	...	3.3	0	0.02	0.02	-
JPKS0423C-205	4 07 36.51	−44 25 38.7	19.63±0.07	21.08	18.72±0.06	19.93	17.15±0.07	18.95	2.48±0.10	4.0	90	0.01	0.01	-
JPKS0423C-206	4 07 36.52	−44 26 18.2	20.22±0.07	21.22	19.60±0.08	20.72	...	...	...	2.7	-6	0.07	0.07	-
JPKS0423C-207	4 07 36.92	−44 23 19.4	19.60±0.08	21.31	19.12±0.06	20.09	18.12±0.12	19.28	1.47±0.15	4.8	51	0.11	0.11	-

Table B.1 continued...

Ident.	RA (J2000) h m s	DEC (J2000) ° ′ ″	J mag	μ_J^c mag/arcsec^2	H mag	μ_H^c mag/arcsec^2	K_s mag	$\mu_{K_s}^c$ mag/arcsec^2	$J-K_s$ mag	D_J ″	PA °	ε	Class	Morph
(1)	(2a)	(2b)	(3)	(4)	(5)	(6)	(7)	(8)	(9)	(10)	(11)	(12)	(13)	(14)
JPKS0423C-208	4 07 36.92	−44 28 52.3	19.32±0.08	21.58	18.98±0.09	20.46	...	...	...	6.9	39	...	...	-
JPKS0423C-209	4 07 37.43	−44 28 16.1	19.69±0.07	20.48	...	...	...	...	...	3.3	87	0.70	0.70	-
JPKS0423C-210	4 07 37.63	−44 25 51.4	19.87±0.11	21.16	19.11±0.10	20.39	18.36±0.16	19.22	1.50±0.20	5.4	39	0.10	0.10	-
JPKS0423C-211	4 07 37.73	−44 22 59.7	19.64±0.06	20.65	18.47±0.04	19.64	17.71±0.09	18.71	1.92±0.11	3.0	24	0.07	0.07	-
JPKS0423C-212	4 07 37.99	−44 28 18.2	19.43±0.08	21.20	19.08±0.10	20.54	...	...	...	6.4	-8	0.07	0.07	-
JPKS0423C-213	4 07 38.28	−44 28 50.9	18.72±0.06	20.41	18.24±0.04	19.42	17.60±0.08	18.64	1.11±0.10	5.2	54	0.02	0.02	-
JPKS0423C-214	4 07 38.37	−44 25 46.6	15.82±0.01	18.60	15.22±0.01	17.85	14.71±0.01	17.30	1.11±0.02	3.4	0	0.03	0.03	3
JPKS0423C-215	4 07 38.39	−44 26 51.9	19.91±0.11	21.36	19.12±0.11	20.83	...	...	...	6.7	70	0.65	0.65	-
JPKS0423C-216	4 07 38.42	−44 23 49.0	19.71±0.11	21.30	19.17±0.06	20.13	...	...	...	5.9	13	0.02	0.02	-
JPKS0423C-217	4 07 38.56	−44 25 39.2	18.21±0.04	19.80	17.53±0.03	19.11	17.29±0.09	18.82	0.91±0.09	4.4	1	0.03	0.03	3
JPKS0423C-218	4 07 38.73	−44 26 23.0	20.55±0.08	21.23	19.72±0.08	20.36	...	...	...	3.0	68	0.30	0.30	3
JPKS0423C-219	4 07 38.99	−44 25 09.3	20.00±0.09	21.30	19.11±0.07	20.52	...	...	...	3.8	-39	0.01	0.01	-
JPKS0423C-220	4 07 39.09	−44 24 45.2	19.44±0.07	20.86	18.58±0.04	19.97	...	...	...	4.1	-38	0.07	0.07	-
JPKS0423C-221	4 07 39.18	−44 23 43.2	19.12±0.06	20.69	18.54±0.05	19.86	17.97±0.08	18.83	1.15±0.10	4.3	38	0.01	0.01	-
JPKS0423C-222	4 07 39.25	−44 27 33.4	19.82±0.06	20.76	18.84±0.05	19.89	17.91±0.09	18.71	1.91±0.11	2.7	33	0.14	0.14	-
JPKS0423C-223	4 07 39.26	−44 25 20.4	18.69±0.04	20.44	17.76±0.03	19.35	17.29±0.06	18.51	1.40±0.07	3.3	17	0.01	0.01	-
JPKS0423C-224	4 07 39.36	−44 21 38.4	19.50±0.10	21.53	18.70±0.09	20.50	17.95±0.11	19.27	1.55±0.15	6.6	32	0.02	0.02	-
JPKS0423C-225	4 07 39.39	−44 27 54.7	19.32±0.06	20.17	...	...	...	...	...	4.0	52	0.88	0.88	-
JPKS0423C-226	4 07 39.79	−44 25 00.7	19.79±0.10	21.34	19.29±0.07	20.90	...	...	...	5.2	-13	0.04	0.04	-
JPKS0423C-227	4 07 40.68	−44 22 15.7	19.79±0.06	20.58	18.76±0.05	19.79	18.01±0.08	18.92	1.78±0.10	2.7	29	0.84	0.84	-
JPKS0423C-228	4 07 40.69	−44 25 48.4	20.18±0.12	21.69	19.70±0.12	21.07	...	...	...	6.4	44	0.06	0.06	-
JPKS0423C-229	4 07 40.98	−44 28 05.0	17.98±0.02	19.91	17.24±0.02	19.21	16.96±0.05	18.45	1.02±0.05	3.3	56	0.02	0.02	3
JPKS0423C-230	4 07 41.19	−44 25 15.5	19.82±0.08	20.77	19.49±0.07	20.34	...	...	...	3.7	13	0.13	0.13	-
JPKS0423C-231	4 07 41.22	−44 23 46.8	19.03±0.04	20.63	18.35±0.04	20.01	18.17±0.09	19.55	0.86±0.10	2.7	24	0.01	0.01	-
JPKS0423C-232	4 07 41.28	−44 27 33.8	20.15±0.13	21.47	19.40±0.09	20.74	...	...	...	5.7	32	0.50	0.50	-
JPKS0423C-233	4 07 41.35	−44 25 05.6	18.83±0.04	20.41	18.18±0.03	19.51	17.24±0.07	18.52	1.59±0.08	3.8	34	0.01	0.01	-
JPKS0423C-234	4 07 41.47	−44 25 51.5	20.17±0.13	21.70	19.29±0.10	20.76	...	...	...	7.4	8	0.55	0.55	-
JPKS0423C-235	4 07 41.56	−44 29 02.0	19.63±0.06	20.99	18.82±0.07	20.18	18.07±0.13	19.16	1.56±0.14	2.8	-34	0.01	0.01	-
JPKS0423C-236	4 07 41.59	−44 25 47.2	19.96±0.10	21.65	19.43±0.11	20.54	...	...	...	7.2	-8	0.48	0.48	-
JPKS0423C-237	4 07 42.15	−44 24 32.2	20.26±0.07	20.93	19.44±0.09	20.21	...	...	...	2.7	82	0.87	0.87	-

Table B.1 continued...

Ident.	RA (J2000) h m s	DEC (J2000) ° ′ ″	J mag	μ_J^c mag/arcsec^2	H mag	μ_H^c mag/arcsec^2	K_s mag	$\mu_{K_s}^c$ mag/arcsec^2	$J-K_s$ mag	D_J ″	PA °	ε	Class	Morph
(1)	(2a)	(2b)	(3)	(4)	(5)	(6)	(7)	(8)	(9)	(10)	(11)	(12)	(13)	(14)
JPKS0423C-238	4 07 42.27	−44 24 54.2	18.64±0.03	19.50	...	...	17.98±0.08	18.40	0.67±0.08	2.7	-9	0.85	0.85	-
JPKS0423C-239	4 07 42.37	−44 26 05.8	19.61±0.06	20.99	18.92±0.07	20.33	...	...	...	2.9	45	...	...	-
JPKS0423C-240	4 07 42.42	−44 23 20.7	20.65±0.13	21.72	20.02±0.11	20.62	...	...	...	4.3	-89	0.08	0.08	-
JPKS0423C-241	4 07 42.56	−44 21 54.9	19.84±0.11	21.32	18.98±0.10	21.05	...	...	...	5.5	-75	0.30	0.30	-
JPKS0423C-242	4 07 42.82	−44 23 55.1	19.62±0.06	20.66	19.15±0.06	19.93	...	...	...	2.9	-87	0.36	0.36	-
JPKS0423C-243	4 07 42.88	−44 23 22.9	19.91±0.11	21.33	18.78±0.08	20.39	17.46±0.10	19.37	2.46±0.15	5.7	-45	0.05	0.05	-
JPKS0423C-244	4 07 43.07	−44 26 21.2	19.04±0.06	20.58	18.14±0.03	19.73	17.46±0.08	19.04	1.58±0.10	4.1	38	0.01	0.01	-
JPKS0423C-245	4 07 43.57	−44 24 22.3	20.14±0.09	21.16	19.64±0.09	20.41	...	...	...	3.3	-42	0.09	0.09	-
JPKS0423C-246	4 07 43.76	−44 22 41.9	20.22±0.09	21.31	19.43±0.07	20.42	18.57±0.15	19.08	1.64±0.17	3.3	-87	0.04	0.04	-
JPKS0423C-247	4 07 43.86	−44 25 20.9	20.63±0.08	21.58	19.67±0.12	21.01	...	...	...	2.7	-24	0.10	0.10	-
JPKS0423C-248	4 07 44.09	−44 22 21.0	19.86±0.09	21.28	19.08±0.06	20.18	...	...	...	4.2	68	...	...	-
JPKS0423C-249	4 07 44.59	−44 26 55.7	20.45±0.12	21.25	19.86±0.09	20.49	...	...	...	4.2	-16	0.35	0.35	-
JPKS0423C-250	4 07 44.60	−44 24 48.6	19.16±0.07	20.91	18.61±0.05	20.12	18.13±0.11	19.10	1.03±0.13	4.3	-30	0.01	0.01	-
JPKS0423C-251	4 07 44.96	−44 27 52.5	19.94±0.07	20.85	18.97±0.07	19.92	...	...	...	2.7	44	0.02	0.02	-
JPKS0423C-252	4 07 44.98	−44 25 46.8	19.05±0.06	20.11	18.74±0.06	19.58	18.43±0.14	19.07	0.62±0.16	4.6	82	0.41	0.41	-
JPKS0423C-253	4 07 45.25	−44 25 44.3	17.87±0.02	19.22	17.10±0.01	18.37	16.55±0.03	17.70	1.33±0.04	3.4	71	0.07	0.07	3
JPKS0423C-254	4 07 45.29	−44 25 50.9	19.90±0.12	21.33	19.34±0.11	20.95	18.21±0.14	19.82	1.69±0.19	5.8	48	0.01	0.01	-
JPKS0423C-255	4 07 45.35	−44 22 05.2	19.82±0.11	21.55	...	...	...	...	...	5.6	66	0.01	0.01	-
JPKS0423C-256	4 07 45.39	−44 28 47.0	20.37±0.14	21.29	19.88±0.08	20.52	...	...	...	4.8	-44	0.07	0.07	-
JPKS0423C-257	4 07 45.60	−44 28 03.1	19.97±0.11	21.30	19.76±0.11	20.72	...	...	...	6.4	28	0.68	0.68	-
JPKS0423C-258	4 07 45.69	−44 22 23.2	19.40±0.06	20.18	...	...	...	...	...	4.0	2	0.79	0.79	-
JPKS0423C-259	4 07 45.84	−44 24 26.2	19.82±0.11	21.35	18.94±0.06	20.21	18.04±0.12	19.21	1.78±0.16	5.2	10	0.01	0.01	-
JPKS0423C-260	4 07 45.87	−44 27 59.9	18.29±0.03	19.94	17.89±0.03	19.23	17.25±0.06	18.53	1.04±0.07	3.7	-81	0.02	0.02	3
JPKS0423C-261	4 07 45.96	−44 22 40.3	20.01±0.12	21.45	19.29±0.08	20.54	18.12±0.12	19.31	1.89±0.17	5.3	2	...	...	-
JPKS0423C-262	4 07 46.23	−44 25 57.0	19.48±0.10	21.42	19.03±0.06	20.39	17.98±0.11	19.24	1.50±0.15	6.5	7	...	...	-
JPKS0423C-263	4 07 46.40	−44 27 48.1	20.28±0.11	21.39	19.31±0.07	20.64	...	...	...	4.3	-1	0.06	0.06	-
JPKS0423C-264	4 07 46.86	−44 25 02.0	18.99±0.06	20.53	18.39±0.04	19.78	18.19±0.12	18.84	0.80±0.14	4.0	34	0.05	0.05	-
JPKS0423C-265	4 07 46.88	−44 25 07.6	19.50±0.09	21.27	19.39±0.07	20.37	...	...	...	5.0	17	...	...	-
JPKS0423C-266	4 07 47.08	−44 22 10.0	17.11±0.01	19.41	16.31±0.01	18.56	15.77±0.02	17.77	1.33±0.02	3.0	-19	0.03	0.03	3
JPKS0423C-267	4 07 47.13	−44 25 44.2	20.48±0.15	21.79	...	...	...	...	...	6.4	-1	0.21	0.21	3

Table B.1 continued...

Ident.	RA (J2000) h m s	DEC (J2000) ° ′ ″	J mag	μ_J^c mag/arcsec^2	H mag	μ_H^c mag/arcsec^2	K_s mag	$\mu_{K_s}^c$ mag/arcsec^2	$J-K_s$ mag	D_J ″	PA °	ε	Class	Morph
(1)	(2a)	(2b)	(3)	(4)	(5)	(6)	(7)	(8)	(9)	(10)	(11)	(12)	(13)	(14)
JPKS0423C-268	4 07 47.15	−44 23 12.9	19.96±0.11	21.95	19.30±0.11	21.28	...	...	...	7.7	-45	0.08	0.08	-
JPKS0423C-269	4 07 47.18	−44 23 19.4	17.59±0.02	19.66	17.10±0.02	19.01	16.66±0.04	18.53	0.93±0.04	3.1	44	0.02	0.02	3
JPKS0423C-270	4 07 47.47	−44 26 20.7	20.47±0.10	21.30	19.15±0.09	20.46	...	...	...	3.2	-45	0.16	0.16	3
JPKS0423C-271	4 07 47.60	−44 28 44.9	20.10±0.11	21.49	19.52±0.10	20.87	...	...	...	4.2	-2	0.01	0.01	3
JPKS0423C-272	4 07 47.67	−44 28 30.4	20.58±0.10	21.35	20.04±0.10	20.77	...	...	...	3.4	88	0.60	0.60	3
JPKS0423C-273	4 07 48.05	−44 22 30.5	19.91±0.06	20.86	19.47±0.10	20.41	...	...	...	2.7	1	0.35	0.35	3
JPKS0423C-274	4 07 48.14	−44 24 07.1	20.16±0.16	21.68	...	...	...	...	...	7.5	13	0.15	0.15	3
JPKS0423C-275	4 07 48.27	−44 27 22.0	18.79±0.04	20.80	17.72±0.04	19.73	17.12±0.05	18.80	1.67±0.06	2.7	-66	...	...	3
JPKS0423C-276	4 07 48.34	−44 25 42.1	17.76±0.02	19.84	16.80±0.01	18.81	15.99±0.03	17.86	1.77±0.03	3.3	-84	0.02	0.02	3
JPKS0423C-277	4 07 48.44	−44 26 54.5	19.49±0.05	20.54	18.28±0.04	19.73	17.99±0.08	18.71	1.50±0.09	2.7	35	0.35	0.35	3
JPKS0423C-278	4 07 48.68	−44 27 15.2	19.83±0.06	20.76	...	...	18.28±0.09	18.81	1.54±0.10	2.7	9	0.06	0.06	3
JPKS0423C-279	4 07 48.80	−44 21 29.0	19.58±0.05	20.79	19.45±0.07	20.13	18.29±0.08	19.26	1.29±0.10	2.7	77	0.06	0.06	3
JPKS0423C-280	4 07 48.82	−44 28 01.3	19.39±0.08	20.76	18.78±0.06	19.99	17.93±0.08	19.19	1.46±0.11	4.5	16	0.01	0.01	-
JPKS0423C-281	4 07 49.23	−44 26 11.8	20.12±0.09	21.09	19.98±0.11	20.13	...	...	...	3.4	42	0.07	0.07	-
JPKS0423C-282	4 07 49.28	−44 26 01.4	19.09±0.06	21.05	18.59±0.09	20.11	17.76±0.12	19.30	1.33±0.13	3.5	74	...	...	-
JPKS0423C-283	4 07 49.63	−44 23 35.9	19.77±0.12	21.27	...	...	18.42±0.16	19.60	1.36±0.20	6.2	2	...	...	-
JPKS0423C-284	4 07 49.85	−44 25 07.1	18.37±0.03	19.63	17.15±0.02	18.64	16.48±0.04	17.86	1.89±0.05	3.4	-4	0.04	0.04	3
JPKS0423C-285	4 07 50.06	−44 22 02.9	17.59±0.03	20.69	17.01±0.04	20.20	16.57±0.07	19.45	1.03±0.07	3.4	9	...	...	-
JPKS0423C-286	4 07 50.17	−44 21 58.3	19.56±0.08	21.26	...	...	...	...	...	4.4	60	...	...	-
JPKS0423C-287	4 07 50.46	−44 25 00.1	19.88±0.11	21.03	19.55±0.14	20.14	...	...	...	5.4	-24	0.38	0.38	-
JPKS0423C-288	4 07 50.49	−44 22 02.2	20.40±0.09	21.23	19.11±0.07	20.63	...	...	...	2.7	-83	0.06	0.06	-
JPKS0423C-289	4 07 50.64	−44 25 29.7	18.64±0.04	20.06	17.80±0.04	19.01	16.94±0.05	18.19	1.70±0.06	4.0	-2	0.03	0.03	-
JPKS0423C-290	4 07 50.84	−44 26 04.7	19.24±0.08	21.75	...	...	...	...	...	6.9	-2	...	...	-
JPKS0423C-291	4 07 50.87	−44 23 19.1	19.12±0.04	20.08	18.63±0.06	19.37	18.20±0.12	19.18	0.91±0.13	2.7	40	0.75	0.75	-
JPKS0423C-292	4 07 51.11	−44 21 37.5	20.28±0.08	21.20	20.27±0.23	20.44	18.13±0.10	19.12	2.15±0.12	2.7	67	0.05	0.05	-
JPKS0423C-293	4 07 51.13	−44 26 19.8	20.10±0.14	21.43	18.83±0.06	20.52	18.24±0.17	19.46	1.86±0.22	4.5	-3	...	...	-
JPKS0423C-294	4 07 51.19	−44 22 57.8	18.47±0.04	19.94	17.87±0.03	19.13	17.13±0.05	18.29	1.34±0.06	4.0	22	0.02	0.02	3
JPKS0423C-295	4 07 51.20	−44 28 04.0	20.18±0.12	21.02	18.98±0.07	19.80	17.82±0.09	18.90	2.35±0.15	4.0	-75	0.01	0.01	3
JPKS0423C-296	4 07 51.30	−44 23 12.4	20.26±0.11	21.32	19.73±0.12	20.43	...	...	...	4.8	49	0.67	0.67	3
JPKS0423C-297	4 07 51.37	−44 22 37.2	18.76±0.04	20.63	18.25±0.04	20.08	18.14±0.12	19.62	0.62±0.12	2.7	-41	0.01	0.01	3

Table B.1 continued...

Ident.	RA (J2000) h m s	DEC (J2000) ° ′ ″	J mag	μ_J^c mag/arcsec^2	H mag	μ_H^c mag/arcsec^2	K_s mag	$\mu_{K_s}^c$ mag/arcsec^2	$J-K_s$ mag	D_J ″	PA °	ε	Class	Morph
(1)	(2a)	(2b)	(3)	(4)	(5)	(6)	(7)	(8)	(9)	(10)	(11)	(12)	(13)	(14)
JPKS0423C-298	4 07 51.57	−44 23 46.3	19.54±0.10	21.76	...	...	18.38±0.19	19.51	1.16±0.21	8.0	-37	0.06	0.06	-
JPKS0423C-299	4 07 51.75	−44 23 26.3	19.16±0.04	20.08	18.58±0.04	19.51	18.51±0.09	18.82	0.64±0.10	2.7	-16	0.44	0.44	-
JPKS0423C-300	4 07 51.79	−44 22 29.1	18.40±0.02	19.82	17.49±0.02	18.89	16.65±0.05	18.03	1.75±0.05	2.7	-68	0.03	0.03	-
JPKS0423C-301	4 07 51.86	−44 25 55.3	18.84±0.05	20.16	17.97±0.03	19.27	17.30±0.06	18.26	1.54±0.08	3.9	2	0.02	0.02	-
JPKS0423C-302	4 07 52.04	−44 25 30.9	20.00±0.08	21.80	19.06±0.07	20.74	...	...	...	2.8	-7	...	...	-
JPKS0423C-303	4 07 52.12	−44 27 38.5	19.74±0.08	21.05	19.35±0.07	20.09	18.35±0.14	19.39	1.39±0.17	4.0	-4	0.30	0.30	-
JPKS0423C-304	4 07 52.14	−44 27 41.2	20.59±0.09	21.18	19.35±0.07	20.09	18.35±0.14	19.39	2.24±0.17	2.7	17	0.56	0.56	-
JPKS0423C-305	4 07 52.38	−44 24 52.1	19.72±0.06	21.03	18.92±0.05	20.28	17.83±0.11	19.24	1.89±0.13	2.7	46	0.10	0.10	-
JPKS0423C-306	4 07 52.43	−44 27 07.4	20.22±0.13	21.73	19.07±0.07	20.91	...	...	...	6.2	-68	0.05	0.05	-
JPKS0423C-307	4 07 52.46	−44 23 06.0	15.91±0.00	17.57	15.17±0.00	16.82	14.73±0.01	16.21	1.18±0.01	2.8	-52	0.03	0.03	2
JPKS0423C-308	4 07 52.66	−44 27 50.3	18.59±0.05	20.78	17.87±0.03	19.94	16.98±0.07	18.92	1.62±0.09	3.8	28	...	...	-
JPKS0423C-309	4 07 52.71	−44 26 43.5	16.30±0.01	18.55	15.60±0.01	17.76	15.00±0.01	17.09	1.30±0.02	2.8	5	0.03	0.03	3
JPKS0423C-310	4 07 52.73	−44 27 44.0	20.09±0.08	20.83	19.01±0.06	19.99	18.05±0.11	19.00	2.03±0.14	3.2	-28	0.56	0.56	3
JPKS0423C-311	4 07 52.85	−44 28 35.2	20.15±0.12	21.32	19.78±0.07	20.73	...	...	...	5.3	1	0.56	0.56	3

Table B.2: Galaxies found in the Northern field.

Ident.	RA (J2000) h m s	DEC (J2000) ° ′ ″	J mag	μ_J^c mag/arcsec^2	H mag	μ_H^c mag/arcsec^2	K_s mag	$\mu_{K_s}^c$ mag/arcsec^2	$J-K_s$ mag	D_J ″	PA °	ε	Class	Morph
(1)	(2a)	(2b)	(3)	(4)	(5)	(6)	(7)	(8)	(9)	(10)	(11)	(12)	(13)	
JPKS0423N-001	4 07 09.60	−44 19 58.1	18.83±0.06	21.31	...	...	...	...	...	4.6	65	...	...	-
JPKS0423N-002	4 07 09.64	−44 18 02.7	19.68±0.09	21.41	...	...	...	...	...	7.1	48	0.54	0.54	-
JPKS0423N-003	4 07 09.65	−44 17 55.4	19.89±0.11	21.29	...	...	...	...	...	6.4	-20	0.57	0.57	-
JPKS0423N-004	4 07 09.66	−44 19 49.6	17.71±0.05	21.18	19.97±0.14	20.57	...	...	...	6.0	30	...	...	-
JPKS0423N-005	4 07 09.67	−44 18 34.4	19.87±0.11	21.55	...	...	...	...	...	6.6	-25	0.01	0.01	-
JPKS0423N-006	4 07 09.68	−44 18 18.2	18.97±0.08	20.76	18.70±0.05	19.72	...	...	...	5.3	16	0.02	0.02	-
JPKS0423N-007	4 07 09.75	−44 19 25.4	20.28±0.08	21.36	...	...	...	...	...	2.7	-45	0.18	0.18	-
JPKS0423N-008	4 07 09.77	−44 19 28.3	20.46±0.11	21.29	...	...	...	...	...	3.9	-46	0.51	0.51	-
JPKS0423N-009	4 07 09.79	−44 20 01.7	19.54±0.10	21.55	...	...	...	...	...	6.4	-56	...	...	-
JPKS0423N-010	4 07 09.85	−44 19 38.1	18.01±0.04	20.17	19.36±0.12	20.74	16.74±0.05	18.02	1.27±0.06	5.0	-62	0.01	0.01	-
JPKS0423N-011	4 07 09.96	−44 18 09.0	20.45±0.12	21.80	...	...	...	...	...	4.8	-84	0.43	0.43	-
JPKS0423N-012	4 07 10.03	−44 17 47.8	19.43±0.11	21.19	...	...	...	...	...	4.4	-24	...	...	-
JPKS0423N-013	4 07 10.06	−44 17 38.6	19.74±0.07	21.04	...	...	...	...	...	2.7	-24	0.01	0.01	-
JPKS0423N-014	4 07 10.11	−44 19 03.9	20.83±0.10	21.35	...	...	...	...	...	2.7	-45	0.52	0.52	-
JPKS0423N-015	4 07 10.36	−44 17 44.0	19.94±0.20	21.21	...	...	...	...	...	6.0	41	...	...	-
JPKS0423N-016	4 07 10.63	−44 16 49.5	20.19±0.13	21.17	...	...	...	...	...	5.8	28	0.49	0.49	-
JPKS0423N-017	4 07 10.64	−44 16 45.2	19.53±0.10	21.22	...	...	...	...	...	6.8	-68	0.59	0.59	-
JPKS0423N-018	4 07 10.75	−44 13 29.4	19.90±0.08	20.91	18.06±0.04	19.85	17.54±0.09	18.70	2.36±0.12	3.3	42	0.11	0.11	-
JPKS0423N-019	4 07 10.76	−44 16 50.5	19.19±0.08	21.29	...	...	...	...	...	7.2	-22	0.35	0.35	-
JPKS0423N-020	4 07 10.79	−44 15 00.2	19.33±0.08	21.03	18.09±0.06	20.25	...	...	...	4.0	9	...	...	-
JPKS0423N-021	4 07 10.87	−44 16 45.7	19.14±0.07	21.38	...	...	...	...	...	7.0	32	0.67	0.67	-
JPKS0423N-022	4 07 10.91	−44 17 23.5	20.59±0.15	21.35	...	...	...	...	...	5.1	90	0.55	0.55	-
JPKS0423N-023	4 07 10.92	−44 14 05.1	19.01±0.07	20.75	19.32±0.10	20.36	...	...	...	5.8	61	0.80	0.80	-
JPKS0423N-024	4 07 10.93	−44 16 10.8	20.20±0.12	21.15	19.51±0.08	20.74	...	...	...	4.9	-16	0.67	0.67	-
JPKS0423N-025	4 07 10.96	−44 14 23.2	20.31±0.14	21.24	...	...	...	...	...	6.0	45	0.64	0.64	-
JPKS0423N-026	4 07 11.18	−44 19 36.8	18.21±0.02	19.18	19.91±0.18	20.48	17.73±0.09	18.26	0.48±0.09	2.7	11	0.81	0.81	-
JPKS0423N-027	4 07 11.23	−44 16 47.5	19.38±0.08	21.45	19.60±0.17	21.22	...	...	...	6.0	49	0.43	0.43	-

Table B.2 continued...

Ident.	RA (J2000) h m s	DEC (J2000) ° ′ ″	J mag	μ_J^c mag/arcsec^2	H mag	μ_H^c mag/arcsec^2	K_s mag	$\mu_{K_s}^c$ mag/arcsec^2	$J-K_s$ mag	D_J ″	PA °	ε	Class	Morph
(1)	(2a)	(2b)	(3)	(4)	(5)	(6)	(7)	(8)	(9)	(10)	(11)	(12)	(13)	
JPKS0423N-028	4 07 11.33	−44 13 29.1	19.58±0.10	21.15	...	...	...	...	...	5.6	-73	0.10	0.10	-
JPKS0423N-029	4 07 11.55	−44 16 45.3	18.69±0.06	21.15	19.60±0.17	21.22	...	...	...	6.2	84	...	...	-
JPKS0423N-030	4 07 11.68	−44 19 55.8	19.44±0.09	21.60	...	...	...	...	...	7.2	-90	0.06	0.06	-
JPKS0423N-031	4 07 11.70	−44 19 46.5	17.91±0.02	18.99	17.67±0.03	18.58	17.50±0.09	18.34	0.41±0.09	3.4	23	0.80	0.80	3
JPKS0423N-032	4 07 11.74	−44 15 04.5	18.75±0.08	20.70	18.16±0.07	19.98	17.63±0.12	18.81	1.12±0.14	6.4	-35	0.01	0.01	-
JPKS0423N-033	4 07 11.94	−44 13 22.9	18.28±0.04	19.92	18.61±0.08	19.62	18.28±0.18	19.22	-0.00±0.18	5.3	-50	0.73	0.73	-
JPKS0423N-034	4 07 11.99	−44 18 43.5	18.98±0.09	21.22	18.76±0.10	20.62	...	...	...	6.6	2	...	...	-
JPKS0423N-035	4 07 12.17	−44 18 40.8	18.96±0.08	20.99	18.76±0.10	20.62	...	...	...	6.3	-28	0.02	0.02	-
JPKS0423N-036	4 07 12.54	−44 18 51.0	19.41±0.08	20.54	18.31±0.07	19.84	...	...	...	4.0	-43	0.01	0.01	-
JPKS0423N-037	4 07 12.80	−44 17 14.2	20.23±0.16	21.38	19.05±0.11	20.49	...	...	...	5.9	22	0.02	0.02	-
JPKS0423N-038	4 07 13.12	−44 14 13.4	19.13±0.05	20.48	18.44±0.05	19.59	17.97±0.13	18.87	1.16±0.14	3.3	-73	0.01	0.01	-
JPKS0423N-039	4 07 13.14	−44 19 58.9	19.36±0.10	20.78	18.37±0.07	19.82	...	...	...	4.3	-36	0.01	0.01	-
JPKS0423N-040	4 07 13.17	−44 20 01.4	20.12±0.15	21.56	18.37±0.07	19.82	...	...	...	5.7	24	0.04	0.04	-
JPKS0423N-041	4 07 13.40	−44 16 21.3	20.95±0.12	21.48	19.27±0.14	20.65	...	...	...	2.7	2	0.23	0.23	-
JPKS0423N-042	4 07 13.62	−44 13 47.9	20.18±0.08	21.06	19.30±0.09	20.16	18.11±0.12	18.87	2.07±0.14	2.7	-21	0.28	0.28	-
JPKS0423N-043	4 07 13.69	−44 14 29.8	18.91±0.03	19.93	18.35±0.04	19.31	18.26±0.13	19.10	0.65±0.14	2.7	25	0.31	0.31	-
JPKS0423N-044	4 07 14.23	−44 19 17.7	20.29±0.14	21.43	19.65±0.13	20.96	...	...	...	6.1	-86	0.56	0.56	-
JPKS0423N-045	4 07 14.58	−44 14 22.6	18.47±0.04	20.85	17.84±0.05	20.15	...	...	...	3.6	-82	...	...	-
JPKS0423N-046	4 07 14.70	−44 14 53.0	20.21±0.14	21.39	...	...	...	...	...	6.4	45	0.24	0.24	-
JPKS0423N-047	4 07 14.94	−44 12 50.4	20.10±0.09	20.99	...	...	...	...	...	3.2	-61	0.33	0.33	-
JPKS0423N-048	4 07 15.54	−44 15 37.7	18.88±0.06	21.24	18.17±0.06	20.47	17.41±0.10	19.29	1.47±0.12	3.5	-81	...	...	-
JPKS0423N-049	4 07 15.63	−44 13 02.1	20.35±0.12	21.48	...	...	...	...	...	4.6	-22	0.16	0.16	-
JPKS0423N-050	4 07 16.00	−44 19 03.7	19.09±0.05	20.26	18.15±0.04	19.59	17.48±0.13	18.75	1.61±0.14	3.4	-26	0.09	0.09	-
JPKS0423N-051	4 07 16.04	−44 12 47.4	20.07±0.07	20.78	19.57±0.08	20.74	...	...	...	2.7	-8	0.53	0.53	-
JPKS0423N-052	4 07 16.22	−44 13 17.8	20.31±0.16	21.85	19.45±0.12	21.25	...	...	...	7.2	-5	0.02	0.02	-
JPKS0423N-053	4 07 16.22	−44 13 34.5	17.85±0.03	19.94	17.10±0.02	19.11	16.46±0.06	18.37	1.38±0.07	3.7	-46	0.02	0.02	3
JPKS0423N-054	4 07 16.75	−44 15 20.1	19.70±0.06	20.76	19.20±0.07	20.12	...	...	...	2.7	-41	0.07	0.07	3
JPKS0423N-055	4 07 16.78	−44 14 56.5	19.80±0.11	20.95	18.95±0.06	20.28	...	...	...	5.3	46	0.51	0.51	-
JPKS0423N-056	4 07 17.02	−44 15 27.8	18.39±0.03	19.64	17.46±0.02	18.89	17.00±0.06	18.11	1.39±0.06	2.7	-12	0.05	0.05	-
JPKS0423N-057	4 07 17.31	−44 19 45.7	20.32±0.15	21.54	...	...	...	...	...	6.1	44	0.14	0.14	-

Table B.2 continued...

Ident.	RA (J2000) h m s	DEC (J2000) ° ′ ″	J mag	μ_J^c mag/arcsec^2	H mag	μ_H^c mag/arcsec^2	K_s mag	$\mu_{K_s}^c$ mag/arcsec^2	$J-K_s$ mag	D_J ″	PA °	ε	Class	Morph
(1)	(2a)	(2b)	(3)	(4)	(5)	(6)	(7)	(8)	(9)	(10)	(11)	(12)	(13)	
JPKS0423N-058	4 07 17.34	−44 14 51.7	19.30±0.06	20.82	18.72±0.05	19.82	17.79±0.13	18.68	1.51±0.15	3.0	-58	0.01	0.01	-
JPKS0423N-059	4 07 17.45	−44 16 32.2	20.20±0.08	21.30	18.56±0.07	20.47	...	...	...	2.8	60	0.04	0.04	-
JPKS0423N-060	4 07 17.76	−44 12 31.5	19.29±0.05	20.35	18.03±0.04	19.59	17.23±0.07	18.48	2.06±0.08	2.7	53	0.12	0.12	-
JPKS0423N-061	4 07 17.81	−44 16 51.4	18.76±0.06	20.90	17.93±0.04	19.74	16.84±0.09	18.64	1.92±0.11	4.2	-44	...	...	-
JPKS0423N-062	4 07 18.12	−44 12 46.8	19.37±0.08	21.04	19.42±0.10	20.49	...	...	...	4.8	-79	0.01	0.01	-
JPKS0423N-063	4 07 18.18	−44 13 59.2	18.46±0.05	20.50	18.35±0.04	20.05	...	...	...	4.6	87	0.01	0.01	-
JPKS0423N-064	4 07 18.28	−44 19 12.8	19.71±0.09	21.05	18.86±0.06	19.99	...	...	...	4.2	9	0.01	0.01	-
JPKS0423N-065	4 07 18.36	−44 14 51.1	20.24±0.14	21.42	...	...	...	...	...	6.0	56	0.56	0.56	-
JPKS0423N-066	4 07 18.57	−44 18 17.8	20.07±0.13	21.44	19.92±0.12	20.62	...	...	...	5.5	-59	...	...	-
JPKS0423N-067	4 07 18.82	−44 18 50.7	18.68±0.03	20.11	17.95±0.04	19.34	17.11±0.11	18.58	1.57±0.11	2.7	-38	0.02	0.02	-
JPKS0423N-068	4 07 18.92	−44 15 50.0	20.16±0.13	21.17	19.22±0.10	20.54	...	...	...	5.6	-13	0.36	0.36	-
JPKS0423N-069	4 07 19.18	−44 13 04.2	19.76±0.06	20.89	19.17±0.07	20.35	...	...	...	2.7	45	0.07	0.07	-
JPKS0423N-070	4 07 19.48	−44 18 22.2	20.21±0.09	21.39	...	...	...	...	...	3.1	-5	...	...	-
JPKS0423N-071	4 07 19.48	−44 19 15.9	19.07±0.06	20.49	18.42±0.04	19.67	17.83±0.14	18.69	1.24±0.15	4.5	-47	0.02	0.02	-
JPKS0423N-072	4 07 19.61	−44 15 48.2	19.84±0.12	21.45	...	...	...	...	...	6.0	-3	0.01	0.01	-
JPKS0423N-073	4 07 19.71	−44 19 24.3	18.62±0.03	19.57	17.99±0.03	18.96	17.38±0.11	18.45	1.23±0.11	2.7	76	0.69	0.69	-
JPKS0423N-074	4 07 19.91	−44 12 26.9	18.09±0.02	18.97	17.40±0.02	18.39	...	...	...	2.7	-87	0.74	0.74	-
JPKS0423N-075	4 07 20.36	−44 18 45.2	19.75±0.09	21.13	18.95±0.06	20.11	17.85±0.13	18.85	1.91±0.16	3.9	1	...	...	-
JPKS0423N-076	4 07 20.45	−44 19 25.9	19.62±0.10	21.24	19.03±0.08	20.52	...	...	...	5.0	0	...	...	-
JPKS0423N-077	4 07 20.51	−44 15 24.7	20.06±0.10	21.30	19.08±0.08	20.46	...	...	...	4.3	42	0.23	0.23	-
JPKS0423N-078	4 07 20.74	−44 16 42.2	19.30±0.05	20.63	18.60±0.06	19.70	17.78±0.10	18.47	1.52±0.12	3.0	48	0.03	0.03	-
JPKS0423N-079	4 07 20.98	−44 17 26.8	19.23±0.05	20.39	18.27±0.05	19.42	17.58±0.08	18.51	1.65±0.10	2.9	11	0.23	0.23	-
JPKS0423N-080	4 07 20.98	−44 16 53.4	20.14±0.13	21.40	19.22±0.12	20.77	...	...	...	4.8	50	0.05	0.05	-
JPKS0423N-081	4 07 21.00	−44 15 26.7	19.65±0.06	20.66	18.49±0.04	19.48	17.57±0.08	18.45	2.08±0.10	2.7	30	0.07	0.07	-
JPKS0423N-082	4 07 21.00	−44 16 59.7	20.67±0.10	21.29	19.14±0.10	20.16	...	...	...	2.9	-1	0.45	0.45	-
JPKS0423N-083	4 07 21.04	−44 15 39.5	16.80±0.01	18.75	16.11±0.01	17.93	15.65±0.02	17.37	1.15±0.03	3.0	-63	0.03	0.03	3
JPKS0423N-084	4 07 21.10	−44 15 20.0	18.93±0.04	20.33	17.98±0.04	19.35	17.52±0.12	18.75	1.41±0.13	3.1	-58	0.01	0.01	-
JPKS0423N-085	4 07 21.13	−44 17 11.3	19.05±0.04	20.03	18.38±0.04	19.29	...	...	...	2.7	34	0.17	0.17	-
JPKS0423N-086	4 07 21.28	−44 18 40.3	19.53±0.10	21.24	19.05±0.11	20.75	...	...	...	5.4	5	...	...	-
JPKS0423N-087	4 07 21.63	−44 13 35.7	18.78±0.05	20.57	18.06±0.04	19.90	17.43±0.11	18.90	1.35±0.13	3.7	-15	0.01	0.01	-

Table B.2 continued...

Ident.	RA (J2000) h m s	DEC (J2000) ° ′ ″	J mag	μ_J^c mag/arcsec^2	H mag	μ_H^c mag/arcsec^2	K_s mag	$\mu_{K_s}^c$ mag/arcsec^2	$J-K_s$ mag	D_J ″	PA °	ε	Class	Morph
(1)	(2a)	(2b)	(3)	(4)	(5)	(6)	(7)	(8)	(9)	(10)	(11)	(12)	(13)	
JPKS0423N-088	4 07 21.91	−44 16 29.6	18.36±0.03	19.67	17.66±0.03	18.88	17.37±0.09	18.33	0.99±0.10	3.0	-65	0.05	0.05	3
JPKS0423N-089	4 07 22.14	−44 15 49.5	20.25±0.08	21.27	19.00±0.09	20.55	...	...	...	2.7	-36	0.01	0.01	3
JPKS0423N-090	4 07 22.76	−44 15 07.7	19.19±0.07	20.36	18.18±0.04	19.48	17.76±0.09	18.40	1.43±0.11	4.3	86	0.02	0.02	-
JPKS0423N-091	4 07 22.98	−44 15 26.0	19.20±0.08	20.78	18.68±0.08	20.40	...	...	...	5.3	28	0.30	0.30	-
JPKS0423N-092	4 07 23.23	−44 17 35.8	19.48±0.10	21.32	19.21±0.08	20.52	...	...	...	7.1	28	0.03	0.03	-
JPKS0423N-093	4 07 23.33	−44 15 29.5	18.71±0.07	20.84	18.52±0.07	20.42	17.79±0.13	18.96	0.92±0.14	6.2	22	0.01	0.01	-
JPKS0423N-094	4 07 23.42	−44 17 06.5	19.96±0.11	21.62	19.48±0.08	20.36	...	...	...	5.4	-25	...	...	-
JPKS0423N-095	4 07 23.81	−44 16 03.1	20.26±0.09	20.99	19.69±0.11	20.23	...	...	...	3.4	9	0.56	0.56	-
JPKS0423N-096	4 07 23.89	−44 16 16.0	19.83±0.08	21.02	18.74±0.06	20.03	...	...	...	3.7	-29	0.27	0.27	-
JPKS0423N-097	4 07 24.01	−44 13 56.5	19.95±0.15	21.59	...	...	...	...	...	6.8	64	...	...	-
JPKS0423N-098	4 07 24.06	−44 19 36.4	19.73±0.10	21.01	18.49±0.07	20.02	...	...	...	4.6	41	0.02	0.02	-
JPKS0423N-099	4 07 24.67	−44 14 01.2	19.40±0.09	20.85	19.31±0.11	20.45	...	...	...	5.4	-29	0.28	0.28	-
JPKS0423N-100	4 07 24.69	−44 14 06.3	19.76±0.13	21.07	19.88±0.16	20.71	...	...	...	5.8	41	0.13	0.13	-
JPKS0423N-101	4 07 24.73	−44 14 15.3	19.00±0.07	20.76	18.58±0.05	19.89	18.28±0.15	18.73	0.71±0.16	5.1	-7	0.01	0.01	-
JPKS0423N-102	4 07 25.14	−44 13 36.0	18.81±0.03	19.80	17.86±0.03	19.10	17.19±0.08	18.17	1.61±0.08	2.7	61	0.60	0.60	-
JPKS0423N-103	4 07 25.51	−44 13 27.1	19.69±0.08	21.01	18.77±0.09	20.08	...	...	...	3.7	60	0.01	0.01	-
JPKS0423N-104	4 07 25.66	−44 14 28.0	18.75±0.03	20.05	17.70±0.04	19.17	17.13±0.08	18.22	1.61±0.09	2.7	-41	0.02	0.02	-
JPKS0423N-105	4 07 25.74	−44 15 34.3	20.29±0.13	21.34	19.75±0.11	20.66	...	...	...	5.0	22	0.23	0.23	-
JPKS0423N-106	4 07 26.11	−44 12 20.9	20.10±0.10	21.09	...	...	...	...	...	4.6	-60	0.42	0.42	-
JPKS0423N-107	4 07 26.19	−44 19 32.7	20.29±0.10	21.14	19.09±0.09	20.22	...	...	...	3.2	-76	0.28	0.28	-
JPKS0423N-108	4 07 26.36	−44 17 09.1	19.47±0.10	21.22	19.15±0.07	20.45	...	...	...	5.6	39	...	...	-
JPKS0423N-109	4 07 26.39	−44 19 11.2	19.70±0.06	20.95	18.91±0.09	20.68	...	...	...	2.8	-67	0.07	0.07	-
JPKS0423N-110	4 07 26.49	−44 19 31.4	17.81±0.03	19.70	17.04±0.02	18.87	16.35±0.05	17.93	1.46±0.05	3.9	-4	0.02	0.02	3
JPKS0423N-111	4 07 26.59	−44 15 59.0	17.56±0.02	19.36	16.71±0.02	18.48	16.20±0.04	17.61	1.36±0.05	4.3	77	0.03	0.03	3
JPKS0423N-112	4 07 26.59	−44 16 11.8	19.82±0.11	21.54	19.21±0.10	21.01	...	...	...	5.4	85	...	...	-
JPKS0423N-113	4 07 26.91	−44 13 42.9	18.45±0.06	21.08	18.16±0.06	20.70	...	...	...	5.0	-6	...	...	-
JPKS0423N-114	4 07 27.06	−44 14 30.3	17.29±0.01	18.86	16.80±0.01	18.31	16.50±0.06	17.88	0.79±0.06	2.7	21	0.03	0.03	-
JPKS0423N-115	4 07 27.14	−44 12 36.7	19.27±0.07	21.38	18.75±0.06	20.53	17.26±0.08	18.95	2.01±0.10	3.8	-41	...	...	-
JPKS0423N-116	4 07 27.23	−44 17 09.6	18.51±0.05	20.38	18.29±0.04	19.71	17.13±0.10	19.07	1.38±0.11	4.8	-79	0.01	0.01	-
JPKS0423N-117	4 07 27.30	−44 12 34.2	20.08±0.12	21.22	18.75±0.06	20.53	17.26±0.08	18.95	2.82±0.14	4.4	-45	0.39	0.39	-

Table B.2 continued...

Ident.	RA (J2000)	DEC (J2000)	J	μ_J^c	H	μ_H^c	K_s	$\mu_{K_s}^c$	$J-K_s$	D_J	PA	ε	Class	Morph
	h m s	° ′ ″	mag	mag/arcsec^2	mag	mag/arcsec^2	mag	mag/arcsec^2	mag	″	°			
(1)	(2a)	(2b)	(3)	(4)	(5)	(6)	(7)	(8)	(9)	(10)	(11)	(12)	(13)	
JPKS0423N-118	4 07 27.34	−44 14 00.4	19.57±0.09	20.87	18.72±0.05	19.68	17.91±0.10	18.76	1.66±0.13	4.5	84	0.22	0.22	-
JPKS0423N-119	4 07 27.44	−44 17 15.7	20.14±0.10	21.43	19.16±0.08	20.56	...	...	...	4.1	55	...	...	-
JPKS0423N-120	4 07 27.45	−44 16 44.8	18.70±0.05	20.13	17.92±0.03	19.45	17.43±0.10	18.73	1.26±0.11	3.8	39	0.02	0.02	-
JPKS0423N-121	4 07 27.55	−44 18 54.5	19.49±0.09	21.10	18.99±0.08	20.37	...	...	...	4.7	7	0.17	0.17	-
JPKS0423N-122	4 07 27.62	−44 17 33.5	19.54±0.09	20.95	18.15±0.04	19.71	17.40±0.09	18.51	2.14±0.13	4.3	-84	0.01	0.01	-
JPKS0423N-123	4 07 27.74	−44 12 30.7	19.16±0.07	21.11	18.51±0.07	20.08	17.47±0.11	18.76	1.68±0.13	4.4	38	...	...	-
JPKS0423N-124	4 07 27.86	−44 19 01.6	20.15±0.13	21.75	19.36±0.11	20.81	...	...	...	6.9	82	0.05	0.05	-
JPKS0423N-125	4 07 28.18	−44 14 43.8	19.51±0.05	20.63	18.70±0.05	19.53	17.83±0.12	18.76	1.68±0.13	2.7	-48	0.19	0.19	-
JPKS0423N-126	4 07 28.21	−44 12 20.9	19.64±0.09	21.64	19.79±0.14	21.27	...	...	...	7.4	90	0.17	0.17	-
JPKS0423N-127	4 07 28.49	−44 16 45.7	20.13±0.07	20.97	...	...	...	...	...	2.7	-41	0.75	0.75	-
JPKS0423N-128	4 07 28.49	−44 17 34.2	20.20±0.08	21.45	19.04±0.06	20.15	...	...	...	2.7	61	...	...	-
JPKS0423N-129	4 07 28.53	−44 19 51.3	19.55±0.06	20.96	18.72±0.05	20.09	17.62±0.08	18.56	1.93±0.10	2.7	38	0.05	0.05	-
JPKS0423N-130	4 07 28.56	−44 18 13.6	19.73±0.09	21.09	18.76±0.06	19.97	17.63±0.12	18.83	2.10±0.15	4.1	62	0.07	0.07	-
JPKS0423N-131	4 07 28.58	−44 13 16.8	16.39±0.01	19.08	15.60±0.01	18.34	14.96±0.03	17.56	1.42±0.03	2.7	34	0.03	0.03	-
JPKS0423N-132	4 07 28.78	−44 18 15.8	19.50±0.05	20.60	19.13±0.10	20.06	...	...	...	2.7	25	0.77	0.77	-
JPKS0423N-133	4 07 28.80	−44 18 22.5	19.63±0.06	20.86	18.75±0.07	20.22	...	...	...	2.7	47	0.04	0.04	-
JPKS0423N-134	4 07 28.90	−44 14 10.8	18.95±0.04	20.21	18.08±0.03	19.42	17.29±0.09	18.44	1.66±0.10	2.7	2	0.06	0.06	-
JPKS0423N-135	4 07 29.37	−44 13 10.6	20.10±0.07	20.78	19.18±0.08	20.45	...	...	...	2.7	9	0.76	0.76	-
JPKS0423N-136	4 07 29.51	−44 19 14.1	18.04±0.02	19.68	17.27±0.02	18.87	16.63±0.05	18.17	1.42±0.05	2.7	58	0.02	0.02	-
JPKS0423N-137	4 07 29.82	−44 15 22.0	18.63±0.04	20.07	17.97±0.03	19.21	17.31±0.09	18.18	1.32±0.10	3.7	-10	0.02	0.02	-
JPKS0423N-138	4 07 30.22	−44 19 01.7	19.64±0.10	21.22	18.88±0.06	20.26	...	...	...	4.8	31	...	...	-
JPKS0423N-139	4 07 30.55	−44 15 11.9	19.05±0.07	20.69	18.16±0.04	19.69	17.19±0.08	18.40	1.86±0.10	4.4	44	0.01	0.01	-
JPKS0423N-140	4 07 31.00	−44 19 34.0	18.42±0.02	19.39	...	...	17.71±0.10	18.44	0.70±0.10	2.7	12	0.66	0.66	-
JPKS0423N-141	4 07 31.16	−44 16 15.9	19.03±0.05	20.43	18.20±0.04	19.62	17.64±0.09	18.47	1.39±0.10	2.9	-36	0.01	0.01	-
JPKS0423N-142	4 07 31.40	−44 16 54.7	20.01±0.07	20.88	19.01±0.06	20.13	18.18±0.14	19.15	1.83±0.16	2.7	79	0.50	0.50	-
JPKS0423N-143	4 07 31.48	−44 15 42.8	18.75±0.03	19.81	17.78±0.03	18.94	16.91±0.07	18.07	1.84±0.08	2.7	73	0.20	0.20	-
JPKS0423N-144	4 07 31.51	−44 19 32.3	17.86±0.02	19.51	16.96±0.02	18.63	16.39±0.05	17.95	1.47±0.05	3.1	-18	0.03	0.03	3
JPKS0423N-145	4 07 31.63	−44 19 48.2	18.69±0.03	19.58	...	...	17.82±0.10	18.65	0.87±0.10	2.7	-16	0.81	0.81	3
JPKS0423N-146	4 07 31.66	−44 19 20.3	20.18±0.11	21.49	19.40±0.08	20.41	...	...	...	4.1	75	...	...	3
JPKS0423N-147	4 07 31.72	−44 12 50.5	18.43±0.03	20.41	17.60±0.03	19.70	17.12±0.11	18.72	1.31±0.11	2.7	61	0.01	0.01	3

Table B.2 continued...

Ident.	RA (J2000) h m s	DEC (J2000) ° ′ ″	J mag	μ_J^c mag/arcsec^2	H mag	μ_H^c mag/arcsec^2	K_s mag	$\mu_{K_s}^c$ mag/arcsec^2	$J-K_s$ mag	D_J ″	PA °	ε	Class	Morph
(1)	(2a)	(2b)	(3)	(4)	(5)	(6)	(7)	(8)	(9)	(10)	(11)	(12)	(13)	
JPKS0423N-148	4 07 31.85	−44 15 34.2	19.84±0.07	20.86	19.22±0.07	20.12	...	...	...	2.7	20	0.08	0.08	3
JPKS0423N-149	4 07 32.10	−44 15 19.1	20.27±0.13	21.23	18.95±0.09	20.45	...	...	...	4.8	-89	0.29	0.29	3
JPKS0423N-150	4 07 32.27	−44 14 43.8	19.02±0.07	20.48	18.15±0.06	19.57	17.77±0.14	18.68	1.25±0.16	5.1	-41	0.03	0.03	-
JPKS0423N-151	4 07 32.35	−44 15 07.0	19.36±0.05	20.37	18.49±0.05	19.79	17.78±0.10	18.75	1.58±0.11	2.7	-77	0.06	0.06	-
JPKS0423N-152	4 07 32.67	−44 12 31.3	17.90±0.04	20.55	18.36±0.06	19.77	17.63±0.12	18.70	0.27±0.12	5.7	-78	...	...	-
JPKS0423N-153	4 07 32.95	−44 18 37.3	19.49±0.07	20.47	18.65±0.07	19.94	...	...	...	3.7	36	0.09	0.09	-
JPKS0423N-154	4 07 33.29	−44 13 01.0	18.12±0.02	19.26	...	...	...	...	...	3.2	-54	0.15	0.15	3
JPKS0423N-155	4 07 33.34	−44 17 22.7	19.90±0.08	21.15	18.83±0.06	20.13	18.12±0.10	18.86	1.78±0.13	3.5	-17	0.03	0.03	-
JPKS0423N-156	4 07 33.43	−44 13 25.0	18.62±0.04	20.17	18.13±0.04	19.43	17.74±0.13	18.56	0.88±0.14	4.0	-4	0.02	0.02	-
JPKS0423N-157	4 07 33.44	−44 17 14.6	19.60±0.06	20.76	18.46±0.04	19.62	17.63±0.11	18.57	1.97±0.13	2.9	-21	0.02	0.02	-
JPKS0423N-158	4 07 33.45	−44 16 51.9	19.59±0.10	21.26	18.90±0.10	20.41	...	...	...	6.3	44	0.04	0.04	-
JPKS0423N-159	4 07 33.65	−44 13 10.6	18.76±0.04	20.31	17.47±0.02	19.13	17.20±0.09	18.28	1.56±0.10	2.7	23	0.01	0.01	-
JPKS0423N-160	4 07 33.72	−44 14 17.2	20.58±0.13	21.32	19.10±0.10	20.01	17.98±0.12	18.62	2.60±0.18	4.3	-44	0.27	0.27	-
JPKS0423N-161	4 07 33.73	−44 18 57.0	20.02±0.12	21.55	19.63±0.15	21.07	...	...	...	5.9	64	0.01	0.01	-
JPKS0423N-162	4 07 33.88	−44 19 06.2	20.36±0.14	21.31	19.82±0.16	20.91	...	...	...	5.7	-88	0.57	0.57	-
JPKS0423N-163	4 07 34.00	−44 18 39.9	19.96±0.12	21.40	19.42±0.13	20.63	...	...	...	5.1	-15	...	...	-
JPKS0423N-164	4 07 34.38	−44 15 17.6	18.92±0.06	20.17	18.62±0.05	19.48	...	...	...	4.6	-58	0.02	0.02	-
JPKS0423N-165	4 07 34.43	−44 13 13.5	20.46±0.09	21.24	18.97±0.09	20.49	...	...	...	2.8	-59	0.22	0.22	-
JPKS0423N-166	4 07 34.43	−44 13 39.0	20.05±0.15	21.43	18.34±0.07	20.29	...	...	...	6.2	-15	0.04	0.04	-
JPKS0423N-167	4 07 34.65	−44 18 08.1	19.97±0.14	21.22	18.96±0.09	20.45	18.01±0.12	19.14	1.97±0.19	5.2	54	...	...	-
JPKS0423N-168	4 07 34.93	−44 19 45.7	20.70±0.21	21.59	19.70±0.09	20.46	...	...	...	5.0	-16	0.01	0.01	-
JPKS0423N-169	4 07 35.11	−44 15 05.9	18.76±0.06	19.97	18.30±0.04	19.18	18.15±0.14	18.96	0.61±0.15	4.9	28	0.04	0.04	3
JPKS0423N-170	4 07 35.23	−44 16 00.0	19.63±0.13	21.79	19.26±0.12	20.98	...	...	...	7.5	-31	...	...	-
JPKS0423N-171	4 07 35.31	−44 16 36.1	19.56±0.12	20.80	19.17±0.07	20.10	...	...	...	5.5	62	0.01	0.01	-
JPKS0423N-172	4 07 35.36	−44 16 04.7	18.69±0.09	20.60	18.32±0.07	19.85	...	...	...	6.6	-43	0.01	0.01	-
JPKS0423N-173	4 07 35.41	−44 18 52.4	18.07±0.05	20.23	18.14±0.04	19.28	17.54±0.08	18.35	0.53±0.09	6.4	72	0.01	0.01	-
JPKS0423N-174	4 07 35.45	−44 15 38.4	19.15±0.10	21.22	19.35±0.12	20.55	...	...	...	7.0	-24	...	...	-
JPKS0423N-175	4 07 35.47	−44 18 33.5	19.25±0.11	21.34	18.73±0.06	20.29	18.06±0.15	19.10	1.19±0.19	6.7	-32	...	...	-
JPKS0423N-176	4 07 35.53	−44 19 22.5	19.98±0.15	21.89	...	...	...	...	...	7.7	-87	0.01	0.01	-
JPKS0423N-177	4 07 35.58	−44 16 26.9	20.33±0.17	21.82	...	...	...	...	...	7.3	-10	0.01	0.01	-

Table B.2 continued...

Ident.	RA (J2000) h m s	DEC (J2000) ° ′ ″	J mag	μ_J^c mag/arcsec^2	H mag	μ_H^c mag/arcsec^2	K_s mag	$\mu_{K_s}^c$ mag/arcsec^2	$J-K_s$ mag	D_J ″	PA °	ε	Class	Morph
(1)	(2a)	(2b)	(3)	(4)	(5)	(6)	(7)	(8)	(9)	(10)	(11)	(12)	(13)	
JPKS0423N-178	4 07 35.62	−44 17 53.8	19.82±0.14	21.90	...	...	...	...	...	7.9	-65	...	...	-
JPKS0423N-179	4 07 35.62	−44 15 44.8	20.56±0.21	21.92	...	...	...	...	...	7.6	-8	0.01	0.01	-
JPKS0423N-180	4 07 35.67	−44 16 09.4	17.99±0.06	20.89	18.18±0.05	19.85	17.85±0.14	18.75	0.14±0.16	6.6	-43	...	...	-
JPKS0423N-181	4 07 35.74	−44 15 34.2	18.34±0.06	20.25	17.72±0.04	19.40	16.88±0.07	18.21	1.47±0.09	5.5	6	0.01	0.01	-
JPKS0423N-182	4 07 35.77	−44 19 11.5	19.36±0.11	21.96	...	...	...	...	...	7.6	-88	...	...	-
JPKS0423N-183	4 07 35.80	−44 16 19.6	18.74±0.09	21.08	18.74±0.06	19.97	18.08±0.15	18.63	0.66±0.17	6.6	-35	...	...	-
JPKS0423N-184	4 07 35.89	−44 17 18.8	18.54±0.06	20.47	17.92±0.04	19.33	17.05±0.08	18.50	1.49±0.10	6.1	-2	0.01	0.01	-
JPKS0423N-185	4 07 36.07	−44 18 36.7	18.98±0.09	21.03	18.87±0.08	20.18	...	...	...	6.8	81	...	...	-
JPKS0423N-186	4 07 36.08	−44 16 48.9	19.65±0.13	21.17	19.17±0.11	20.37	...	...	...	6.9	14	0.02	0.02	-
JPKS0423N-187	4 07 36.10	−44 14 15.1	16.84±0.01	18.50	16.15±0.01	17.64	15.64±0.02	16.82	1.20±0.03	4.0	-23	0.03	0.03	3
JPKS0423N-188	4 07 36.19	−44 13 25.0	18.19±0.05	20.48	17.91±0.04	19.41	17.55±0.11	18.65	0.64±0.12	5.9	68	0.01	0.01	-
JPKS0423N-189	4 07 36.24	−44 16 03.1	20.27±0.20	21.63	...	...	...	...	...	6.0	-37	...	...	-
JPKS0423N-190	4 07 36.32	−44 19 48.2	20.78±0.23	21.67	...	...	...	...	...	5.7	21	...	...	-
JPKS0423N-191	4 07 36.49	−44 14 15.7	19.72±0.11	20.38	18.90±0.09	19.85	...	...	...	4.1	79	0.03	0.03	-
JPKS0423N-192	4 07 36.91	−44 14 25.5	15.53±0.00	17.99	14.73±0.00	17.21	14.20±0.01	16.48	1.33±0.01	3.0	-24	0.03	0.03	2
JPKS0423N-193	4 07 37.04	−44 13 42.6	17.60±0.02	18.81	16.84±0.02	18.11	16.64±0.07	17.74	0.96±0.07	3.0	30	0.19	0.19	3
JPKS0423N-194	4 07 37.17	−44 16 07.7	20.20±0.08	20.82	19.50±0.08	20.16	...	...	...	2.7	17	0.55	0.55	3
JPKS0423N-195	4 07 37.22	−44 14 46.3	19.00±0.07	20.67	18.36±0.07	20.03	17.88±0.14	19.22	1.12±0.16	4.3	72	0.01	0.01	-
JPKS0423N-196	4 07 37.24	−44 14 13.6	19.24±0.05	20.61	18.83±0.08	19.86	...	...	...	2.8	-46	0.01	0.01	-
JPKS0423N-197	4 07 37.40	−44 13 10.5	20.62±0.15	21.36	19.66±0.08	20.66	...	...	...	4.9	-9	0.65	0.65	-
JPKS0423N-198	4 07 37.50	−44 14 50.9	18.16±0.03	20.32	17.46±0.03	19.27	16.85±0.07	18.17	1.31±0.08	3.0	13	0.01	0.01	-
JPKS0423N-199	4 07 37.64	−44 16 27.4	19.51±0.09	20.78	19.64±0.09	20.63	...	...	...	4.9	15	0.08	0.08	-
JPKS0423N-200	4 07 37.65	−44 18 40.9	19.37±0.06	21.13	18.79±0.06	20.02	18.18±0.13	19.14	1.19±0.14	2.7	-5	...	...	-
JPKS0423N-201	4 07 37.70	−44 16 04.7	18.11±0.02	19.53	17.46±0.02	18.84	17.05±0.09	18.35	1.06±0.09	2.9	-78	0.03	0.03	3
JPKS0423N-202	4 07 37.71	−44 17 20.8	19.17±0.05	20.23	18.76±0.05	19.51	17.80±0.08	18.56	1.36±0.09	2.8	-26	0.10	0.10	-
JPKS0423N-203	4 07 37.89	−44 14 07.5	20.21±0.13	21.17	...	...	...	...	...	5.6	70	0.58	0.58	-
JPKS0423N-204	4 07 38.00	−44 13 48.8	18.93±0.05	20.47	18.07±0.03	19.53	17.29±0.10	18.30	1.65±0.11	3.4	5	0.02	0.02	-
JPKS0423N-205	4 07 38.10	−44 15 17.7	15.10±0.00	17.04	14.35±0.00	16.37	13.95±0.01	15.64	1.15±0.01	3.0	-66	0.03	0.03	1
JPKS0423N-206	4 07 38.14	−44 17 08.2	18.14±0.03	20.10	17.53±0.03	19.42	17.13±0.06	18.68	1.01±0.07	3.6	-42	0.01	0.01	-
JPKS0423N-207	4 07 38.17	−44 19 10.7	20.01±0.07	21.25	18.79±0.08	20.37	...	...	...	2.7	-85	...	...	-

Table B.2 continued...

Ident.	RA (J2000) h m s	DEC (J2000) ° ′ ″	J mag	μ_J^c mag/arcsec^2	H mag	μ_H^c mag/arcsec^2	K_s mag	$\mu_{K_s}^c$ mag/arcsec^2	J–K_s mag	D_J ″	PA °	ε	Class	Morph
(1)	(2a)	(2b)	(3)	(4)	(5)	(6)	(7)	(8)	(9)	(10)	(11)	(12)	(13)	
JPKS0423N-208	4 07 38.31	−44 19 04.5	19.95±0.09	21.10	18.93±0.06	20.31	...	...	...	3.3	5	0.05	0.05	-
JPKS0423N-209	4 07 38.40	−44 13 19.7	19.74±0.11	21.48	19.68±0.10	21.10	...	...	...	5.8	76	...	...	-
JPKS0423N-210	4 07 38.96	−44 17 17.1	20.23±0.14	21.36	...	...	...	...	...	5.9	-73	0.20	0.20	-
JPKS0423N-211	4 07 39.08	−44 14 22.2	17.91±0.02	18.89	...	...	17.83±0.08	18.27	0.08±0.09	2.7	38	0.86	0.86	-
JPKS0423N-212	4 07 39.17	−44 12 26.5	19.87±0.11	21.08	19.00±0.07	20.25	...	...	...	4.3	-42	0.01	0.01	-
JPKS0423N-213	4 07 39.51	−44 16 54.3	19.43±0.10	21.31	19.30±0.10	20.76	...	...	...	6.3	6	...	...	-
JPKS0423N-214	4 07 39.96	−44 19 33.2	19.48±0.06	20.81	18.22±0.04	19.45	17.27±0.08	18.43	2.22±0.10	2.7	-75	0.01	0.01	-
JPKS0423N-215	4 07 40.25	−44 18 57.0	18.14±0.02	19.15	...	...	...	...	...	2.7	-6	0.67	0.67	-
JPKS0423N-216	4 07 40.35	−44 13 51.7	18.65±0.04	20.38	17.93±0.03	19.85	17.50±0.14	18.99	1.15±0.14	2.9	44	0.01	0.01	-
JPKS0423N-217	4 07 40.82	−44 16 32.8	20.18±0.13	21.73	19.29±0.11	20.75	...	...	...	6.7	9	0.03	0.03	-
JPKS0423N-218	4 07 40.99	−44 12 45.1	18.94±0.08	20.78	18.86±0.09	20.09	...	...	...	5.5	43	...	...	-
JPKS0423N-219	4 07 41.14	−44 13 21.8	19.29±0.10	21.63	19.06±0.12	20.60	...	...	...	6.3	75	...	...	-
JPKS0423N-220	4 07 41.22	−44 14 22.1	19.04±0.08	20.84	18.69±0.07	19.95	18.06±0.15	18.62	0.98±0.17	6.3	21	0.16	0.16	-
JPKS0423N-221	4 07 41.27	−44 15 27.7	18.49±0.03	19.54	...	...	17.47±0.12	18.44	1.02±0.12	3.1	11	0.49	0.49	3
JPKS0423N-222	4 07 41.35	−44 18 52.8	16.22±0.01	18.51	15.49±0.01	17.64	14.78±0.02	16.85	1.43±0.02	3.3	-77	0.03	0.03	3
JPKS0423N-223	4 07 41.68	−44 13 43.3	19.74±0.07	21.26	19.04±0.10	20.48	18.11±0.17	19.20	1.63±0.18	2.7	-14	...	...	3
JPKS0423N-224	4 07 41.76	−44 12 55.4	19.66±0.11	21.19	19.13±0.09	20.40	...	...	...	5.9	-26	0.05	0.05	-
JPKS0423N-225	4 07 41.95	−44 16 48.9	14.52±0.00	17.09	13.78±0.00	16.21	13.49±0.01	15.61	1.03±0.01	2.9	82	0.03	0.03	1
JPKS0423N-226	4 07 42.25	−44 12 36.8	19.74±0.11	21.65	...	...	...	...	...	6.7	-76	...	...	-
JPKS0423N-227	4 07 42.29	−44 16 00.2	19.02±0.06	20.33	18.04±0.04	19.33	17.26±0.09	18.41	1.76±0.11	4.0	15	0.02	0.02	-
JPKS0423N-228	4 07 42.40	−44 13 40.7	18.75±0.06	21.04	17.79±0.05	19.92	17.63±0.12	19.07	1.12±0.14	3.6	-16	...	...	-
JPKS0423N-229	4 07 42.59	−44 13 44.9	19.99±0.11	21.31	18.80±0.10	20.62	...	...	...	5.0	50	0.32	0.32	-
JPKS0423N-230	4 07 42.67	−44 19 30.6	19.22±0.05	20.98	18.31±0.06	20.24	17.76±0.13	19.18	1.46±0.14	2.9	-35	...	...	-
JPKS0423N-231	4 07 42.73	−44 18 18.8	18.57±0.03	19.58	17.99±0.04	18.94	17.90±0.10	18.61	0.67±0.10	2.7	84	0.76	0.76	-
JPKS0423N-232	4 07 42.90	−44 18 00.2	19.38±0.08	20.32	18.34±0.08	19.80	...	...	...	4.1	56	0.21	0.21	-
JPKS0423N-233	4 07 42.94	−44 14 24.3	20.03±0.11	21.34	...	...	...	...	...	4.8	-46	0.10	0.10	-
JPKS0423N-234	4 07 43.06	−44 12 38.1	19.84±0.13	21.49	...	...	...	...	...	7.8	54	0.41	0.41	-
JPKS0423N-235	4 07 43.09	−44 17 53.9	18.92±0.04	20.05	18.40±0.06	19.62	...	...	...	2.7	56	0.18	0.18	-
JPKS0423N-236	4 07 43.14	−44 18 06.7	15.07±0.00	17.94	14.32±0.00	17.14	14.07±0.01	16.68	1.00±0.01	3.2	-68	0.03	0.03	2
JPKS0423N-237	4 07 43.33	−44 15 58.9	19.34±0.05	20.89	18.70±0.09	20.12	17.58±0.13	19.20	1.75±0.14	2.7	-87	...	...	2

Table B.2 continued...

Ident.	RA (J2000) h m s	DEC (J2000) ° ′ ″	J mag	μ_J^c mag/arcsec^2	H mag	μ_H^c mag/arcsec^2	K_s mag	$\mu_{K_s}^c$ mag/arcsec^2	$J-K_s$ mag	D_J ″	PA °	ε	Class	Morph
(1)	(2a)	(2b)	(3)	(4)	(5)	(6)	(7)	(8)	(9)	(10)	(11)	(12)	(13)	
JPKS0423N-238	4 07 43.41	−44 14 44.2	18.70±0.04	19.68	18.04±0.03	19.06	17.64±0.10	18.52	1.06±0.11	3.2	-68	0.86	0.86	3
JPKS0423N-239	4 07 43.47	−44 16 36.5	20.09±0.09	21.54	19.59±0.17	21.20	...	...	...	3.3	84	...	...	3
JPKS0423N-240	4 07 43.63	−44 18 52.7	20.27±0.08	21.31	18.97±0.08	20.24	...	...	...	2.7	-45	0.49	0.49	3
JPKS0423N-241	4 07 43.67	−44 18 40.3	18.90±0.04	20.08	18.04±0.03	19.14	17.30±0.07	18.29	1.60±0.08	2.7	-13	0.09	0.09	3
JPKS0423N-242	4 07 43.91	−44 14 14.5	20.35±0.10	21.34	19.08±0.09	20.23	...	...	...	3.4	50	0.18	0.18	3
JPKS0423N-243	4 07 43.95	−44 15 45.9	20.50±0.14	21.53	19.05±0.10	20.64	...	...	...	4.8	44	0.15	0.15	3
JPKS0423N-244	4 07 44.28	−44 15 46.9	18.25±0.04	20.07	17.33±0.03	19.15	16.63±0.07	18.12	1.62±0.08	3.8	35	0.01	0.01	-
JPKS0423N-245	4 07 44.50	−44 15 59.9	18.37±0.04	19.96	17.52±0.03	18.84	16.92±0.07	17.92	1.44±0.08	4.4	-11	0.03	0.03	3
JPKS0423N-246	4 07 44.68	−44 15 55.5	20.08±0.14	21.32	18.92±0.10	20.64	...	...	...	5.9	16	0.20	0.20	3
JPKS0423N-247	4 07 45.14	−44 17 29.0	18.07±0.04	19.83	17.48±0.03	18.95	16.94±0.08	18.28	1.13±0.09	4.8	8	0.03	0.03	3
JPKS0423N-248	4 07 45.40	−44 15 59.8	20.24±0.14	21.30	18.61±0.06	20.30	18.04±0.16	18.87	2.20±0.22	4.6	-75	...	...	3
JPKS0423N-249	4 07 45.61	−44 12 55.6	19.72±0.06	20.48	19.29±0.07	20.10	...	...	...	2.7	-85	0.45	0.45	3
JPKS0423N-250	4 07 46.08	−44 12 20.9	19.96±0.09	20.89	18.99±0.09	20.29	...	...	...	3.4	-73	0.21	0.21	-
JPKS0423N-251	4 07 46.19	−44 17 58.0	19.87±0.11	21.50	19.55±0.13	20.30	...	...	...	6.7	46	0.60	0.60	-
JPKS0423N-252	4 07 46.20	−44 15 54.0	18.81±0.07	20.47	18.37±0.06	19.68	17.93±0.15	18.79	0.87±0.16	6.3	36	0.01	0.01	-
JPKS0423N-253	4 07 46.38	−44 13 16.8	19.92±0.12	21.60	19.35±0.12	20.80	...	...	...	6.5	64	0.01	0.01	-
JPKS0423N-254	4 07 46.41	−44 14 43.3	19.23±0.08	21.08	19.20±0.07	20.45	...	...	...	5.3	-43	0.05	0.05	-
JPKS0423N-255	4 07 46.82	−44 19 59.6	19.85±0.06	20.68	...	...	...	...	...	2.7	87	0.09	0.09	-
JPKS0423N-256	4 07 46.85	−44 17 17.6	19.92±0.07	20.80	19.08±0.10	20.24	...	...	...	2.7	37	0.14	0.14	-
JPKS0423N-257	4 07 46.87	−44 18 27.4	19.93±0.12	21.42	18.74±0.09	20.15	...	...	...	5.8	-55	0.11	0.11	-
JPKS0423N-258	4 07 47.00	−44 12 53.0	19.44±0.08	20.74	17.87±0.05	20.01	...	...	...	3.9	-40	0.02	0.02	-
JPKS0423N-259	4 07 47.06	−44 17 50.1	15.90±0.00	17.17	...	...	...	...	...	2.7	-26	0.79	0.79	-
JPKS0423N-260	4 07 47.21	−44 18 31.9	19.76±0.09	20.87	18.85±0.08	20.11	18.00±0.13	18.85	1.77±0.16	4.2	22	0.41	0.41	-
JPKS0423N-261	4 07 47.74	−44 18 09.2	20.27±0.15	21.50	...	...	...	...	...	6.3	-45	0.52	0.52	-
JPKS0423N-262	4 07 47.88	−44 15 03.8	17.64±0.01	19.10	16.88±0.01	18.25	16.33±0.04	17.46	1.31±0.04	2.7	1	0.03	0.03	-
JPKS0423N-263	4 07 47.91	−44 17 49.4	19.60±0.10	21.21	19.20±0.13	20.69	...	...	...	6.4	-61	0.27	0.27	-
JPKS0423N-264	4 07 47.98	−44 15 14.7	20.33±0.08	20.94	19.76±0.08	20.32	...	...	...	2.7	-43	0.34	0.34	-
JPKS0423N-265	4 07 48.14	−44 19 35.8	19.62±0.06	20.67	18.91±0.09	20.01	...	...	...	2.7	-52	0.12	0.12	-
JPKS0423N-266	4 07 48.25	−44 18 57.7	20.27±0.14	21.58	19.73±0.11	20.90	...	...	...	5.6	-17	0.07	0.07	-
JPKS0423N-267	4 07 48.36	−44 17 49.5	17.71±0.02	18.81	...	...	...	...	...	3.2	-22	0.81	0.81	3

Table B.2 continued...

Ident.	RA (J2000) h m s	DEC (J2000) ° ′ ″	J mag	μ_J^c mag/arcsec^2	H mag	μ_H^c mag/arcsec^2	K_s mag	$\mu_{K_s}^c$ mag/arcsec^2	$J-K_s$ mag	D_J ″	PA °	ε	Class	Morph
(1)	(2a)	(2b)	(3)	(4)	(5)	(6)	(7)	(8)	(9)	(10)	(11)	(12)	(13)	
JPKS0423N-268	4 07 48.42	−44 17 45.8	18.82±0.04	19.98	18.17±0.05	19.20	18.13±0.12	18.83	0.69±0.13	3.7	-34	0.50	0.50	3
JPKS0423N-269	4 07 48.49	−44 19 25.8	18.86±0.04	20.47	17.99±0.03	19.50	17.08±0.08	18.39	1.78±0.09	2.7	34	0.01	0.01	3
JPKS0423N-270	4 07 48.51	−44 13 47.9	19.00±0.07	20.84	18.53±0.06	20.46	...	...	...	4.2	31	...	...	-
JPKS0423N-271	4 07 48.53	−44 13 18.2	18.45±0.04	19.85	...	...	17.90±0.13	18.73	0.54±0.14	4.0	60	0.11	0.11	3
JPKS0423N-272	4 07 48.54	−44 19 54.2	20.06±0.13	21.62	...	...	...	...	...	6.2	64	0.02	0.02	3
JPKS0423N-273	4 07 48.67	−44 12 34.8	19.85±0.12	21.34	19.22±0.09	20.63	...	...	...	5.2	-88	...	...	-
JPKS0423N-274	4 07 49.26	−44 19 38.6	18.99±0.08	21.42	18.81±0.09	20.38	17.95±0.13	19.10	1.04±0.15	6.3	6	...	...	-
JPKS0423N-275	4 07 49.58	−44 17 53.7	20.50±0.09	21.26	19.75±0.15	20.57	...	...	...	2.7	85	0.19	0.19	-
JPKS0423N-276	4 07 49.63	−44 12 20.4	19.98±0.12	21.60	...	...	...	...	...	6.7	36	0.47	0.47	-
JPKS0423N-277	4 07 49.91	−44 18 14.6	19.70±0.06	20.65	19.03±0.06	20.06	...	...	...	2.7	-58	0.37	0.37	-
JPKS0423N-278	4 07 50.00	−44 17 49.4	18.58±0.03	20.10	17.71±0.03	19.05	16.90±0.08	18.09	1.68±0.08	2.7	-4	0.02	0.02	-
JPKS0423N-279	4 07 50.10	−44 12 57.7	18.96±0.04	20.18	18.01±0.04	19.35	17.41±0.07	18.35	1.56±0.08	2.7	-24	0.06	0.06	-
JPKS0423N-280	4 07 50.19	−44 17 39.5	18.91±0.05	20.81	17.75±0.03	19.42	17.03±0.08	18.66	1.89±0.09	3.1	-23	...	...	-
JPKS0423N-281	4 07 50.21	−44 16 52.5	18.56±0.03	20.10	17.56±0.02	19.13	17.01±0.08	18.39	1.55±0.08	2.7	67	0.01	0.01	-
JPKS0423N-282	4 07 51.53	−44 16 31.4	19.75±0.11	21.43	19.15±0.10	20.91	...	...	...	6.4	-55	0.04	0.04	-
JPKS0423N-283	4 07 51.82	−44 17 45.3	20.01±0.12	21.76	...	...	...	...	...	6.8	-68	0.05	0.05	-
JPKS0423N-284	4 07 51.95	−44 17 25.7	19.74±0.12	21.45	...	...	...	...	...	6.7	47	...	...	-
JPKS0423N-285	4 07 51.96	−44 15 54.3	16.96±0.03	20.56	16.94±0.02	20.05	...	...	...	4.6	-46	...	...	-
JPKS0423N-286	4 07 51.97	−44 13 47.5	19.81±0.12	21.17	...	...	...	...	...	5.3	88	0.06	0.06	-
JPKS0423N-287	4 07 52.10	−44 15 15.8	17.72±0.01	18.73	...	...	...	...	...	2.7	82	0.74	0.74	-
JPKS0423N-288	4 07 52.13	−44 15 43.4	19.64±0.07	20.94	18.79±0.05	20.22	17.89±0.14	19.17	1.74±0.16	3.0	30	0.03	0.03	-
JPKS0423N-289	4 07 52.24	−44 13 48.6	19.82±0.13	21.26	...	...	...	...	...	5.3	47	0.01	0.01	-
JPKS0423N-290	4 07 52.30	−44 18 49.5	20.67±0.11	20.97	20.19±0.10	20.83	...	...	...	3.2	24	0.69	0.69	-

Table B.3: Galaxies found in the Western field.

Ident.	RA (J2000) h m s	DEC (J2000) ° ′ ″	J mag	μ_J^c mag/arcsec^2	H mag	μ_H^c mag/arcsec^2	K_s mag	$\mu_{K_s}^c$ mag/arcsec^2	$J-K_s$ mag	D_J ″	PA °	ε	Class	Morph
(1)	(2a)	(2b)	(3)	(4)	(5)	(6)	(7)	(8)	(9)	(10)	(11)	(12)	(13)	
JPKS0423W-001	4 06 19.04	−44 26 22.1	19.79±0.08	21.16	...	...	...	...	...	3.3	-70	0.40	0.40	-
JPKS0423W-002	4 06 19.05	−44 27 00.7	19.52±0.07	20.96	...	...	...	...	...	2.7	-4	0.03	0.03	-
JPKS0423W-003	4 06 19.13	−44 27 16.3	19.52±0.10	21.05	...	...	...	...	...	4.8	51	0.03	0.03	-
JPKS0423W-004	4 06 19.24	−44 26 53.8	20.50±0.17	21.22	...	...	...	...	...	5.6	-46	0.49	0.49	-
JPKS0423W-005	4 06 19.30	−44 22 39.5	19.15±0.09	20.73	...	...	...	...	...	5.2	77	0.11	0.11	-
JPKS0423W-006	4 06 19.30	−44 22 57.4	20.40±0.10	21.21	...	...	...	...	...	2.9	21	0.39	0.39	-
JPKS0423W-007	4 06 19.34	−44 25 37.2	19.63±0.11	21.18	20.11±0.23	21.04	...	...	...	3.9	-47	...	...	-
JPKS0423W-008	4 06 19.45	−44 23 30.6	20.33±0.09	20.77	19.75±0.09	20.30	...	...	...	2.7	3	0.60	0.60	-
JPKS0423W-009	4 06 19.49	−44 23 21.8	18.56±0.03	19.56	18.44±0.05	19.45	...	...	...	2.7	20	0.11	0.11	-
JPKS0423W-010	4 06 19.55	−44 22 34.3	20.13±0.11	20.70	...	...	...	...	...	4.4	-37	0.55	0.55	-
JPKS0423W-011	4 06 19.57	−44 22 38.2	20.31±0.09	20.96	...	...	...	...	...	3.6	-1	0.38	0.38	-
JPKS0423W-012	4 06 19.59	−44 28 04.5	20.04±0.09	21.14	19.48±0.09	20.92	...	...	...	3.6	11	0.15	0.15	-
JPKS0423W-013	4 06 19.61	−44 27 50.6	19.88±0.11	21.02	18.54±0.05	19.81	...	...	...	4.4	19	0.34	0.34	-
JPKS0423W-014	4 06 19.69	−44 23 11.6	20.39±0.10	21.34	...	...	...	...	...	2.7	19	0.08	0.08	-
JPKS0423W-015	4 06 19.80	−44 24 55.4	19.36±0.05	20.49	18.05±0.04	19.22	17.00±0.07	18.31	2.36±0.08	2.7	-10	0.05	0.05	-
JPKS0423W-016	4 06 20.15	−44 28 18.9	19.43±0.06	20.51	18.24±0.06	19.67	18.07±0.12	18.66	1.36±0.13	2.7	-35	0.06	0.06	-
JPKS0423W-017	4 06 20.36	−44 22 26.4	19.58±0.10	20.89	...	...	...	...	...	6.1	-64	0.54	0.54	-
JPKS0423W-018	4 06 20.54	−44 25 50.0	20.11±0.08	20.74	...	...	...	...	...	2.7	87	0.65	0.65	-
JPKS0423W-019	4 06 20.60	−44 25 56.4	19.03±0.09	20.67	18.17±0.08	19.89	...	...	...	4.9	-29	0.01	0.01	-
JPKS0423W-020	4 06 20.76	−44 24 54.2	20.24±0.16	21.23	...	...	...	...	...	5.6	-3	0.51	0.51	-
JPKS0423W-021	4 06 20.84	−44 22 43.4	20.04±0.11	21.26	...	...	...	...	...	4.8	-41	0.57	0.57	-
JPKS0423W-022	4 06 21.23	−44 22 49.1	19.33±0.08	20.90	18.47±0.09	20.40	...	...	...	4.0	-63	0.02	0.02	-
JPKS0423W-023	4 06 21.27	−44 27 52.4	19.80±0.13	21.33	...	...	...	...	...	7.3	22	0.11	0.11	-
JPKS0423W-024	4 06 21.27	−44 29 03.3	19.46±0.09	21.20	...	...	...	...	...	7.5	-8	0.65	0.65	-
JPKS0423W-025	4 06 21.28	−44 28 28.1	19.58±0.11	21.42	...	...	...	...	...	6.9	-27	0.10	0.10	-
JPKS0423W-026	4 06 21.29	−44 26 27.8	20.24±0.14	21.22	...	...	...	...	...	5.4	-36	0.53	0.53	-
JPKS0423W-027	4 06 21.29	−44 28 58.6	18.76±0.07	20.86	...	...	...	...	...	6.6	-69	0.19	0.19	-

Table B.3 continued...

Ident.	RA (J2000) h m s	DEC (J2000) ° ′ ″	J mag	μ_J^c mag/arcsec^2	H mag	μ_H^c mag/arcsec^2	K_s mag	$\mu_{K_s}^c$ mag/arcsec^2	$J-K_s$ mag	D_J ″	PA °	ε	Class	Morph
(1)	(2a)	(2b)	(3)	(4)	(5)	(6)	(7)	(8)	(9)	(10)	(11)	(12)	(13)	
JPKS0423W-028	4 06 21.30	−44 27 40.1	19.93±0.14	21.27	...	...	...	...	...	6.1	-26	0.52	0.52	-
JPKS0423W-029	4 06 21.30	−44 28 43.8	18.39±0.04	19.96	17.78±0.05	19.37	17.12±0.07	18.56	1.27±0.08	3.4	-22	0.02	0.02	3
JPKS0423W-030	4 06 21.30	−44 24 21.4	19.19±0.10	21.31	...	...	...	...	...	7.2	-7	...	...	-
JPKS0423W-031	4 06 21.31	−44 28 48.3	18.83±0.07	21.17	...	...	...	...	...	6.4	-10	0.31	0.31	-
JPKS0423W-032	4 06 21.31	−44 25 14.3	19.63±0.12	21.09	...	...	...	...	...	6.4	-10	0.27	0.27	-
JPKS0423W-033	4 06 21.31	−44 28 52.8	19.26±0.09	21.21	...	...	...	...	...	6.9	-28	0.10	0.10	-
JPKS0423W-034	4 06 21.32	−44 28 55.1	19.20±0.09	21.21	...	...	...	...	...	5.7	50	...	...	-
JPKS0423W-035	4 06 21.33	−44 23 43.5	19.20±0.10	21.22	18.50±0.09	20.66	...	...	...	7.1	-5	0.01	0.01	-
JPKS0423W-036	4 06 21.33	−44 26 13.0	19.29±0.09	21.34	...	...	...	...	...	6.9	4	0.09	0.09	-
JPKS0423W-037	4 06 21.33	−44 26 31.1	19.41±0.11	21.13	...	...	...	...	...	6.2	-27	0.54	0.54	-
JPKS0423W-038	4 06 21.33	−44 25 03.7	19.84±0.12	21.39	...	...	...	...	...	7.0	9	0.52	0.52	-
JPKS0423W-039	4 06 21.34	−44 27 49.4	20.37±0.16	21.40	...	...	...	...	...	5.4	45	0.15	0.15	-
JPKS0423W-040	4 06 21.35	−44 22 34.7	19.82±0.12	21.12	...	...	...	...	...	5.5	10	0.46	0.46	-
JPKS0423W-041	4 06 21.56	−44 26 35.9	19.74±0.13	21.20	...	...	...	...	...	6.8	-1	0.43	0.43	-
JPKS0423W-042	4 06 21.93	−44 24 25.0	19.64±0.08	20.65	19.23±0.08	19.91	...	...	...	3.5	-60	0.59	0.59	-
JPKS0423W-043	4 06 21.99	−44 27 08.5	19.66±0.07	20.76	19.22±0.08	20.11	...	...	...	3.0	1	0.07	0.07	-
JPKS0423W-044	4 06 22.11	−44 28 05.1	19.53±0.06	20.84	18.83±0.10	20.02	...	...	...	2.7	86	...	...	-
JPKS0423W-045	4 06 22.21	−44 23 55.3	19.20±0.07	20.70	18.71±0.06	19.74	...	...	...	3.7	7	0.07	0.07	-
JPKS0423W-046	4 06 22.97	−44 23 16.6	20.02±0.14	21.33	...	...	...	...	...	7.1	-45	0.63	0.63	-
JPKS0423W-047	4 06 23.22	−44 28 52.3	18.09±0.04	19.58	17.44±0.03	18.75	16.79±0.07	17.93	1.31±0.08	4.1	-23	0.02	0.02	3
JPKS0423W-048	4 06 23.38	−44 25 01.9	19.58±0.09	20.80	19.29±0.10	20.08	...	...	...	4.6	-16	0.08	0.08	-
JPKS0423W-049	4 06 23.57	−44 28 19.7	16.98±0.02	19.62	16.54±0.02	19.06	16.06±0.05	18.38	0.92±0.05	3.6	3	0.02	0.02	3
JPKS0423W-050	4 06 23.84	−44 28 58.7	16.09±0.01	18.10	15.31±0.01	17.22	14.69±0.02	16.46	1.40±0.02	3.3	29	0.03	0.03	2
JPKS0423W-051	4 06 24.01	−44 23 17.7	18.10±0.05	20.23	17.50±0.03	19.27	16.89±0.07	18.09	1.21±0.09	4.8	43	0.01	0.01	-
JPKS0423W-052	4 06 24.06	−44 28 05.0	19.94±0.13	21.40	19.29±0.11	20.39	...	...	...	5.5	33	...	...	-
JPKS0423W-053	4 06 24.36	−44 24 33.6	19.16±0.10	21.63	18.57±0.09	20.85	...	...	...	6.4	-58	...	...	-
JPKS0423W-054	4 06 24.44	−44 26 47.1	18.87±0.04	20.26	17.99±0.04	19.47	17.64±0.14	18.69	1.24±0.14	2.7	0	0.02	0.02	-
JPKS0423W-055	4 06 25.00	−44 21 46.1	20.39±0.08	20.84	19.52±0.14	21.18	...	...	...	2.7	-29	0.60	0.60	-
JPKS0423W-056	4 06 25.30	−44 28 07.0	18.48±0.05	20.20	19.59±0.14	20.89	17.37±0.11	18.43	1.11±0.12	4.8	44	0.01	0.01	-
JPKS0423W-057	4 06 25.32	−44 28 01.6	17.14±0.01	18.22	...	...	...	...	...	2.7	11	0.86	0.86	-

Table B.3 continued...

Ident.	RA (J2000) h m s	DEC (J2000) ° ′ ″	J mag	μ_J^c mag/arcsec^2	H mag	μ_H^c mag/arcsec^2	K_s mag	$\mu_{K_s}^c$ mag/arcsec^2	$J-K_s$ mag	D_J ″	PA °	ϵ	Class	Morph
(1)	(2a)	(2b)	(3)	(4)	(5)	(6)	(7)	(8)	(9)	(10)	(11)	(12)	(13)	
JPKS0423W-058	4 06 25.73	−44 27 31.7	18.90±0.06	20.25	18.35±0.05	19.43	17.76±0.14	18.63	1.14±0.15	3.9	-3	0.12	0.12	-
JPKS0423W-059	4 06 25.79	−44 23 03.6	19.25±0.06	20.24	18.20±0.04	19.39	17.48±0.07	18.19	1.77±0.10	3.2	50	0.25	0.25	-
JPKS0423W-060	4 06 26.48	−44 23 55.8	19.97±0.14	21.47	...	...	...	...	...	7.4	4	0.50	0.50	-
JPKS0423W-061	4 06 26.55	−44 27 25.2	18.24±0.03	19.61	17.69±0.03	18.97	17.15±0.11	18.56	1.09±0.12	3.7	-59	0.04	0.04	3
JPKS0423W-062	4 06 26.69	−44 28 01.5	19.64±0.09	20.92	19.13±0.08	20.12	...	...	...	4.0	24	0.10	0.10	-
JPKS0423W-063	4 06 27.05	−44 25 31.3	20.14±0.08	20.87	18.86±0.10	20.41	...	...	...	2.7	74	0.58	0.58	-
JPKS0423W-064	4 06 27.17	−44 23 11.7	18.05±0.03	19.62	17.26±0.02	18.98	16.76±0.06	18.04	1.30±0.07	2.7	-18	0.02	0.02	-
JPKS0423W-065	4 06 27.20	−44 24 19.9	19.51±0.07	21.34	18.96±0.12	20.93	...	...	...	2.7	65	...	...	-
JPKS0423W-066	4 06 27.21	−44 22 19.2	19.89±0.10	21.32	18.98±0.13	20.82	...	...	...	3.9	25	...	...	-
JPKS0423W-067	4 06 27.55	−44 27 25.3	19.14±0.08	20.77	18.39±0.06	19.96	...	...	...	5.2	13	0.05	0.05	-
JPKS0423W-068	4 06 27.81	−44 22 21.3	19.39±0.10	21.35	19.35±0.12	20.34	...	...	...	7.2	-74	0.08	0.08	-
JPKS0423W-069	4 06 28.53	−44 23 56.5	18.92±0.05	20.43	18.09±0.04	19.68	17.17±0.11	18.58	1.75±0.12	3.2	-37	0.01	0.01	-
JPKS0423W-070	4 06 28.57	−44 26 11.3	17.08±0.02	19.63	16.39±0.02	19.08	16.09±0.07	18.61	0.98±0.07	2.7	61	0.01	0.01	-
JPKS0423W-071	4 06 28.58	−44 28 26.3	20.07±0.08	21.01	19.41±0.11	20.16	...	...	...	2.7	19	0.39	0.39	-
JPKS0423W-072	4 06 28.67	−44 24 26.7	19.45±0.10	20.72	18.68±0.06	19.84	...	...	...	4.9	-22	0.10	0.10	-
JPKS0423W-073	4 06 28.88	−44 22 28.2	19.73±0.12	21.16	18.79±0.09	20.20	...	...	...	5.3	-16	0.01	0.01	-
JPKS0423W-074	4 06 29.60	−44 27 59.6	19.95±0.12	21.25	...	...	...	...	...	6.8	-44	0.59	0.59	-
JPKS0423W-075	4 06 29.64	−44 22 07.5	20.43±0.14	21.05	19.23±0.11	20.63	...	...	...	4.2	-22	0.65	0.65	-
JPKS0423W-076	4 06 29.90	−44 22 06.6	19.28±0.08	20.41	18.30±0.06	19.87	...	...	...	4.8	40	0.29	0.29	-
JPKS0423W-077	4 06 30.15	−44 29 01.4	19.63±0.11	21.24	19.26±0.10	20.52	...	...	...	4.7	52	...	...	-
JPKS0423W-078	4 06 30.18	−44 28 25.1	19.87±0.09	20.95	19.25±0.11	20.39	...	...	...	3.5	57	0.06	0.06	-
JPKS0423W-079	4 06 30.31	−44 25 37.1	19.56±0.06	20.45	18.72±0.06	19.52	...	...	...	2.7	-4	0.33	0.33	-
JPKS0423W-080	4 06 30.37	−44 26 51.6	18.27±0.03	19.18	...	...	17.82±0.11	18.27	0.46±0.12	3.0	1	0.78	0.78	3
JPKS0423W-081	4 06 31.04	−44 24 46.0	18.79±0.07	20.50	18.04±0.04	19.70	17.77±0.15	18.98	1.02±0.16	4.7	23	0.01	0.01	-
JPKS0423W-082	4 06 31.84	−44 28 24.8	16.79±0.01	18.36	16.05±0.01	17.52	15.63±0.03	16.92	1.16±0.03	2.8	-37	0.03	0.03	3
JPKS0423W-083	4 06 32.34	−44 21 45.2	18.95±0.05	19.90	18.26±0.04	19.30	...	...	...	3.1	-8	0.64	0.64	3
JPKS0423W-084	4 06 32.42	−44 21 40.0	19.44±0.09	20.95	19.22±0.07	20.27	17.86±0.13	18.75	1.58±0.16	4.5	40	0.04	0.04	-
JPKS0423W-085	4 06 32.45	−44 21 56.7	20.28±0.15	21.32	...	...	...	...	...	5.8	2	0.23	0.23	-
JPKS0423W-086	4 06 32.49	−44 27 54.9	19.41±0.06	20.83	18.81±0.06	20.04	...	...	...	2.7	-9	...	...	-
JPKS0423W-087	4 06 33.14	−44 22 04.0	20.01±0.14	21.21	...	...	...	...	...	6.1	-69	0.26	0.26	-

Table B.3 continued...

Ident.	RA (J2000) h m s	DEC (J2000) ° ′ ″	J mag	μ_J^c mag/arcsec^2	H mag	μ_H^c mag/arcsec^2	K_s mag	$\mu_{K_s}^c$ mag/arcsec^2	$J-K_s$ mag	D_J ″	PA °	ε	Class	Morph
(1)	(2a)	(2b)	(3)	(4)	(5)	(6)	(7)	(8)	(9)	(10)	(11)	(12)	(13)	
JPKS0423W-088	4 06 33.21	−44 27 48.1	18.76±0.06	20.07	18.42±0.06	19.62	...	...	...	4.5	52	0.12	0.12	-
JPKS0423W-089	4 06 33.38	−44 24 20.5	18.60±0.03	19.78	17.82±0.04	19.08	17.32±0.08	18.23	1.28±0.08	2.7	44	0.04	0.04	-
JPKS0423W-090	4 06 33.40	−44 27 03.9	20.02±0.13	21.59	19.08±0.11	20.64	...	...	...	5.8	-20	0.01	0.01	-
JPKS0423W-091	4 06 33.55	−44 28 33.7	18.17±0.03	20.02	17.44±0.03	18.92	16.84±0.07	18.10	1.33±0.07	2.9	-71	0.01	0.01	-
JPKS0423W-092	4 06 34.26	−44 22 07.7	19.03±0.04	19.88	18.57±0.05	19.50	...	...	...	2.7	74	0.74	0.74	-
JPKS0423W-093	4 06 34.36	−44 27 22.1	19.04±0.05	20.44	18.17±0.04	19.44	17.34±0.09	18.27	1.70±0.11	3.1	2	0.02	0.02	-
JPKS0423W-094	4 06 34.67	−44 27 13.0	18.63±0.06	19.91	17.45±0.04	19.09	17.22±0.10	18.34	1.41±0.12	4.4	25	0.13	0.13	3
JPKS0423W-095	4 06 34.74	−44 27 18.9	18.72±0.05	20.12	17.70±0.04	19.40	16.88±0.09	18.44	1.83±0.11	3.5	38	0.02	0.02	-
JPKS0423W-096	4 06 35.15	−44 27 57.6	19.00±0.05	20.73	18.33±0.06	20.05	17.63±0.14	18.98	1.37±0.15	3.0	40	...	...	-
JPKS0423W-097	4 06 35.29	−44 21 58.2	20.03±0.12	20.89	19.15±0.07	20.27	...	...	...	4.4	35	0.40	0.40	-
JPKS0423W-098	4 06 35.52	−44 28 57.7	20.09±0.12	21.26	...	...	...	...	...	5.0	54	0.09	0.09	-
JPKS0423W-099	4 06 35.53	−44 29 03.7	18.21±0.04	19.83	17.54±0.03	19.03	17.12±0.07	17.95	1.09±0.08	3.7	51	0.03	0.03	3
JPKS0423W-100	4 06 35.95	−44 28 19.2	17.34±0.02	19.84	16.68±0.02	19.21	16.29±0.06	18.42	1.06±0.06	2.7	-0	0.01	0.01	3
JPKS0423W-101	4 06 36.17	−44 24 33.7	18.72±0.07	20.72	18.00±0.05	19.78	17.36±0.12	18.59	1.36±0.14	4.7	-23	...	...	-
JPKS0423W-102	4 06 36.18	−44 22 20.8	18.58±0.04	19.98	17.85±0.03	19.10	17.23±0.08	18.15	1.35±0.09	2.9	-36	0.02	0.02	3
JPKS0423W-103	4 06 36.45	−44 28 14.8	18.34±0.04	19.45	17.89±0.03	18.98	17.71±0.09	18.56	0.64±0.10	4.2	-36	0.86	0.86	3
JPKS0423W-104	4 06 36.51	−44 28 08.2	19.78±0.08	20.59	19.42±0.11	20.25	...	...	...	3.2	44	0.80	0.80	-
JPKS0423W-105	4 06 37.57	−44 28 25.3	18.23±0.03	20.43	17.63±0.03	19.83	...	...	...	2.7	-19	...	...	-
JPKS0423W-106	4 06 37.81	−44 21 52.4	19.91±0.07	20.81	18.91±0.08	19.95	...	...	...	2.7	-0	0.19	0.19	-
JPKS0423W-107	4 06 38.03	−44 22 47.8	17.35±0.02	19.02	16.35±0.01	18.10	15.68±0.04	17.14	1.67±0.04	3.3	9	0.03	0.03	3
JPKS0423W-108	4 06 38.20	−44 27 31.7	18.96±0.05	20.29	18.08±0.04	19.34	17.64±0.12	18.47	1.31±0.13	3.1	-31	0.03	0.03	-
JPKS0423W-109	4 06 38.22	−44 27 15.4	19.97±0.13	21.46	19.59±0.10	20.32	...	...	...	6.7	-1	0.12	0.12	-
JPKS0423W-110	4 06 38.28	−44 22 49.1	18.33±0.04	20.09	17.70±0.03	19.05	16.77±0.08	18.27	1.56±0.09	4.5	18	0.01	0.01	-
JPKS0423W-111	4 06 38.32	−44 25 19.4	19.13±0.07	20.96	19.01±0.07	20.44	...	...	...	3.5	15	...	...	-
JPKS0423W-112	4 06 38.54	−44 23 39.1	19.39±0.10	21.15	18.87±0.06	20.05	...	...	...	5.9	-1	0.19	0.19	-
JPKS0423W-113	4 06 38.64	−44 28 13.0	17.70±0.01	18.73	...	...	...	...	...	2.7	8	0.54	0.54	-
JPKS0423W-114	4 06 39.40	−44 23 42.3	20.17±0.10	21.38	19.19±0.11	20.53	...	...	...	3.9	69	0.01	0.01	-
JPKS0423W-115	4 06 39.58	−44 24 56.0	19.27±0.09	20.84	18.36±0.05	19.70	16.91±0.10	18.51	2.36±0.13	5.1	-44	0.01	0.01	-
JPKS0423W-116	4 06 39.78	−44 23 56.2	19.89±0.13	21.45	19.71±0.13	20.67	...	...	...	7.3	-78	0.48	0.48	-
JPKS0423W-117	4 06 39.92	−44 23 24.2	20.27±0.12	21.37	19.74±0.13	20.73	...	...	...	4.4	45	0.28	0.28	-

Table B.3 continued...

Ident.	RA (J2000) h m s	DEC (J2000) ° ′ ″	J mag	μ_J^c mag/arcsec^2	H mag	μ_H^c mag/arcsec^2	K_s mag	$\mu_{K_s}^c$ mag/arcsec^2	$J-K_s$ mag	D_J ″	PA °	ϵ	Class	Morph
(1)	(2a)	(2b)	(3)	(4)	(5)	(6)	(7)	(8)	(9)	(10)	(11)	(12)	(13)	
JPKS0423W-118	4 06 40.37	−44 28 56.1	20.53±0.10	21.14	19.30±0.08	20.26	...	...	...	2.7	-70	0.24	0.24	-
JPKS0423W-119	4 06 40.40	−44 22 15.5	18.75±0.04	19.92	18.04±0.03	19.13	17.05±0.08	18.26	1.71±0.09	3.2	28	0.31	0.31	3
JPKS0423W-120	4 06 40.53	−44 22 04.8	18.44±0.05	20.19	17.90±0.04	19.26	16.70±0.09	18.22	1.74±0.10	4.3	-77	0.03	0.03	-
JPKS0423W-121	4 06 40.87	−44 25 37.8	18.02±0.03	19.05	...	...	17.46±0.08	18.01	0.56±0.09	3.7	20	0.79	0.79	3
JPKS0423W-122	4 06 41.00	−44 28 55.9	20.16±0.08	21.11	19.27±0.07	20.20	...	...	...	2.7	33	0.27	0.27	3
JPKS0423W-123	4 06 41.26	−44 22 22.9	19.85±0.08	20.60	19.22±0.07	20.06	...	...	...	3.1	64	0.32	0.32	-
JPKS0423W-124	4 06 41.28	−44 25 08.6	19.35±0.10	20.86	19.11±0.07	20.20	...	...	...	5.1	41	0.50	0.50	-
JPKS0423W-125	4 06 41.35	−44 24 02.6	19.90±0.13	21.18	19.44±0.12	20.57	...	...	...	5.6	-90	0.62	0.62	-
JPKS0423W-126	4 06 41.58	−44 27 49.3	19.15±0.10	21.46	18.58±0.09	20.67	...	...	...	6.6	44	...	...	-
JPKS0423W-127	4 06 41.58	−44 24 03.7	19.28±0.10	21.10	19.18±0.11	19.89	...	...	...	6.2	25	0.26	0.26	-
JPKS0423W-128	4 06 41.87	−44 28 56.1	19.84±0.11	21.31	...	...	...	...	...	4.4	24	...	...	-
JPKS0423W-129	4 06 41.91	−44 27 59.4	19.79±0.13	21.30	18.99±0.10	20.15	...	...	...	5.5	-88	...	...	-
JPKS0423W-130	4 06 41.93	−44 21 49.4	20.16±0.08	20.80	19.10±0.07	20.02	...	...	...	2.7	40	0.29	0.29	-
JPKS0423W-131	4 06 41.95	−44 25 07.2	18.55±0.05	19.80	...	...	17.90±0.14	18.83	0.65±0.15	4.3	-8	0.75	0.75	3
JPKS0423W-132	4 06 42.27	−44 26 31.6	19.66±0.12	21.01	19.62±0.10	20.76	...	...	...	5.3	74	0.04	0.04	-
JPKS0423W-133	4 06 42.52	−44 25 07.4	19.23±0.05	20.00	...	...	...	...	...	2.7	10	0.69	0.69	-
JPKS0423W-134	4 06 42.64	−44 23 49.7	19.05±0.06	19.84	18.26±0.06	19.33	...	...	...	3.5	22	0.37	0.37	3
JPKS0423W-135	4 06 42.74	−44 25 48.3	19.59±0.10	20.43	...	...	...	...	...	4.4	89	0.79	0.79	-
JPKS0423W-136	4 06 43.04	−44 23 41.0	18.79±0.06	20.31	17.75±0.04	19.32	17.35±0.08	18.36	1.44±0.10	4.0	-3	0.01	0.01	-
JPKS0423W-137	4 06 43.15	−44 23 08.1	18.43±0.03	19.46	17.66±0.03	18.80	17.98±0.15	18.29	0.46±0.15	2.7	-6	0.53	0.53	-
JPKS0423W-138	4 06 43.30	−44 28 37.0	16.91±0.02	19.56	16.25±0.02	18.94	15.88±0.04	18.38	1.03±0.05	3.3	-19	0.01	0.01	3
JPKS0423W-139	4 06 43.47	−44 26 47.9	19.55±0.06	20.69	18.60±0.05	19.51	17.59±0.14	18.76	1.96±0.15	2.7	-15	0.01	0.01	-
JPKS0423W-140	4 06 43.63	−44 22 45.8	19.62±0.06	20.73	19.11±0.07	20.01	...	...	...	2.7	-76	0.09	0.09	-
JPKS0423W-141	4 06 43.68	−44 21 32.9	17.19±0.02	19.63	16.56±0.01	18.84	15.97±0.04	18.09	1.22±0.04	3.5	32	0.02	0.02	3
JPKS0423W-142	4 06 43.68	−44 25 22.8	19.38±0.06	20.56	18.53±0.06	19.80	17.81±0.17	18.83	1.57±0.19	3.1	9	0.01	0.01	-
JPKS0423W-143	4 06 43.80	−44 26 31.2	20.00±0.14	21.46	19.24±0.13	21.02	...	...	...	6.1	22	0.03	0.03	-
JPKS0423W-144	4 06 43.85	−44 27 44.5	19.17±0.07	20.16	18.46±0.05	19.40	...	...	...	3.8	19	0.25	0.25	-
JPKS0423W-145	4 06 43.95	−44 21 32.8	17.49±0.02	18.71	17.16±0.02	18.46	16.83±0.08	17.87	0.65±0.08	3.1	-20	0.08	0.08	3
JPKS0423W-146	4 06 44.20	−44 27 12.2	20.59±0.19	21.50	19.43±0.13	20.98	...	...	...	5.7	-89	0.40	0.40	3
JPKS0423W-147	4 06 44.26	−44 26 47.1	18.67±0.06	20.02	18.35±0.06	19.50	...	...	...	3.9	-18	0.03	0.03	-

Table B.3 continued...

Ident.	RA (J2000) h m s	DEC (J2000) ° ′ ″	J mag	μ_J^c mag/arcsec^2	H mag	μ_H^c mag/arcsec^2	K_s mag	$\mu_{K_s}^c$ mag/arcsec^2	J–K_s mag	D_J ″	PA °	ε	Class	Morph
(1)	(2a)	(2b)	(3)	(4)	(5)	(6)	(7)	(8)	(9)	(10)	(11)	(12)	(13)	
JPKS0423W-148	4 06 44.33	−44 26 45.0	19.37±0.08	20.56	18.35±0.06	19.50	...	...	...	5.3	-46	0.50	0.50	-
JPKS0423W-149	4 06 44.44	−44 24 18.5	20.28±0.17	21.45	19.53±0.11	20.99	...	...	...	5.2	38	...	...	-
JPKS0423W-150	4 06 44.45	−44 28 04.6	19.48±0.12	21.39	...	...	...	...	...	6.4	25	...	...	-
JPKS0423W-151	4 06 44.60	−44 22 34.7	18.53±0.04	19.54	...	...	17.82±0.12	18.29	0.71±0.13	3.6	9	0.81	0.81	3
JPKS0423W-152	4 06 44.78	−44 26 03.0	18.47±0.06	20.26	17.93±0.05	19.36	17.28±0.09	18.09	1.19±0.10	5.2	-51	0.04	0.04	-
JPKS0423W-153	4 06 44.79	−44 28 31.3	19.28±0.11	21.32	18.97±0.08	20.19	...	...	...	6.7	-41	...	...	-
JPKS0423W-154	4 06 44.86	−44 24 25.4	19.66±0.12	20.61	19.21±0.09	19.99	...	...	...	5.1	9	0.05	0.05	-
JPKS0423W-155	4 06 45.10	−44 28 58.7	17.58±0.04	19.89	17.79±0.05	19.20	17.30±0.09	18.50	0.27±0.10	5.6	22	0.01	0.01	-
JPKS0423W-156	4 06 45.24	−44 24 03.9	18.72±0.04	20.19	17.75±0.03	19.22	17.38±0.12	18.39	1.34±0.12	3.2	20	0.01	0.01	-
JPKS0423W-157	4 06 45.29	−44 21 29.6	19.02±0.08	21.16	...	...	...	...	...	7.4	-11	0.13	0.13	-
JPKS0423W-158	4 06 45.34	−44 22 46.6	19.98±0.13	21.15	19.73±0.14	20.67	...	...	...	5.5	17	0.30	0.30	-
JPKS0423W-159	4 06 45.34	−44 26 32.0	19.14±0.08	20.32	18.74±0.06	19.52	...	...	...	4.5	25	0.03	0.03	-
JPKS0423W-160	4 06 45.96	−44 28 33.1	18.32±0.05	20.42	17.76±0.05	19.86	17.28±0.12	19.22	1.04±0.13	3.9	37	...	...	-
JPKS0423W-161	4 06 46.10	−44 22 20.6	19.84±0.07	21.27	19.28±0.07	20.53	...	...	...	2.7	25	...	...	-
JPKS0423W-162	4 06 46.12	−44 27 10.2	18.33±0.06	20.76	17.88±0.05	19.94	...	...	...	4.8	12	...	...	-
JPKS0423W-163	4 06 46.21	−44 24 15.5	18.67±0.04	20.43	17.81±0.05	19.86	17.61±0.10	18.91	1.05±0.11	2.7	-66	0.01	0.01	-
JPKS0423W-164	4 06 46.39	−44 28 24.8	19.85±0.10	21.05	18.93±0.10	20.48	17.69±0.13	18.96	2.16±0.17	4.1	-1	0.01	0.01	-
JPKS0423W-165	4 06 46.52	−44 28 45.2	20.28±0.13	21.29	...	...	...	...	...	4.3	81	0.20	0.20	-
JPKS0423W-166	4 06 46.83	−44 23 19.4	19.51±0.10	20.80	18.97±0.08	19.87	17.93±0.11	18.65	1.58±0.15	4.7	33	0.10	0.10	-
JPKS0423W-167	4 06 46.96	−44 23 52.9	18.25±0.05	20.01	17.43±0.03	19.02	16.69±0.06	17.96	1.56±0.08	4.8	29	0.01	0.01	3
JPKS0423W-168	4 06 47.20	−44 23 59.3	18.75±0.04	20.06	17.56±0.04	19.18	16.95±0.07	18.07	1.81±0.08	3.1	-2	0.03	0.03	-
JPKS0423W-169	4 06 47.50	−44 25 38.3	19.17±0.07	20.00	...	...	...	...	...	4.1	38	0.63	0.63	-
JPKS0423W-170	4 06 47.88	−44 28 16.7	20.06±0.14	21.27	...	...	...	...	...	5.7	-81	0.51	0.51	-
JPKS0423W-171	4 06 47.92	−44 28 41.1	19.07±0.09	20.86	18.21±0.06	20.11	...	...	...	5.5	-47	...	...	-
JPKS0423W-172	4 06 48.12	−44 28 11.1	18.41±0.07	20.70	17.57±0.05	20.35	...	...	...	5.5	-28	...	...	-
JPKS0423W-173	4 06 48.31	−44 28 06.5	20.18±0.14	21.36	19.87±0.14	20.49	...	...	...	5.1	-4	...	...	-
JPKS0423W-174	4 06 48.54	−44 22 28.7	20.34±0.12	20.99	19.12±0.11	20.19	...	...	...	3.6	-89	0.14	0.14	-
JPKS0423W-175	4 06 48.61	−44 25 17.6	19.65±0.06	20.75	18.60±0.06	19.76	17.88±0.09	18.68	1.77±0.11	2.7	-11	0.22	0.22	-
JPKS0423W-176	4 06 48.80	−44 24 39.7	18.50±0.06	20.41	17.89±0.04	19.58	17.26±0.10	18.62	1.24±0.11	5.1	19	0.01	0.01	-
JPKS0423W-177	4 06 48.81	−44 23 51.2	18.77±0.07	20.57	18.24±0.07	19.81	17.51±0.13	19.07	1.26±0.15	4.6	-28	0.03	0.03	-

Table B.3 continued...

Ident.	RA (J2000) h m s	DEC (J2000) ° ′ ″	J mag	μ_J^c mag/arcsec^2	H mag	μ_H^c mag/arcsec^2	K_s mag	$\mu_{K_s}^c$ mag/arcsec^2	$J-K_s$ mag	D_J ″	PA °	ε	Class	Morph
(1)	(2a)	(2b)	(3)	(4)	(5)	(6)	(7)	(8)	(9)	(10)	(11)	(12)	(13)	
JPKS0423W-178	4 06 48.89	−44 23 39.0	18.25±0.03	19.21	...	...	...	...	...	3.1	23	0.78	0.78	3
JPKS0423W-179	4 06 49.15	−44 23 48.8	19.90±0.12	21.36	18.79±0.10	20.40	...	...	...	6.3	-45	0.16	0.16	-
JPKS0423W-180	4 06 49.53	−44 27 25.7	20.01±0.13	21.11	19.16±0.11	20.48	...	...	...	5.7	21	0.29	0.29	-
JPKS0423W-181	4 06 49.80	−44 26 41.3	19.85±0.11	21.17	18.63±0.09	20.34	17.57±0.13	18.86	2.29±0.17	4.3	-90	...	...	-
JPKS0423W-182	4 06 49.90	−44 27 46.1	19.51±0.10	21.08	18.71±0.07	19.95	17.50±0.09	18.72	2.01±0.14	4.4	-15	...	...	-
JPKS0423W-183	4 06 50.00	−44 27 36.7	18.96±0.08	20.95	18.81±0.09	20.36	...	...	...	5.2	77	...	...	-
JPKS0423W-184	4 06 50.25	−44 28 35.9	18.78±0.06	20.32	17.74±0.04	19.32	17.20±0.07	18.43	1.58±0.09	4.2	39	0.01	0.01	-
JPKS0423W-185	4 06 50.26	−44 24 34.8	17.63±0.02	18.79	...	...	...	...	...	2.7	24	0.57	0.57	3
JPKS0423W-186	4 06 50.42	−44 23 45.9	18.31±0.03	19.32	...	...	17.62±0.12	18.44	0.69±0.13	2.7	7	0.51	0.51	3
JPKS0423W-187	4 06 50.53	−44 25 42.0	20.11±0.14	21.38	19.28±0.10	20.19	...	...	...	5.5	22	0.12	0.12	3
JPKS0423W-188	4 06 50.55	−44 22 35.5	20.54±0.10	21.35	19.24±0.11	20.40	...	...	...	2.7	-22	0.16	0.16	3
JPKS0423W-189	4 06 50.70	−44 28 37.3	19.94±0.13	21.38	...	...	...	...	...	6.4	69	0.10	0.10	-
JPKS0423W-190	4 06 50.83	−44 29 01.2	19.98±0.15	21.39	19.17±0.09	20.33	17.85±0.14	19.06	2.14±0.21	6.0	88	...	...	-
JPKS0423W-191	4 06 51.36	−44 28 38.2	19.70±0.07	20.37	19.05±0.09	20.00	...	...	...	2.7	-49	0.76	0.76	-
JPKS0423W-192	4 06 52.05	−44 25 44.3	19.69±0.07	20.99	18.73±0.06	19.75	...	...	...	2.7	45	...	...	-
JPKS0423W-193	4 06 52.40	−44 26 32.9	20.15±0.14	21.28	19.64±0.14	20.37	...	...	...	5.7	-70	0.61	0.61	-
JPKS0423W-194	4 06 52.77	−44 27 17.9	16.99±0.01	18.62	16.36±0.01	17.89	15.98±0.03	17.16	1.01±0.03	3.2	-17	0.03	0.03	3
JPKS0423W-195	4 06 52.93	−44 27 47.2	18.55±0.04	19.54	...	...	17.43±0.13	18.34	1.12±0.13	3.6	-11	0.10	0.10	3
JPKS0423W-196	4 06 53.12	−44 22 47.6	18.99±0.06	20.12	...	...	...	...	...	3.6	23	0.30	0.30	-
JPKS0423W-197	4 06 53.15	−44 28 09.0	19.40±0.10	21.17	18.98±0.08	20.71	...	...	...	5.0	46	...	...	-
JPKS0423W-198	4 06 53.39	−44 27 46.1	18.48±0.04	19.87	17.56±0.03	18.99	16.65±0.08	18.14	1.83±0.09	3.1	46	0.02	0.02	3
JPKS0423W-199	4 06 53.79	−44 26 33.6	20.14±0.16	21.38	19.14±0.08	20.34	...	...	...	6.5	46	0.60	0.60	3
JPKS0423W-200	4 06 53.80	−44 24 28.1	20.06±0.12	21.27	19.12±0.07	20.22	...	...	...	4.8	-17	0.20	0.20	3
JPKS0423W-201	4 06 54.04	−44 26 20.5	20.29±0.13	21.35	...	...	...	...	...	5.0	-44	0.44	0.44	3
JPKS0423W-202	4 06 54.21	−44 23 53.0	19.62±0.11	21.32	19.15±0.07	20.35	...	...	...	5.1	-0	...	...	-
JPKS0423W-203	4 06 54.37	−44 25 25.8	19.56±0.11	21.01	18.69±0.06	20.04	...	...	...	5.4	45	0.06	0.06	-
JPKS0423W-204	4 06 54.53	−44 25 01.2	17.27±0.02	19.31	16.71±0.02	18.70	16.51±0.07	18.16	0.77±0.07	3.9	13	0.03	0.03	3
JPKS0423W-205	4 06 54.55	−44 23 14.5	17.91±0.05	20.77	17.25±0.04	20.33	...	...	...	5.9	-42	...	...	-
JPKS0423W-206	4 06 54.80	−44 22 01.5	19.06±0.05	20.48	18.08±0.04	19.48	17.56±0.12	18.67	1.50±0.13	2.7	81	0.01	0.01	-
JPKS0423W-207	4 06 55.12	−44 29 06.4	20.03±0.12	21.38	19.76±0.12	20.74	...	...	...	5.7	47	0.17	0.17	-

Table B.3 continued...

Ident.	RA (J2000) h m s	DEC (J2000) ° ′ ″	J mag	μ_J^c mag/arcsec^2	H mag	μ_H^c mag/arcsec^2	K_s mag	$\mu_{K_s}^c$ mag/arcsec^2	$J-K_s$ mag	D_J ″	PA °	ε	Class	Morph
(1)	(2a)	(2b)	(3)	(4)	(5)	(6)	(7)	(8)	(9)	(10)	(11)	(12)	(13)	
JPKS0423W-208	4 06 55.31	−44 26 06.3	17.67±0.02	20.27	17.16±0.02	19.34	16.55±0.07	18.54	1.13±0.08	2.7	-68	...	...	-
JPKS0423W-209	4 06 55.37	−44 23 33.7	19.43±0.11	21.39	19.65±0.08	20.39	...	...	...	7.0	-54	0.02	0.02	-
JPKS0423W-210	4 06 55.44	−44 24 16.3	20.07±0.14	21.38	...	...	...	...	...	5.8	27	0.09	0.09	-
JPKS0423W-211	4 06 55.54	−44 23 27.3	19.47±0.11	21.16	...	...	...	...	...	5.1	52	...	...	-
JPKS0423W-212	4 06 55.54	−44 23 07.8	20.15±0.12	21.33	19.34±0.10	20.30	...	...	...	4.6	-1	0.01	0.01	-
JPKS0423W-213	4 06 55.54	−44 22 34.4	19.21±0.05	20.12	...	...	...	...	...	2.7	38	0.36	0.36	-
JPKS0423W-214	4 06 55.57	−44 27 06.2	18.73±0.05	20.11	17.69±0.03	19.14	16.92±0.07	18.15	1.81±0.09	3.9	-5	0.03	0.03	-
JPKS0423W-215	4 06 55.64	−44 23 31.5	19.96±0.12	20.80	19.11±0.07	20.01	...	...	...	4.5	-76	0.73	0.73	-
JPKS0423W-216	4 06 55.84	−44 24 28.5	19.63±0.07	21.11	18.54±0.05	20.38	...	...	...	2.7	-45	...	...	-
JPKS0423W-217	4 06 56.06	−44 26 57.6	19.62±0.06	20.51	18.41±0.05	19.69	17.94±0.11	18.52	1.68±0.12	2.7	42	0.39	0.39	-
JPKS0423W-218	4 06 56.21	−44 21 27.6	18.34±0.03	20.30	17.82±0.03	19.34	16.89±0.10	18.61	1.45±0.11	2.7	48	...	...	-
JPKS0423W-219	4 06 56.47	−44 25 38.5	19.76±0.09	20.96	18.46±0.08	20.17	17.50±0.12	19.11	2.26±0.15	3.6	-3	0.01	0.01	-
JPKS0423W-220	4 06 56.82	−44 28 16.3	20.39±0.16	21.57	19.92±0.12	20.63	...	...	...	5.9	87	0.03	0.03	-
JPKS0423W-221	4 06 56.83	−44 24 01.4	19.12±0.05	20.96	18.36±0.05	20.15	17.31±0.12	18.87	1.81±0.13	2.9	-18	...	...	-
JPKS0423W-222	4 06 56.83	−44 25 12.4	18.91±0.09	21.09	19.18±0.12	20.22	...	...	...	6.9	-80	...	...	-
JPKS0423W-223	4 06 56.86	−44 24 24.0	19.45±0.09	20.87	19.19±0.07	20.21	...	...	...	3.9	41	0.02	0.02	-
JPKS0423W-224	4 06 57.06	−44 26 34.7	19.80±0.11	21.27	19.35±0.13	20.87	...	...	...	4.7	62	...	...	-
JPKS0423W-225	4 06 57.16	−44 22 22.7	18.86±0.05	19.79	...	...	17.76±0.11	18.75	1.09±0.12	3.7	14	0.47	0.47	3
JPKS0423W-226	4 06 57.57	−44 24 11.8	19.19±0.09	20.71	19.40±0.08	20.23	...	...	...	6.1	37	0.68	0.68	-
JPKS0423W-227	4 06 57.74	−44 22 08.4	18.34±0.05	20.04	17.73±0.03	19.16	16.85±0.09	18.18	1.48±0.10	4.8	29	0.01	0.01	3
JPKS0423W-228	4 06 57.84	−44 21 43.1	19.43±0.07	20.53	19.41±0.10	20.37	...	...	...	3.4	-16	0.17	0.17	-
JPKS0423W-229	4 06 57.89	−44 22 47.5	19.21±0.10	20.77	18.33±0.07	19.96	...	...	...	5.9	7	0.03	0.03	-
JPKS0423W-230	4 06 58.15	−44 25 07.6	19.68±0.07	21.13	18.70±0.08	20.41	...	...	...	2.7	-22	...	...	-
JPKS0423W-231	4 06 58.36	−44 24 16.5	18.92±0.07	21.05	18.77±0.05	20.34	...	...	...	5.0	17	...	...	-
JPKS0423W-232	4 06 58.69	−44 27 08.5	19.86±0.10	21.14	18.49±0.05	20.01	...	...	...	4.0	63	0.04	0.04	-
JPKS0423W-233	4 06 58.71	−44 27 33.9	19.84±0.11	21.40	19.07±0.08	20.43	...	...	...	4.9	-11	...	...	-
JPKS0423W-234	4 06 58.87	−44 22 06.8	18.70±0.03	19.77	18.32±0.04	19.27	17.98±0.12	18.57	0.72±0.12	2.7	-23	0.48	0.48	-
JPKS0423W-235	4 06 58.91	−44 25 15.6	19.24±0.10	21.24	19.54±0.12	20.69	...	...	...	6.9	78	0.01	0.01	-
JPKS0423W-236	4 06 59.12	−44 21 56.8	20.13±0.11	20.94	19.18±0.10	20.19	...	...	...	3.7	24	0.50	0.50	-
JPKS0423W-237	4 06 59.37	−44 26 18.5	18.77±0.04	19.75	...	...	...	...	...	3.5	-12	0.82	0.82	3

Table B.3 continued...

Ident.	RA (J2000) h m s	DEC (J2000) ° ′ ″	J mag	μ_J^c mag/arcsec^2	H mag	μ_H^c mag/arcsec^2	K_s mag	$\mu_{K_s}^c$ mag/arcsec^2	$J-K_s$ mag	D_J ″	PA °	ε	Class	Morph
(1)	(2a)	(2b)	(3)	(4)	(5)	(6)	(7)	(8)	(9)	(10)	(11)	(12)	(13)	
JPKS0423W-238	4 06 59.49	−44 28 12.1	18.63±0.04	19.66	18.00±0.03	19.03	17.48±0.13	18.60	1.15±0.13	3.8	2	0.39	0.39	3
JPKS0423W-239	4 06 59.64	−44 28 44.0	19.26±0.07	20.17	...	...	...	...	...	3.5	68	0.20	0.20	-
JPKS0423W-240	4 06 59.66	−44 25 18.7	20.03±0.14	21.48	18.99±0.12	20.75	...	...	...	6.2	69	0.11	0.11	-
JPKS0423W-241	4 06 59.73	−44 25 43.9	20.02±0.08	20.89	19.20±0.07	20.09	...	...	...	2.7	52	0.64	0.64	-
JPKS0423W-242	4 06 59.77	−44 28 06.8	19.29±0.07	20.87	18.30±0.05	20.07	17.16±0.11	18.79	2.14±0.13	3.5	32	0.01	0.01	-
JPKS0423W-243	4 06 59.94	−44 24 50.4	17.91±0.03	19.42	17.05±0.02	18.52	16.58±0.05	17.63	1.33±0.06	3.3	12	0.04	0.04	3
JPKS0423W-244	4 06 59.99	−44 25 16.8	19.90±0.13	21.18	17.78±0.06	20.09	...	...	...	6.3	-61	0.16	0.16	-
JPKS0423W-245	4 07 00.35	−44 21 26.9	19.58±0.10	20.96	18.21±0.08	19.91	...	...	...	4.4	-63	0.01	0.01	-
JPKS0423W-246	4 07 00.50	−44 21 53.0	19.47±0.06	20.56	18.33±0.07	19.80	18.01±0.14	18.70	1.46±0.15	2.7	12	0.04	0.04	-
JPKS0423W-247	4 07 00.52	−44 24 35.1	18.81±0.04	19.68	18.15±0.04	19.17	17.95±0.09	18.45	0.86±0.10	2.7	7	0.20	0.20	-
JPKS0423W-248	4 07 00.61	−44 22 27.7	20.59±0.10	21.25	...	...	...	...	...	3.1	46	0.54	0.54	-
JPKS0423W-249	4 07 00.64	−44 22 43.4	19.39±0.06	20.39	18.88±0.08	19.86	...	...	...	2.7	24	0.38	0.38	-
JPKS0423W-250	4 07 00.65	−44 23 25.7	20.03±0.12	21.07	19.56±0.08	20.30	...	...	...	4.8	17	0.68	0.68	-
JPKS0423W-251	4 07 00.71	−44 26 27.3	18.98±0.10	21.21	18.74±0.06	20.52	...	...	...	5.7	19	...	...	-
JPKS0423W-252	4 07 00.76	−44 25 23.6	15.11±0.00	17.24	14.35±0.00	16.49	14.04±0.01	15.83	1.07±0.01	3.2	13	0.03	0.03	1
JPKS0423W-253	4 07 00.88	−44 25 03.1	20.04±0.12	21.14	18.86±0.08	20.22	...	...	...	4.9	-13	0.27	0.27	-
JPKS0423W-254	4 07 01.06	−44 21 48.7	20.11±0.15	20.88	19.68±0.11	20.65	...	...	...	5.9	-81	0.38	0.38	-
JPKS0423W-255	4 07 01.09	−44 24 36.9	19.86±0.14	20.97	18.89±0.06	20.28	...	...	...	6.7	-27	0.61	0.61	-
JPKS0423W-256	4 07 01.18	−44 27 08.3	17.79±0.03	19.62	17.11±0.02	18.83	16.40±0.06	18.09	1.39±0.07	3.8	37	0.02	0.02	3
JPKS0423W-257	4 07 01.33	−44 28 39.3	19.62±0.11	20.98	18.85±0.10	20.13	...	...	...	5.7	-49	0.16	0.16	-
JPKS0423W-258	4 07 01.39	−44 27 50.7	19.66±0.11	21.41	19.30±0.08	20.68	...	...	...	5.8	-23	...	...	-
JPKS0423W-259	4 07 01.41	−44 23 40.6	19.41±0.09	20.52	19.18±0.06	20.13	...	...	...	4.7	13	0.14	0.14	-
JPKS0423W-260	4 07 01.45	−44 24 26.1	19.54±0.10	21.04	19.27±0.07	20.10	17.99±0.12	18.64	1.55±0.15	5.1	-26	0.09	0.09	-
JPKS0423W-261	4 07 01.70	−44 26 52.8	20.18±0.13	21.19	19.96±0.13	20.55	...	...	...	5.3	46	0.58	0.58	-
JPKS0423W-262	4 07 01.71	−44 28 21.7	20.15±0.16	20.84	...	...	...	...	...	5.8	19	0.50	0.50	-
JPKS0423W-263	4 07 01.73	−44 22 01.5	18.40±0.04	20.59	17.77±0.04	19.94	16.79±0.10	18.80	1.61±0.11	3.3	-11	...	...	-
JPKS0423W-264	4 07 01.75	−44 22 22.8	19.91±0.14	20.71	19.10±0.08	20.23	...	...	...	5.6	51	0.58	0.58	-
JPKS0423W-265	4 07 01.85	−44 24 25.0	18.89±0.08	21.03	19.09±0.10	20.68	...	...	...	5.4	-61	...	...	-
JPKS0423W-266	4 07 01.88	−44 26 50.3	18.80±0.07	20.53	19.96±0.13	20.55	...	...	...	5.5	-42	0.17	0.17	-
JPKS0423W-267	4 07 01.94	−44 25 00.6	17.90±0.02	19.04	17.32±0.02	18.39	17.21±0.08	17.96	0.69±0.08	3.2	26	0.39	0.39	3

Table B.3 continued...

Ident.	RA (J2000)	DEC (J2000)	J	μ_J^c	H	μ_H^c	K_s	$\mu_{K_s}^c$	$J-K_s$	D_J	PA	ε	Class	Morph
	h m s	° ′ ″	mag	mag/arcsec^2	mag	mag/arcsec^2	mag	mag/arcsec^2	mag	″	°			
(1)	(2a)	(2b)	(3)	(4)	(5)	(6)	(7)	(8)	(9)	(10)	(11)	(12)	(13)	

Bibliography

Abadi, M. G., Moore, B., Bower, R. G., 1999, *MNRAS* **308**, 947.

Abell, G. O., 1958, *ApJS* **3**, 211.

Andreon, S., Cuillandre, J. -C., Pelló, R., 2000, Constructing the Universe with Clusters of Galaxies, IAP 2000 meeting, eds. F. Durret and D. Gerbal.

Baker, A. J., Davies, R. I., Lehnert, M. D., Thatte N. A. *et al.*, 2003, *A&A* **406**, 593.

Balogh, M., Eke, V., Miller, C., Lewis, I. *et al.*, 2004, *MNRAS* **348**, 1355.

Bekki, K., 1998, *ApJ* **499**, 635.

Bertin, E., 1999, SExtractor User manual **v2.3**.

Bicker, J., Fritze - v. Alvensleben, U., Fricke, K. J., 2002, *A&A* **387**, 412.

Bicker, J., Fritze - v. Alvensleben, U., Möller, C. S., Fricke, K. J., 2004, *A&A* **413**, 37

Bicker, J., Fritze - v. Alvensleben, U., 2005, *A&A* **443**, L19.

Bravo-Alfaro, H., Cayatte, V., van Gorkom, J. H., Balkowski, C., 2000, *AJ* **119**, 580.

Butcher, H., Oemler, A., 1978, *ApJ* **219**, 18.

Cayatte, V., van Gorkom, J. H., Balkowski, C., Kontanyi, C., 1990, *AJ* **100**, 604.

Cluver, M. E., 2005, Probing distant clusters - a pre-SALT photometric study of intermediate redshift galaxy clusters, MSc. thesis, University of Cape Town.

Cortese, L., Marcillac, D., Richard, J., Bravo-Alfaro, H. *et al.*, 2007, *MNRAS* **376**, 157.

Couch, W. J., Ellis, R. S., Sharples, R. M., Smail, I., 1994, *ApJ* **430**, 121.

Couch, W. J., Barger, A. J., Smail I., Ellis, R. S., Sharples, R. M., 1998, *ApJ* **497**, 188.

Dahlén, T., Fransson C., Östlin G., Näslund M., 2004, *MNRAS* **350**, 253.

Dressler, A., Oemler Jr., A., Couch, W. J., Smail, I. *et al.*, 1997, *ApJ* **490**, 577.

Einasto, J., Hütsi, G., Einasto, M., Saar, E. *et al.*, 2003, *A&A* **405**, 425.

Einasto, J., Einasto, M., Hütsi, G., Saar, E. *et al.*, 2003, *A&A* **410**, 425.

Fasano, G., Poggianti, B. M., Couch, W. J., Bettoni, D. *et al.*, 2000, *ApJ* **542**, 673.

Fasano, G., Poggianti, B., M., Couch, W., J., Bettoni, D. *et al.*, 2001, *Ap&SS* **277**, 417.

Fritze - v. Alvensleben, U., 1998, *A&A* **336**, 83.

Fritze - v. Alvensleben, U., 1999, *A&A* **342**, L25.

Fritze - v. Alvensleben, U., 2000, preprint (astro-ph/0003416).

Fritze - v. Alvensleben, U., 2004, preprint (astro-ph/0407358).

Garilli, B., Maccagni, D., Andreon, S., 1999, *A&A* **342**, 408.

Gerken, B., Ziegler, B., Balogh, M., Gilbank, D. *et al.*, 2004, *A&A* **421**, 59.

Ghigna, S., Moore, B., Governato, F., Lake, G. *et al.*, 1998, *MNRAS* **300**, 146.

Girardi, M., Giuricin, G., Mardirossian, F., Mezzetti, M., Boschin, W., 1998, *ApJ* **505**, 74.

Glass, I. S., 1999, Handbook of Infrared Astronomy, Cambridge University Press, Cambridge, UK.

Glazebrook, K., Peacock, J. A., Collins, C. A., Miller, L., 1994, *MNRAS* **266**, 65.

Gómez, P. L., Nichol, R. C., Miller, C. J., Balogh, M. L. *et al.*, 2003, *ApJ* **584**, 210.

Gunn, J. E., Gott, J. R., 1972, *ApJ* **176**, 1.

Howell, S. B., 1989, *PASP* **101**, 616

Jarrett, T. H., 2000, *PASP* **112**, 1008.

Jarrett, T. H., Chester, T., Cutri, R. *et al.*, 2003, *AJ* **125**, 525.

Jarrett, T. H., 2004, *PASA* **21**, 396.

Kron, G. E., 1980, *ApJS* **43**, 305.

Landolt, A. U., 1992, *AJ* **104**, 340.

Larson, R. B., Tinsley, B. M., Caldwell, C. N., 1980, *ApJ* **237**, 692.

Lewis, I., Balogh, M., De Propis, R., Couch, W. *et al.*, 2002, *MNRAS* **334**, 673.

Lisker, T., Glatt, K., Westera, P., Grebel, E. K., 2006, *AJ* **132**, 2432.

Maddox, S. J., Efstathiou, G., Sutherland, W. J., Loveday, J., 1990, *MNRAS* **243**, 692.

Maddox, S. J., Efstathiou, G., Sutherland, W. J., 1990, *MNRAS* **246**, 433.

Massey, P., Davis, L. E., 1992, A User's Guide to Stellar CCD Photometry with IRAF.

McCall, M. L., 2004, *AJ* **128**, 2144.

Mihos, C. J., 2004, Clusters of Galaxies: Probes of Cosmological Structure and Galaxy Evolution, eds., Mulchaey J. S., Dressler, A., Oemler Jr., A., Cambridge Univ. Press, Cambridge, p. 277.

Moore, B., Katz, N., Lake, G., Dressler, A., Oemler Jr., A., 1995, *Nat* **379**, 613.

Moore, B., Lake, G., Katz, N., 1998, *ApJ* **495**, 139.

Moss, C., 2006, *MNRAS* **373**, 167.

Mould, J., Martin, S., Bothun, G., Huchra, J., Schommer, B., 1999, *ApJS* **96**, 1

Nagashima, C., Nagayama, T., Tamura, M., Sugitani, K. *et al.*, 2002, Science with SIRIUS: Simultaneous-color InfraRed Imager for Unbiased Surveys, eds., Tyson, J. A., Wolff, S., Proceedings of the SPIE, **4836**, *29*.

Oemler Jr., A., Dressler, A., Butcher, H. R., 1997, *ApJ* **474**, 561.

Persson, S. E., Murphy, D. C., Krzeminski, W., Roth, M., Rieke, M. J., 1998, *AJ* **116**, 2475.

Poggianti, B. M., Bridges, T. J, Carter, D., Mobasher, B. *et al.*, 2001, *ApJ* **563**, 118.

Schechter, P., 1976, *ApJ* **203**, 297.

Shectman, S. A., Landy, S. D., Oemler, A., Tucker, D. L. *et al.*, 1996, *ApJ* **470**, 172.

Skelton, R. E., 2007, The Near Infrared Luminosity Function of the Norma Cluster, MSc. thesis, University of Cape Town.

Skrutskie, M. F., Cutri, R. M., Stiening, R., Weinberg, M. D. *et al.*, 2006, *AJ* **131**, 1163.

Smail, I., Dressler, A., Couch, W. J., Ellis, R. S. *et al.*, 1997, *ApJS* **110**, 213.

Stetson, P. B., 1990, *PASP* **102**, 932.

Tanaka, I., Yamada, T., Turner, E. L., Suto, Y., 2001, *ApJ* **547**, 521.

van den Bergh, S., 1976, *ApJ* **206**, 883.

van Dokkum, P. G., Franx, Fabricant, D. M., Kelson, D. D., Illingworth, G. D., 1999, *ApJ* **520**, L95.

van Dokkum, P. G., Franx, M., Kelson, D. D., Illingworth, G. D., 2001, *ApJ* **553**, 39.